

# ~~Dual-hemisphere sea ice thickness reference measurements~~ A First Approach Towards Dual-Hemisphere Sea Ice Reference Measurements ~~from multiple data sources~~ Multiple Data Sources Tailored for evaluation ~~Evaluation and product inter-comparison~~ Product Intercomparison of satellite altimetry ~~Satellite Altimetry~~

Ida Birgitte Lundtorp Olsen<sup>1,9,\*</sup>, Henriette Skourup<sup>1,\*</sup>, Heidi Sallila<sup>2</sup>, Stefan Hendricks<sup>3</sup>, Renée Mie Fredensborg Hansen<sup>1,4</sup>, Stefan Kern<sup>5</sup>, Stephan Paul<sup>3</sup>, Marion Bocquet<sup>6</sup>, Sara Fleury<sup>6</sup>, Dmitry Divine<sup>7</sup>, and Eero Rinne<sup>8</sup>

<sup>1</sup>Department of Geodesy and Earth Observation, National Space Institute, Technical University of Denmark (DTU Space), Elektrovej Building 327, 2800 Kgs. Lyngby, Denmark

<sup>2</sup>Marine Research Unit, Finnish Meteorological Institute (FMI), Helsinki, Finland

<sup>3</sup>Alfred Wegener Institute (AWI), Helmholtz Centre for Polar and Marine Research, Bremerhaven, Germany

<sup>4</sup>Department of Civil and Environmental Engineering, Norwegian University of Science and Technology (NTNU), Trondheim, Norway

<sup>5</sup>Integrated Climate Data Center (ICDC), Center for Earth System Research and Sustainability (CEN), University of Hamburg, Hamburg, Germany

<sup>7</sup>Norwegian Polar Institute (NPI), Tromsø, Norway

<sup>8</sup>Arctic Geophysics, University Centre in Svalbard (UNIS), Longyearbyen, Svalbard, Norway

<sup>9</sup>National Center for Climate Research (NCKF), Danish Meteorological Institute, Copenhagen, 2100, Denmark

\*These authors contributed equally to this work.

**Correspondence:** Ida Birgitte Lundtorp Olsen (ilo@dmi.dk)

## Abstract.

Sea ice altimetry currently remains the primary method for estimating sea ice thickness from space, however ~~time-series of sea ice thickness~~, time series of such satellite-derived estimates are of limited use without having been quality-controlled against reference measurements. Such reference ~~observations for sea ice thickness validation measurements~~ (a term encapsulating  
5 in situ observations and remotely sensed measurements from ground, air, and below the ice) for validation of altimetry measurements over sea ice in the polar regions are sparse and rarely presented in a ~~format matching the manner where the time-space averaging matches that of the~~ satellite-derived products. Here, the first published comprehensive collection of sea ice reference ~~observations~~ measurements tailored for satellite altimetry observations over sea ice is presented, including free-board, thickness, draft and snow depth from sea ice-covered regions in the Northern Hemisphere (NH) and the Southern Hemisphere (SH) ~~is presented. The observations. The measurements~~ have been collected using ~~airbor~~ Ja, det er da meget underligt  
10 Jeg kigger på det om lidt, så vi kan få det afsted. ne airborne sensors, autonomous drifting buoys, moored and submarine-mounted upward-looking sonars, and visual observations. The data package has been prepared to match the spatial (25 km for NH and 50 km for SH) and temporal (monthly) resolutions of conventional satellite altimetry-derived sea ice thickness data

products for a direct evaluation of these, and the code is publicly available and distributed for users to change depending on their aim. This data package, also known as the Climate Change Initiative (CCI) sea ice thickness (SIT) Round Robin Data Package (RRDP), was produced within the ESA CCI ~~sea ice~~ Sea Ice project. The current version of the CCI SIT RRDP covers the polar satellite altimetry era (~~1993–2021~~) ~~and is part of ongoing efforts to keep the dataset updated~~ 1993–2024 ~~and has ongoing efforts aimed at continuously updating the datasets~~. The CCI SIT RRDP has been collocated ~~to with~~ satellite-derived sea ice thickness products from CryoSat-2, Envisat, and ERS-1/2 produced within the ESA CCI and the Fundamental Data Records for Altimetry (FDR4ALT) ~~project~~ projects to demonstrate the overlap and inter-comparison between the reference ~~observations~~ measurements and satellite-derived products. Here, the CCI SIT RRDP is introduced along with examples of its use as a validation source for satellite altimetry products, where the averaging, collocation and uncertainty methodology is presented ~~and their~~, and advantages and limitations are discussed.

## 1 Introduction

~~Satellite altimetry is often used to derive sea ice thickness at reasonable temporal and spatial resolutions by detecting and converting freeboard i.e., the height of the sea ice above the local sea level depending on scattering horizon, into thickness assuming the ice to be in hydrostatic equilibrium (e.g., Laxon et al., 2003, 2013; Rieker et al., 2014; Kacimi and Kwok, 2020; Fons et al., 2020).~~

~~Typically, either radar (Ku-band) or laser altimetry is used to obtain derived freeboards and thicknesses. This is achieved based on the assumption that a laser measures the total freeboard (snow + sea ice freeboard), whereas for~~

Reference measurements are key to a successful satellite mission, forming the foundation for building confidence in satellite-derived Ku-band radar observations it is commonly assumed to measure the sea ice freeboard once a correction of the slow-down of the radar wave propagation in snow ( $c_s$ ) (Ulaby et al., 1986) has been applied. Without such correction, the freeboard measured by the Ku-band radar is commonly referenced as the radar freeboard. The assumption of full penetration is based on laboratory experiments over cold and dry snow conditions Beaven et al. (1995). To estimate the correction for the slow-down of the radar wave propagation in snow, a measure of snow depth and snow density is necessary (Mallett et al., 2020).

~~The radar freeboard will in principle be located below the snow-ice surface as illustrated in Fig. 1. However, this is not a physical signal, but simply caused by the fact that the speed of light in air ( $c$ ) is larger than the speed of light in snow ( $c_s$ ), causing the conversion of travel-time to range (when not accounting for slow-down) being longer than reality. The height of the radar freeboard also includes other factors that impacts the scattering horizon and thereby the derived freeboard, such as e.g., roughness (Landy et al., 2020), basal snow salinity (Nandan et al., 2017), flooding (King et al., 2018; Kacimi and Kwok, 2020; Fons et al., 2020) and in-complete penetration (e.g. Willatt et al., 2010, 2011; Rieker et al., 2014; Stroeve et al., 2020b). These factors prevents the radar signal from penetrating all the way to the snow-ice surface.~~

geophysical products. However, over sea ice, such reference observations are limited in both spatial and temporal coverage—particularly during the earlier years of the satellite altimetry era. In addition, meaningful comparisons between reference observations and satellite altimetry data are complicated by differences in spatial resolution, temporal frequency, and sampling methodologies.

The different freeboards (total or sea ice freeboard) can be converted into an estimate of sea ice thickness assuming that sea ice is in hydrostatic equilibrium and additional information on the snow depth and the densities of snow, sea ice and water is available (Wadhams et al., 1992). From these parameters, the snow depth and sea ice densities comprise the largest uncertainties in the sea ice freeboard to thickness conversion (e.g. Giles et al., 2007; Zygmuntowska et al., 2014; Ricker et al., 2014; Kern et al., 2014) with a higher sensitivity to snow depth errors in the total freeboard to sea ice freeboard conversion (Giles et al., 2007). While the impact of snow mass (snow depth and density) error decreases with increasing total freeboard due to a lower snow to ice mass ratio, the impact of snow mass error increases with increasing total freeboard. In this study, we adopt the term *reference measurements* to refer to a collection of non-satellite observations (from e.g., in situ, airborne, moorings, drifting buoys, and ships) that can be used for comparison with satellite remote sensing data. This should not be confused with the term *Fiducial Reference Measurements (FRMs)*, which are required to follow specific standards. Protocols and procedures for individual FRMs, and their comparison to altimetry-derived sea ice thickness (SIT) measurements, are currently being defined by the scientific community (e.g. Da Silva et al., 2023). Comprehensive validation of satellite-derived sea ice thickness products necessitates coincident observations of sea ice density scales with sea ice freeboard. Thus, for thinner sea ice the snow load error may be more relevant for the sea ice thickness error budget, while for thicker sea ice errors in sea ice density may be the largest retrieval error component. The point where sea ice density error contribution exceeds the snow mass error contribution depends on the actual sea ice and snow conditions.

The snow depth uncertainties arises primarily due to the fact that there is currently no consistent snow depth dataset at the same temporal and spatial resolution as the satellite altimetry observations, thickness, snow depth, and the densities of snow, ice, and water (Fig. 1, following the assumption that sea ice is in hydrostatic equilibrium), ideally at matching spatial and temporal scales covering the entire polar satellite altimetry era (1993–present). The Arctic available monthly climatologies (e.g. Warren et al., 1999; Shalina and Sandven, 2018) or modified versions (Kurtz and Farrell, 2011) based on field observations often lack information of inter-annual variations and trends, and various snow depth products from models or temporally limited multi-sensor observations have shown large discrepancies (Zhou et al., 2021), thus there is limited consensus between the available snow depth estimates. In the Antarctic, one must currently rely on snow depths derived from e.g. passive microwave sensors (e.g. Markus and Cavalieri, 1998; Comiso et al., 2003; Shen et al., 2022), where the methods are most reliant over first-year ice, which is the predominant ice type. The record dates back to the early 1990s and thus covers the entire polar satellite era. However, the method is challenged by the fact that it cannot reliably measure snow depths exceeding 50 cm, which are common in the Antarctic (Lawrence et al., 2024). Additionally, numerous publications (e.g. Worby et al., 2008a; Markus et al., 2011; Ozsoy-Cicek et al., 2011) have demonstrated that the method underestimates snow depth over deformed sea ice by a factor of 2 or even 3. Snow depth models are lacking in the Antarctic, but first efforts have recently been published by Lawrence et al. (2024). Dual-frequency satellite altimetry derived snow depth estimates for both Arctic (Guerreiro et al., 2016; Lawrence et al., 2018; Kwok et al., 2020; Garnier et al., 2021; Kacimi and Kwok, 2022; Fredensborg-Hansen et al., 2022) and Antarctic (Kacimi and Kwok, 2020; Garnier et al., 2021) are promising, but limited to the period when the NASA ICESat mission was operational (2003–2008) and after SARAL/AltiKa was launched (in 2013) and thus, do not cover the entire polar satellite era dating back to 1993. In addition, efforts are being made to better understand the penetration capabilities of Ku-band

throughout the seasons and how that impacts the signal in preparation for the upcoming dual-frequency radar altimetry mission, CRISTAL (Copernicus Polar Ice and Snow Topography Altimeter, see Kern et al., 2020).

Schematic of the different sea ice altimetry-related terms. Radar (Ku-band) and laser altimetry observations and their expected penetration into the snow pack are shown by the red and green beams, respectively. Not to scale. The shaded area denote the uncertainty related to penetration of radar and slow-down of propagation speed, which is depending on the snow conditions, and impacts (along with other things) the retrieved radar freeboard.

Conventional methods for estimating Arctic sea ice thicknesses from satellite altimetry use sea ice densities depending on sea ice types i.e., first-year ice (FYI) and multi-year ice (MYI) following Alexandrov et al. (2010). According to Jutila et al. (2022a), these sea ice densities might not represent the present state of the sea ice as their results show higher average bulk densities for both ice types. The dual-density approach also introduce auxiliary sea ice types to be included in the sea ice freeboard to thickness conversion, which in case of miss-classification may introduce relatively large errors (e.g. Haas et al., 2017; Kern et al., 2015). For the Antarctic sea ice, either a singular value for sea ice density assuming full coverage of FYI is used (Kacimi and Kwok, 2020) or, alternatively, the sea ice freeboard to thickness conversion takes into account a single combined density for snow and ice to accommodate for the special sea ice conditions in the Antarctic with negative freeboards and flooded ice (e.g. Kern et al., 2016; King et al., 2017). More recent attempts by Fons et al. (2023) uses seasonal variable ice densities, however, most methods rely on in situ measurements collected by Worby et al. (2008a) and Buynitskiy (1967).

With altimetry observations ranging back to the beginning of 1990, there is a potential for developing long time-series of sea ice freeboard and thickness for climate analyses (Quartly et al., 2019). The European Space Agency (ESA) Climate Change Initiative (CCI) for sea ice (last access: 28 February 2024) has the ultimate objective of producing Climate Data Records (CDR) of the Essential Climate Variable (ECV) sea ice thickness (SIT) (and sea ice concentration) from various altimetry (and passive-microwave-radiometry) missions without inter-satellite-mission biases. This presents challenges due to the differences in coverage, resolution and instrument design between the missions. The CCI SIT project utilizes observations from the European Remote Sensing Satellites-1 and -2 (ERS-1/2, ESA, 2013), the Environmental Satellite (Envisat, Dubock et al., 2001) and CryoSat-2 (Wingham et al., 2006). ERS-1 launched in 1991 (in orbit until 2000) and its follow-up mission, ERS-2, launched in 1995 (in orbit until 2011), were equipped with However, such reference measurements are sparse and unevenly distributed across the Arctic and even more limited in the Antarctic, amongst others, the Radar Altimeter (RA) instrument. RA was a pulse-limited Ku-band radar altimeter (13.8 GHz), that acquired data in two operating modes: ocean or ice, and had a footprint diameter of 16-20 km (depending on sea state) due to logistical challenges and high operational costs. Moreover, most existing reference measurements provide only a subset of the required variables. Here, we include and assess existing publicly available reference measurements of freeboard, thickness, draft, and snow depth from a variety of sources to support long-term altimeter-derived sea ice thickness Climate Data Records (CDRs). We do not include reference measurements of snow, sea ice, or water densities, as these are extremely limited. We implement a simple approach developed in accordance with current community practices, intended as a first step toward a consistent collection of harmonized reference measurements. We note, that RA on ERS-1 was only active for specific sea ice or geodetic campaigns from 1993-1996 and thus, the satellite-

115 ~~The sea ice altimetry time-series currently only range back to 1993. To continue data acquisition, Envisat was launched in 2002 (in orbit until 2012) which carried RA-2, a dual-frequency pulse-limited radar altimeter operating at Ku-band (13.575 GHz) and S-band (3.2 GHz) with a footprint diameter of 20 km for Ku-band (Roca et al., 2009). ERS-1 community - particularly when using radar altimeters - rarely validates data in its native form (i.e., along-track Level-2 data products). Examples can be found in studies such as Laxon et al. (2003); Kern et al. (2015); Giles and Hvidegaard (2006); ?; Fredensborg Hansen et al. (2024b)~~  
120 ~~, where some spatial averaging is applied and/2 and Envisat flew in sun-synchronous polar orbits and acquired data up to 81.5°N/S latitude. In 2010, or the data are restricted in time and space. For instance, Laxon et al. (2003) use only satellite data within 100 km and 15 days of the first-ever synthetic aperture radar (SAR) interferometric radar altimeter (SIRAL) was launched on the CryoSat-2 mission (Wingham et al., 2006). CryoSat-2's SIRAL measures in Ku-band (13.575 GHz), reaches 88° N/S latitude and has an improved spatial resolution with a footprint size of about ~300 m reference measurements, while~~  
125 ~~Fredensborg Hansen et al. (2024b) smooth airborne underflight measurements using an along-track and ~1.65 km across-track (e.g. European Space Agency, 2019) when operating in SAR, which is the main mode used over sea ice, and provides observations acquired in interferometric SAR (SARIn) mode for coastal areas or over ice margins. The improved spatial resolution of CryoSat-2 when operating in SAR mode paved the way for more recently launched satellites (Sentinel-3A search radius of 7 km to match a processed satellite along-track product. In fact, community practice, based on numerous publications~~  
130 ~~(e.g., Laxon et al., 2013; Tilling et al., 2018; Carret et al., 2025; Bocquet et al., 2024; Landy et al., 2022; Guerreiro et al., 2017; Kwok and~~  
~~, is to compare monthly, gridded altimetry-derived geophysical variables (e.g., SD or SIT) with monthly averages of reference data gridded to the same resolution as the satellite product. This approach allows for comparison with reference measurements obtained at locations other than directly beneath the satellite track (e.g., from moorings or buoys), by utilizing a full month of satellite orbits to generate maps with pan-Arctic or Antarctic coverage. As such, most validation and inter-comparison studies~~  
135 ~~are performed on monthly grids (commonly used grids such as EASE/B and upcoming CEASE2.0 or North/D, and Sentinel-6 Michael Freilich), which all use this technique. ERS-1/2, Envisat and CryoSat-2 have together covered a period of 30 years, and therefore present an opportunity of creating consistent and quality-controlled time-series of sea ice freeboards and thicknesses.~~  
~~South Polar Stereographic) with a resolution ranging between 12.5-80 km depending on the product (see e.g., Carret et al., 2025; Landy et al.~~  
~~allowing for inter-comparison with other products (e.g., model-based or other satellite-derived composites) available in similar~~  
140 ~~formats. Processing the reference measurements into such formats provides composites, otherwise tailored for validation of the satellite altimeters, that can be used more widely by the community.~~

~~During the first phase of the CCI sea ice project, time-series of consistent sea ice freeboards and thicknesses were produced for the period of 2002–2021 using observations from Envisat and CryoSat-2 (Kern et al., 2015; Schwegmann et al., 2016; Paul et al., 2018) for both hemispheres. These are herein referred to as The Data Package (DP) of reference measurements presented here,~~  
145 ~~were collected and prepared in the framework of the European Space Agency (ESA) Climate Change Initiative (CCI) for Sea Ice project (<https://climate.esa.int/en/projects/sea-ice/>, last accessed: 23 May 2025) Round Robin (RR) exercise, and is referred to as the CCI SIT RRD. To facilitate these comparisons, the reference measurements have been gridded to match the temporal (monthly) and spatial resolution of the CCI SIT CDR. Stand-alone CDRs are of little use unless the products have been quality-controlled against relevant reference measurements for consistency. Evaluation of the satellite-derived sea~~

150 ice freeboards and thicknesses is a crucial part of the CCI-SIT project. For a complete validation of the satellite-derived sea ice  
freeboards and thicknesses we need coincident observations of sea ice freeboards, sea ice thickness, snow depth and densities  
of snow, ice and water with the same temporal and spatial scales covering the polar satellite altimetry era. However, reference  
measurements are sparsely and unevenly distributed in the Arctic, with even less availability in the Antarctic, due to the harsh  
environment and cost-expensive access and often only measure one of the variables e.g., freeboard, total thickness, draft or  
155 snow depth.

In this manuscript, we present a collection of publicly available sea ice reference measurements (to our knowledge the first  
set tailored for satellite data validation) relevant for sea ice thickness evaluation; including primary variables of freeboard,  
thickness, draft and snow depth acquired during the period 1993–2021 from different sources. Upon availability, surface and  
air temperature are provided as secondary variables. The collection of reference measurements is herein referred to as the CCI  
160 SIT RRDP. In the CCI-SIT RRDP, the reference measurements have been gridded to align with the scales and resolution of  
commonly provided satellite-derived sea ice thickness and freeboard products (25 km in the NH and SIT products (25 km  
in the Northern Hemisphere and 50 km in the SH), and collocated with km in the Southern Hemisphere) according to the  
community practice. We present the CCI SIT RRDP in detail, including detailed description of the reference measurements  
with emphasis on methods, inherent biases and preferential sampling, pre-processing steps, as well as the characterization of  
165 their uncertainties. Since the reference observations originate from diverse instruments and methods, their uncertainties vary  
significantly. As an example some older datasets (pre-2010) lack detailed uncertainty information, and others (e.g., visual  
ship-based observations) provide only a single uncertainty estimate per dataset. As a result, estimating the uncertainty for each  
measurement in the RRDP is complex but essential, and has been a major focus of this work. Given the complexity of the  
uncertainty budget, including sampling biases and the conversion of freeboard to thickness, we adopt a simplified approach  
170 rather than relying on advanced statistical methods that may not fully capture the underlying uncertainties.

We collocate the reference measurements with the CCI SIT CDR version 3.0 (~~(, last accessed on April 26, 2024)~~) including  
time-series <http://cci.esa.int>, last accessed: 26 April 2024), which includes time series from CryoSat-2 and Envisat. We have  
further collocated the CCI-SIT RRDP with time-series of (2010–present) and Envisat (2002–2012). Additionally, the RRDP is  
collocated with ERS-1/2 radar freeboards produced within (1993–2003) radar freeboard time series from the ESA Fundamental  
175 Data Records for Altimetry (FDR4ALT) project (Bocquet et al., 2023) ~~to show the data availability throughout the~~, providing  
coverage across the polar satellite altimetry era. The aim of CCI-SIT RRDP is to provide a data package useful for evaluating  
satellite-derived sea ice thickness products by collocating the sea ice freeboards, thicknesses and derived drafts from the  
CCI-SIT CDR processors with the observations included in the CCI-SIT RRDP. We further include reference observations  
of snow depth, and collocate to the auxiliary snow depths provided in the CDRs as the snow depths are used both in the  
180 radar-freeboard-to-sea-ice-freeboard and sea-ice-freeboard-to-thickness conversions, as already described. We do not include  
sea ice, snow or water densities, as there are limited overlapping reference observations of these. This is done to demonstrate  
the usage and the performance of the reference measurement with a focus on evaluating their reliability for satellite altimetry  
inter-comparison. Erroneous observations are systematically rejected, and our performance analysis is grounded in several  
key criteria: spatial and temporal representativeness, methodological biases, and threshold-based outlier detections. These

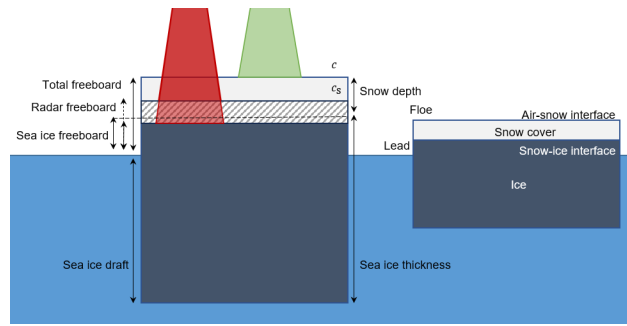


**Figure 1.** Schematic of the different sea-ice-altimetry-related terms. Radar (Ku-band) and laser altimetry observations and their expected penetration into the snow pack are shown by the red and green beams, respectively. Not to scale. The shaded area denotes the uncertainty related to penetration of radar and slowdown of propagation speed, which depends on the snow conditions, and impacts (along with other things) the retrieved radar freeboard.

185 aspects are examined through sensitivity studies and insights from previous research. In line with metrological principles, we recognize that reference measurements themselves require validation, a condition, which is not always met. Therefore, we describe the validation status of each reference dataset through a comprehensive literature review, highlighting limitations such as preferential sampling and inherent biases. To support data usability, we assess the spatial and temporal representativeness of each dataset and assign quality flags accordingly. These flags assist users in identifying data with potential representativeness issues, and we provide illustrative examples demonstrating the impact of excluding low-quality data in the evaluation of satellite products. Ultimately, we aim to enhance transparency and usability by providing uncertainty estimates and user-oriented quality flags, which through guided examples enables informed decision-making tailored to specific validation needs. Finally, we share the reference measurements in their final format, collocated with the CCI and FDR4ALT altimetry-derived sea ice thickness datasets (Olsen and Skourup, 2024a). We also provide the associated code and scripts (Olsen and Skourup, 2024b), and links to the native reference measurements (Table 2) allowing users to easily access and adapt the reference data to their desired temporal and spatial resolutions.

195 Since the reference observations are acquired by different instruments and methods, the uncertainties of the measurements are important to take into consideration. Some of the reference measurements are relatively old (before 2010), and have limited uncertainty information in the provided data product. Furthermore, some reference measurements (e.g., visual observations from ships) only include one constant uncertainty estimate per data product and not per measurement. Thus, determining the uncertainty of each estimate in the CCI-SIT-RRDP is not a trivial task, but is nonetheless important and has been a significant part of producing this RRDP (see Sect. 5).

205 This paper presents the CCI-SIT-RRDP, explaining in detail the collocation and averaging methodology as well as the uncertainty characterisation. Furthermore, a comparison with satellite data is presented to demonstrate the usage and performance of the CCI-SIT-RRDP. Since the CCI-SIT-RRDP provides already pre-processed comparable data for evaluation of sea ice altimetry-derived freeboards and thicknesses, as well as auxiliary snow depth estimates – for both hemispheres – this data

package and the methodologies applied herein have the potential of becoming the reference for future comparisons of current and future SIT products. The collection of reference measurements is presented in [The manuscript is organized as follows](#); Section 2 ~~Access to the CCI SIT RRDP and related software code is provided in Section 8~~ describes the RRDP reference measurements with emphasis on methods, inherent biases and preferential sampling. Pre-processing steps, and ~~the uncertainties of each data product and the applied uncertainty methodology~~ representativeness quality flags are presented in Section 3 and Section 5, respectively. ~~The satellite 4, respectively, followed by their uncertainties and the applied uncertainty methodology in Section 5. Satellite~~ SIT CDRs are described in Section 6.1, followed by a description of the comparability and ~~location of the location of~~ CCI SIT RRDP and satellite SIT CDRs in Section 6.1. Results and discussions of the CCI SIT RRDP and inter-comparison with satellite-derived products are presented in Section 7 including the availability of the reference measurements and their advantages and limitations. [Access to the CCI SIT RRDP and related software code is provided in Section 8.](#) Finally, Section 9 concludes the paper.

## 2 Description of RRDP reference measurements

The CCI SIT RRDP includes observations of freeboard (FRB), thickness (SIT), draft (SID) and snow depth (SD) in both the Arctic and Antarctic regions. Here, we use the term FRB as a general term for freeboard, including total freeboard and sea ice freeboard as both are available in the CCI SIT RRDP. In addition, SIT includes total thickness (snow + sea ice thickness) and sea ice thickness. Some reference measurements provide additional information on surface temperature and air temperature. As the temperature has an impact on radar penetration depths (e.g. ~~Willatt et al., 2011~~) (e.g. [Giles and Hvidegaard, 2006](#); [Willatt et al., 2011](#)) we have included the temperature observations in the CCI SIT RRDP. All available reference observations (from the included sources) for the polar regions for both hemispheres are part of the CCI SIT RRDP, providing us with observations throughout the entire year, although the coverage and availability are seasonally dependent, as can be seen in Fig. 5. Reference observations north of the satellite altimeter coverage i.e., the polar gap, has been included to prepare for evaluation of potential future satellite CDR gap filling products (e.g. by use of statistical methods such as kriging or optimal interpolation, see Gregory et al., 2021), but also to be used as reference observations for models.

In total, data from ~~10-14~~ different sources in the Arctic and 4 different sources in the Antarctic are included in CCI SIT RRDP. The measurements are obtained from different platforms using varying methods i.e., airborne measurements, measurements from moorings and autonomous drifting buoys, ships, and submarines. These methods and data products will be described more thoroughly in the following sections. A complete overview of the data sources used in the CCI SIT RRDP for both hemispheres is presented in Table 1 and links to the raw data are available from Table 2. Data sources are further illustrated in the Sankey diagram in Fig. 2, where the platform and methods of measurements are shown, along with the name of the data sources and the associated geophysical sea ice variables included in the CCI SIT RRDP. From here on, the data sources will be referred to by their abbreviations as provided in Table 1.

**Table 1.** Overview of reference measurements and their sources included in the CCI SIT RRDP for both the Northern (NH) and Southern (SH) hemispheres.

Campaign name or responsible	Description	Location	Abbreviation
<i>Northern Hemisphere (NH)</i>			
North Pole Environmental Observatory	Stationary moored upward-looking sonar	North Pole	NPEO
Fram Strait Arctic Outflow Observatory	Stationary moored upward-looking sonar	Fram Strait	NPI-FS
Beaufort Gyre Exploration Project	Four stationary moored upward-looking sonars	Beaufort Sea	BGEP
Russian-German TRANSDRIFT project	Four stationary moored upward-looking sonar	Laptev Sea	TRANSDRIFT
Arctic Shipborne Sea Ice Standardization Tool (ASSIST)	Visual observations from <del>ice-breakers</del> ships	Arctic Ocean	ASSIST
Submarine Arctic Science Program (SCICEX)	Submarine-mounted upward-looking sonar	Arctic Ocean	SCICEX
Cold Regions Research and Engineering Laboratory (CRREL)	Ice mass balance buoys (IMB)	Arctic Ocean	IMB-CRREL
Alfred Wegener Institute (AWI)	Snow depth buoys (SB)	Arctic Ocean	SB-AWI
Alfred Wegener Institute (AWI)	Airborne electromagnetic (AEM) measurements	Lincoln Sea/Beaufort Sea	AEM-AWI
NASA's Operation IceBridge (OIB)	Airborne laser and radar altimetry and snow radar	Lincoln Sea/Beaufort Sea	OIB
Multidisciplinary drifting Observatory for the Study of Arctic Climate (MOSAIC)	Airborne electromagnetic measurements and ice mass balance buoys	Arctic Ocean	MOSAIC
Nansen Legacy project	bottom-anchored ocean moorings and AEM measurements	Arctic Ocean	Nansen Legacy
<i>Southern Hemisphere (SH)</i>			
Alfred Wegener Institute (AWI)	Stationary moored upward-looking sonar (ULS)	Weddell Sea	AWI-ULS
NASA's Operation Ice Bridge (OIB)	Airborne laser and radar altimetry	Weddell Sea	OIB-SH
Alfred Wegener Institute (AWI)	Snow depth buoys (SB)	Weddell Sea	SB-AWI-SH
Antarctic Sea ice Processes and Climate (ASPeCt)	Visual observations from <del>ice-breakers</del> ships	Southern Ocean	ASPeCt

**Table 2.** Direct data access is provided to all included reference data by using the DOI/url links. DOI's are used when available.

Campaign	Reference	DOI/URL	Additional notes
OIB (NH, SH)	Kurtz et al. (2016), Kurtz et al. (2015)	<a href="https://doi.org/10.5067/GRIXZ91DE0L9">https://doi.org/10.5067/GRIXZ91DE0L9</a> <a href="https://doi.org/10.5067/G519SHCKWQV6">https://doi.org/10.5067/G519SHCKWQV6</a>	QuickLooks (QLs) IDSC4. SH data is available from Operation IceBridge Data Portal, similar to IDCS4
AEM-AWI	Grosfeld et al. (2016)	<a href="https://data.meereisportal.de/relaunch/airborne?lang=de">https://data.meereisportal.de/relaunch/airborne?lang=de</a>	Snow depth measurements available for 2017 and 2019 (Jutila et al., 2024a, b)
ASSIST	ASSIST (2006)	<a href="https://icewatch.met.no/">https://icewatch.met.no/</a>	Data is repeatedly added, hence, providing more data than what is used in this study
ASPeCt	Worby et al. (2008b) Kern (2020)	<a href="https://aspect.amarctica.gov.au/data.html">https://aspect.amarctica.gov.au/data.html</a> <a href="https://doi.org/10.26050/WDC/ESACCIPSMVBSIOV2">https://doi.org/10.26050/WDC/ESACCIPSMVBSIOV2</a>	
IMB-CRREL	Perovich et al. (2022)	<a href="https://imb-crrel-dartmouth.org/archived-data/">https://imb-crrel-dartmouth.org/archived-data/</a>	
SB-AWI (NH & SH)	Nicolaus et al. (2017)	<a href="https://doi.org/10.2312/polfor.2016.011">https://doi.org/10.2312/polfor.2016.011</a>	Data available by: Maps & Data -> Method -> Autonomous measurements -> Snowbuoy
MOSAIC	von Albedyll et al. (2021) Lei et al. (2021)	<a href="https://doi.pangaea.de/10.1594/PANGAEA.934578">https://doi.pangaea.de/10.1594/PANGAEA.934578</a> <a href="https://doi.pangaea.de/10.1594/PANGAEA.938244">https://doi.pangaea.de/10.1594/PANGAEA.938244</a>	Airborne Electromagnetic Measurements (AEM) Snow and Ice Mass Balance Array (SIMBA)
Nansen Legacy	Øyvind and Sundford (2025) Cristea et al. (2023) Divine et al. (2023)	<a href="https://data.npolar.no/dataset/1a68b156-6f96-4824-8b10-40f07acb4632">https://data.npolar.no/dataset/1a68b156-6f96-4824-8b10-40f07acb4632</a> <a href="https://data.npolar.no/dataset/1a9cc2df-e48c-4286-aad8-e7d0ca94904c">https://data.npolar.no/dataset/1a9cc2df-e48c-4286-aad8-e7d0ca94904c</a> <a href="https://data.npolar.no/dataset/c1cfd5dd-71c8-4b00-b2f2-fd4f85a4d6af">https://data.npolar.no/dataset/c1cfd5dd-71c8-4b00-b2f2-fd4f85a4d6af</a>	Data from moorings Data from AEM Data from AEM
BGEP	BGEP (2003)	<a href="https://www2.whoi.edu/site/beaufortgyre/data/mooring-data/">https://www2.whoi.edu/site/beaufortgyre/data/mooring-data/</a>	
AWI-ULS	Behrendt et al. (2013b)	<a href="https://doi.org/10.1594/PANGAEA.785565">https://doi.org/10.1594/PANGAEA.785565</a>	
TRANSDRIFT	Belter et al. (2019), Belter et al. (2020)	<a href="https://doi.pangaea.de/10.1594/PANGAEA.899275">https://doi.pangaea.de/10.1594/PANGAEA.899275</a> <a href="https://doi.pangaea.de/10.1594/PANGAEA.912927">https://doi.pangaea.de/10.1594/PANGAEA.912927</a>	
NPI-FS	Sumata et al. (2021)	<a href="https://doi.org/10.21334/npolar.2021.5b717274">https://doi.org/10.21334/npolar.2021.5b717274</a>	
NPEO	Morison et al. (2016)	<a href="https://doi.org/10.5065/D6P84921">https://doi.org/10.5065/D6P84921</a>	
SCICEX	NSIDC (1998) SCICEX (2009, 2014)	<a href="https://doi.org/10.7265/N5930R3Z">https://doi.org/10.7265/N5930R3Z</a> <a href="https://doi.org/10.7265/N54Q7RWK">https://doi.org/10.7265/N54Q7RWK</a>	From 1993-2014 From 1960-2005
ERS-1 & ERS2	(Bocquet, 2023)	<a href="https://doi.org/10.6096/croh_sit_2023_01">https://doi.org/10.6096/croh_sit_2023_01</a>	
CryoSat-2	(Hendricks, 2024c), (Hendricks, 2024b)	<a href="https://catalogue.ceda.ac.uk/uuid/6c50437878c4cc0f83960434023eff">https://catalogue.ceda.ac.uk/uuid/6c50437878c4cc0f83960434023eff</a> <a href="https://catalogue.ceda.ac.uk/uuid/861ad3c7f3a34ebd8be6f618a92bd8e3">https://catalogue.ceda.ac.uk/uuid/861ad3c7f3a34ebd8be6f618a92bd8e3</a>	Northern Hemisphere Southern Hemisphere
Envisat	(Hendricks, 2024b), (Hendricks, 2024d)	<a href="https://catalogue.ceda.ac.uk/uuid/92eb2ba942074bec804af6a8b5436bee">https://catalogue.ceda.ac.uk/uuid/92eb2ba942074bec804af6a8b5436bee</a> <a href="https://catalogue.ceda.ac.uk/uuid/af96a1ecc493f49caa39dc912d15f2b17">https://catalogue.ceda.ac.uk/uuid/af96a1ecc493f49caa39dc912d15f2b17</a>	Northern Hemisphere Southern Hemisphere

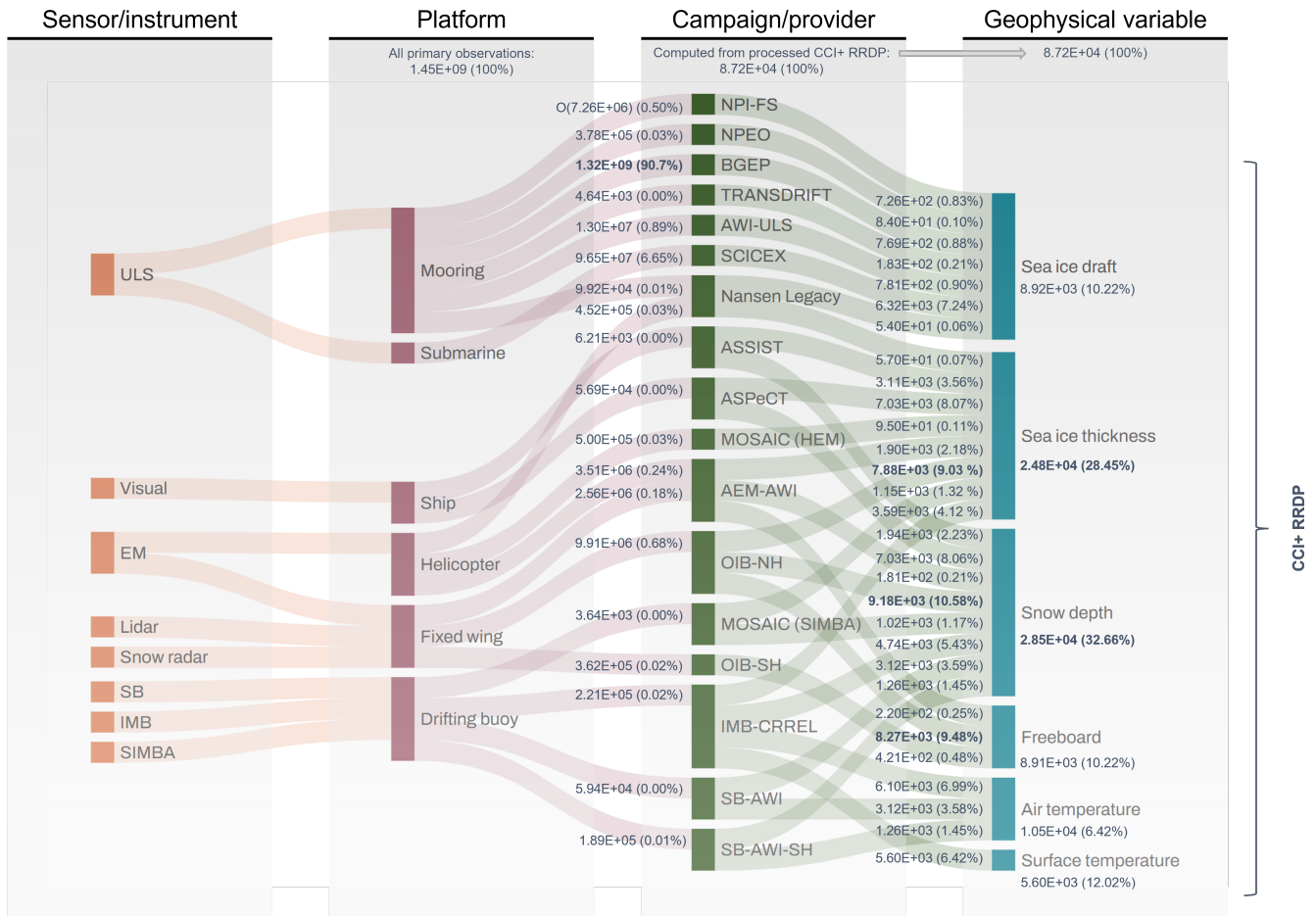


**Figure 2.** Sankey diagram providing an overview of the data sources used in the CCI SIT RRDP and how they are acquired, by whom/when and what has been observed. The diagram is shown by four categories; sensor or measurement type, platform, campaigns (Table 2), derived geophysical variable, and their dependencies. We note that the data volume included in the CCI SIT RRDP is represented here by numbers (in scientific notation) and percentages, and it is dependent on the processing level. Platform data volume denotes raw data, while campaign/geophysical variables refer to processed data. Note that the dominant-highest contributing data sources (at different processing levels) are highlighted in bold, defined as the the three highest contributing (in %) unless there is a large gap to the lesser contributors. In particular, the platform/mooring contributes more than 80% of the data, which primarily reflects the large time-series, high sampling frequency, and temporal coverage of the buoys. In contrast, campaign (OIB-NH, ASPeCTASPeCt, or SCICEX) primarily reflect spatial coverage, since these numbers refer to the processed CCI SIT RRDP. In total, SIT and SD account for approximately 60% of the CCI SIT RRDP. The notation O(number) denotes an approximation.

## 2.1 Airborne measurements

240 ~~Measurements from both OIB and~~ Measurements from OIB, AEM-AWI, MOSAiC and the Nansen Legacy are conducted from  
airborne platforms, either fixed-wing aircraft or helicopters (see Fig. 2). These measurements provide a higher spatial resolution  
than satellite measurements, and a larger spatial coverage than in situ observations, however, they are usually temporally limited  
to a few days to weeks in specific months, primarily spring (March–April) in the NH and austral summer (October) in the SH,  
depending on when and whether an airborne campaign was conducted (see Fig. 5).

## 245 **2.2 Campaign details: OIB and AEM-AWI**

OIB's primary objective was to bridge the gap between NASA's ICESat (2003–2009) and ICESat-2 (2018–onwards) satellite  
missions. ~~Over~~ During its duration from 2009 to 2019, more than 12 different ~~aircraft types was used during its duration from~~  
~~2009–2019~~ types of aircraft were used and within this time span, several updates to the instruments used for surveying were  
made. For a detailed overview of instruments used for different periods, along with an assessment of the impact on the ob-  
tained data, see MacGregor et al. (2021). The OIB reference measurements used in this study consist of data from the IceBridge  
"L4 Sea Ice Freeboard, Snow Depth, and Thickness", Version 001 (IDCS4), data product in the period of 2009–2013. Data  
~~subsequent to after~~ this are provided as ~~quick-looks~~ quicklooks (Kurtz et al., 2016), which means that significantly less process-  
ing has been ~~done~~. ~~Quick-looks performed~~. Quicklooks are processed from 2012–2019, but are only used from 2014–2019 due  
to IDCS4 being available until 2014. The measurands that we compare to satellite observations are the sea ice FRB (total FRB  
subtracted the snow depth) and SD as well ~~SIF that as~~ SIT which is derived from laser and radar observations with additional  
sea ice density ~~parametrization~~ parametrisation. The officially published Antarctic campaign data ~~is are~~ limited to total FRBs  
from the airborne topographic mapper (ATM) for the 2009 and 2010 campaigns, with no snow depth estimates provided and,  
hence, no sea ice thickness estimates. ~~For~~ The sensors used to produce the OIB product, post-processing algorithms have been  
~~used (Kurtz et al., 2013), which are based on observations from used herein, are~~ the ATM laser altimeter system (Section 2.1.1),  
a digital camera (Section 2.1.1) and a snow radar (Section 2.1.2).

AEM-AWI, MOSAiC and the Nansen Legacy measurements are conducted using an electromagnetic (EM) sounding de-  
vice (known as the "EM-Bird", see Section 2.1.3) dedicated to measuring the total thickness. In total, ~~25–27~~ campaigns are  
included in the AEM-AWI dataset as provided in Olsen and Skourup (2024a) along with information on the platform and  
measurement type for each campaign. AEM-AWI ~~has~~ includes data from 2001–2019, but has not been measured consistently  
~~each year~~. every year. For campaigns in 2017 and 2019, snow depth measurements (Section 2.1.2) were also obtained using  
an airborne frequency-modulated continuous-wave ultrawideband radar (Jutilla et al., 2024a, b). Additionally, total thicknesses  
from Airborne Electromagnetic (AEM) measurements were obtained during both the Nansen Legacy project (2019–2021)  
and the MOSAiC Expedition (2019–2020) using helicopters from ships. MOSAiC AEM measurements (also called HEM, as  
measurements were obtained from a helicopter) were provided with quality flags, described in the data product user manual  
(von Albedyll et al., 2021). The following flags were used to filter the data QF\_Reliability<2, Filter\_Moderate\_filter=1 Filter\_Strict\_filter=  
Total freeboards are provided for 2004 (IRIS, GreenIce) and 2007 (POLICE) campaigns in the AEM-AWI dataset (Olsen and Skourup, 2024a)  
, derived from the EM-integrated laser.

### 2.1.1 Airborne topographic mapper (ATM) and digital camera

The main components of ATM are two conically scanning laser altimeters that measure the surface elevation along the path of the aircraft at 15° and 2.5° off-nadir angle, respectively (MacGregor et al., 2021). The ATM measures surface elevation with respect relative to the WGS-84 reference ellipsoid by incorporating measurements from global navigation satellite system (GNSS) receivers and inertial navigation system attitude sensors. Measurements from ATM are subsequently converted to measurements of total freeboard  $\bar{r}$  by subtracting the instantaneous sea surface height (the local sea level obtained from lead measurements) from the measured elevation height. Determination of the sea surface height involves corrections of geoid height, tides, atmospheric pressure and the dynamic sea surface e.g. waves. During these procedures, information from the geo-referenced images from the digital cameras is used to support the identification of leads, which are used as tie-points for the instantaneous sea surface height. For more information about the ATM and the subsequent processing, see Kurtz et al. (2013).

### 2.1.2 Snow radar

SD is recorded using an ultra-wide frequency-modulated-continuous-wave (FMCW) radar at either S/C (2-8 GHz) or S/Ku (2-18 GHz) band (MacGregor et al., 2021)(MacGregor et al., 2021; Jutila et al., 2022b). The snow radar measures the return radar signal as a function of time, which is scattered from the illuminated area below the aircraft. SD is determined by identifying the air-snow and snow-ice interfaces (see Fig. 1 for the definition of the interfaces) in the received signal and converting the time difference between these interfaces to SD accounting for slow-down of propagation speed, accounting for the slowdown of the propagation speed in snow, by using the refractive index of snow (Kurtz et al., 2013).

Several different data products are available from snow radars, which are primarily caused by the use of different re-trackers (methodology to identify the air-snow and snow-ice interfaces, as shown in Fig. 1). Five different processing methods were compared with extensive in situ field measurements averaged to scales of 40 m (from the BROMEX, Ozone, and Mercury EXperiment/BROMEX at Barrow, Alaska, and observations acquired near Eureka, Nunavut, Canada), as well as reanalysis data (ERA-Interim) in Kwok et al. (2017, henceforth K17). Within this RRDP, three different re-trackers are employed in the three different data products (IDCS4, QLS, AEM-AWI-SD; two of which were inter-compared in K17).

- **IDCS4** (denoted NSIDC in K17): A full description of the algorithm is available from Kurtz et al. (2013), which utilises an empirical method that selects the air-snow interface either as the first significant peak above a defined threshold or the fit point when the rise in radar return power reaches a specified threshold, for the cases where no peaks are detected. The snow-ice interface is selected as the maxima in the radar signal below the air-snow interface.
- **QLS** (denoted GSFC-NK in K17): The full details of the algorithm methodology are described in the product documentation at NSIDC, but are based on the waveform fitting method described in Kurtz et al. (2014). The algorithm fits a model waveform to the snow-radar data, and both interfaces are selected from the model fit results. The model fit is highly sensitive to the parameters used in the fitting process, where the most important include the initial guess and model fit bounds for the interfaces along with the maximum number of iterations.

– AEM-AWI-SD: Jutila et al. (2022b) implemented a peakiness-based method, adapted from satellite radar altimetry, to enhance the detection of air–snow and snow–ice interfaces. This method is more robust in picking the right surface especially when the air–snow interface is the dominant scattering surface, compared to e.g. the Haar wavelet method. Their method is specifically tailored for the snow radar system deployed during the AWI IceBird campaigns, which has smaller footprints due to a lower flight altitude and slower speed of the aircraft.

310

According to K17, the QLs snow depth product exhibits a negative bias of approximately 5 cm compared to the IDCS4 product, based on comparisons with in situ measurements from the BROMEX and Eureka in situ field campaigns. Biases of similar magnitude (-4.5 to -6.7 cm) were found by King et al. (2015) and Petty et al. (2023) depending on sea ice type and settings (i.e. deformed ice versus level ice). The performance of the AEM-AWI-SD derived snow depth measurements over level, landfast first-year sea ice shows a mean bias of 0.86 cm between radar-derived estimates and ground truth (Jutila et al., 2022b), aligning closely with the performance (with biases of 0.3 m and -0.8 m when compared to the same in situ field observations as the the QLs in K17) of the OIB IDCS4 product. While alternative processing algorithms exist, their lack of consistency across datasets (Stroeve et al., 2020a; Kwok et al., 2017) led us to implement only a single approach in this study. However, this choice may introduce biases that exceed the provided uncertainties in the OIB QLs product, see Section 5.2.1.

315

### 320 2.1.3 EM-Bird

The EM-bird senses the distance of the sensor to the ice-water interface using frequency-domain EM induction sounding capitalizing on the substantial difference of electrical conductivity between the sea ice and snow layers compared to the ocean (Haas et al., 2009). Subtracting the instrument distance to the air-snow surface, measured by an integrated laser, from the distance to the ice-water surface yields the total thickness. The EM probe is towed by a helicopter or fixed-wing aircraft approximately 10-20 m above the surface of the sea ice. ~~The temporal extent of available relevant total thickness data in the AEM-AWI dataset is 2001, 2003-2017 and 2019. Measurements of the total freeboard are provided for 2004 (IRIS, GreenIce) and 2007 (PoHCE) campaigns in the AEM-AWI dataset (Olsen and Skourup, 2024a). These were derived from the helicopter EM-integrated laser~~We further emphasize that helicopters tend to avoid certain ice types, such as thin or young ice, and open water areas for safety reasons, and therefore preferentially sample sea ice thicker than 0.30 m. Comparison with drill-hole data shows that helicopter-borne EM derived ice thicknesses agree within  $\pm 0.1$  m over level ice (e.g., Haas et al., 2007). However, the accuracy can be heavily underestimated over deformed ice (by as much as 50 to 60% in worst case) due to the footprint size of EM measurements over those 3D structures, and the presence of air pockets between the ice floes that have been pushed together (Haas et al., 2009; Mahoney et al., 2015; Haas et al., 2007).

325

330

## 2.2 Stationary moorings

In the CCI SIT RRDP, we have included data from stationary moorings equipped with upward-looking upward-looking sonar (ULS). The observations are the only sea ice reference measurements, which are fixed to a specific geographic location, and provide continuous measurements throughout the year. Even though the individual measurements are point measurements,

335

the sea ice drift causes time-averaged sea ice drafts from ULS' to provide information of the sea ice pack representative of a larger area. Many of the existing ULS' provide long time-series (Fig. 4), and thus provide reference measurements ideal for evaluation of long-term multi-satellite climate data records. ~~An~~ A ULS is an instrument targeted at measuring the sea ice draft (the submerged part of the ice). The instrument emits sound pulses ~~and~~ and detects their echo return after being reflected on the bottom of the ice or the water level ~~in~~ between the ice floes. From these observations, the sea ice draft is derived after ~~applied~~ applying corrections. For basic principles, see Melling et al. (1995).

In the Arctic, we include ~~four~~ five sources providing stationary ULS data; the North Pole Environmental Observatory (NPEO) located at the North Pole with data from 2001–2010, the Fram Strait Arctic Outflow Observatory of the Norwegian Polar Institute (NPI-FS) located in the Fram Strait with data from 1990–2018, the Beaufort Gyre Exploration Project (BGEP) in the Beaufort Sea providing data from ~~2003–2018, 2003–2023, the Nansen Legacy project providing data from 2019–2021,~~ and the Russian-German TRANSDRIFT project (TRANSDRIFT) in the Lincoln Sea and Beaufort Sea with data from 2003 to 2016. ~~Data from the TRANSDRIFT project consist of ULS data from~~ Where the NPEO, NPI-FS, BGEP and TRANSDRIFT (2013–2015 and Upward-Looking acoustic Doppler current profiler (ADCP) from 2003–2016 (Belter et al., 2020).) moorings are measuring using an Ice Profiling Sonar (IPS), the Nansen Legacy and TRANSDRIFT (2003–2016) are using upward-looking Acoustic Doppler Current Profilers (ADCPs) (Belter et al., 2020). These different measurement techniques might introduce biases in the measured draft.

In the Antarctic, there are ULS draft observations from AWI (AWI-ULS) moorings in the Weddell Sea, where data ~~was~~ were collected from 1990 to 2011. We note ~~that~~ that currently there are several ULS ~~is~~ stationed around the Arctic and Antarctic, ensuring the continuation of the mooring time-series of ice draft, however, data is not available in near-real-time due to the sensor being submerged under water. Routine deployment and collection efforts are needed to deploy and retrieve ULS data, which is then processed afterwards. Hence, the ~~lag-time~~ lag time for data collection is significant compared to other data sources, e.g., autonomous drifting buoys equipped with Iridium link.

To our knowledge, there are no community practices w.r.t. direct validation of ULS derived sea ice drafts. However, different methods to extract the drafts from raw measurements can impact the resulting uncertainties, see Section 5.2.2.

### 2.3 Drifting buoys

Drifting buoys are autonomous systems, installed on selected sea ice floes, that drift freely with the ice compared to being anchored to one location as moorings. Depending on the buoy model, drifting buoys provide, along with other variables, the evolution of the thermodynamic growth and melt of the ice and/or changes in the snow depth at the specific point where they are deployed, and representativeness of the data acquired by these buoys ~~depend~~ depends on the initial snow and ice conditions at the time of deployment.

The derived information from drifting buoys ~~are~~ is limited to point measurements, and do not capture ice distribution on larger spatial scales nor the changes in the ice thickness distribution due to deformation, unless they are deployed in an array.

In the CCI SIT RRDP, we have included data from ice mass balance (IMB) buoys ~~with data from 2003–2015, and from~~ maintained by the Cold Regions Research and Engineering Laboratory (CRREL) (Perovich et al., 2022), covering the period

2003–2018; the Snow and Ice Mass Balance Array (SIMBA) deployed during the MOSAiC expedition in 2019–2020; and dedicated acoustic snow depth buoys (SB) ~~with data from 2013–2020. SB also has data available~~ deployed by AWI during the time period 2013–2023. While the IMB-CRREL and SIMBA buoys are only available for the Northern Hemisphere, SB data are available for both hemispheres. Data from IMB-CRREL for ~~the southern hemisphere from 2013–2023. 2017 is found to be faulty, as all recorded values are identical. These data were therefore excluded from the CCI SIT RRDP.~~

~~IMB-buoys measure~~ The Snow and Ice Mass Balance (IMB) buoys measure the thermodynamic contribution to changes in the mass balance of the sea ice. The main component is thermistor strings mounted vertically throughout the snow and ice column measuring the temperature profile, along with acoustic sounders placed above and below the ice, measuring the top of the snow/ice and the bottom of the ice, respectively. In addition, the buoys are typically equipped with a barometer and an air temperature sensor. ~~The IMB-buoy data in the CCI SIT RRDP is obtained from the Cold Regions Research and Engineering Laboratory (IMB-CRREL) (Perovich et al., 2022).~~ From the IMB-CRREL buoys, we include measurements of SIT and SD, along with surface and air temperature. Typically, 3–6 IMB buoys are deployed each year in the Arctic Ocean, with the most regular deployments focused in the Beaufort Sea and at the North Pole with a typical survival period of 1–2 seasons. The time interval between subsequent mass balance data measurements (SD and SIT) varies for different buoys and ~~depend~~ depends on the buoy model and the year of deployment. In general, the mass balance data ~~is~~ are measured approximately every four hours for the majority of buoys, but several buoys provide measurements every two hours and some (2002A, 2003A) only twice a day, while others (2015I, 2015J, 2015K) have measurements every hour. ~~SIMBA consists of an array of IMB buoys and hence also measures vertical temperature profiles through the air-snow-ice-water column using a thermistor string.~~ As such, ~~the IMB buoys provide spatially local~~ an individually deployed IMB buoy (IMB-CRREL) provides spatially localized measurements, due to ~~their fixed location~~ its fixed position on an ice floe, but with a relatively high temporal resolution. ~~Whereas, an array of IMB buoys (SIMBA) is expected to better represent a larger spatial variation of ice thicknesses and snow depths on the scales of the array, while keeping the high temporal sampling. The automatic detection of snow depth and ice thickness from SIMBA has been evaluated against in situ data by Zeliang Liao and Cheng (2019) when deployed in landfast ice (in vicinity of Zhongshan station in Prydz Bay, East Antarctic). In situ snow depth and ice thickness were measured on a weekly bases, where boreholes were drilled through the ice and the distance was measured using an ice gauge to determine ice thickness, and snow depth was measured with a stainless ruler from three close (less than 1 m) random sites near the ice boreholes (within 2 m), with accuracies of 0.01 m and 0.005 m for ice and snow measurements, respectively. No in situ comparison was recorded over drifting ice. Comparisons of ice thickness records a bias of 0.025 m, a RMSE of 0.09 m, and a correlation of 0.99, and the snow depth comparison was not reported. Cheng et al. (2020) compared SIMBA observations acquired in a frozen lake in Finland, where the interfaces of snow detection and ice thickness were compared with in situ observations acquired from the lake at observation sites 500 m apart from each other.~~

The IMB-CRREL ~~buoys initial thicknesses~~ and SIMBA buoys' initial thicknesses, i.e., the ice thickness at deployment, are shown in Fig. 3. Of the ~~87–92 IMB-CRREL~~ buoys included here, only ~~1-buoy-two buoys~~ (2015H, 2018D) has an initial SIT < 0.5 m. In general, they tend to be deployed in ice thicker than 1 m with few exceptions (2003C, 2013A, 2015H, 2015I, 2015K) ~~and most of them (21 out of 29 buoys),~~ 2018D and 2018E) with 37 of them deployed in the perennial sea ice

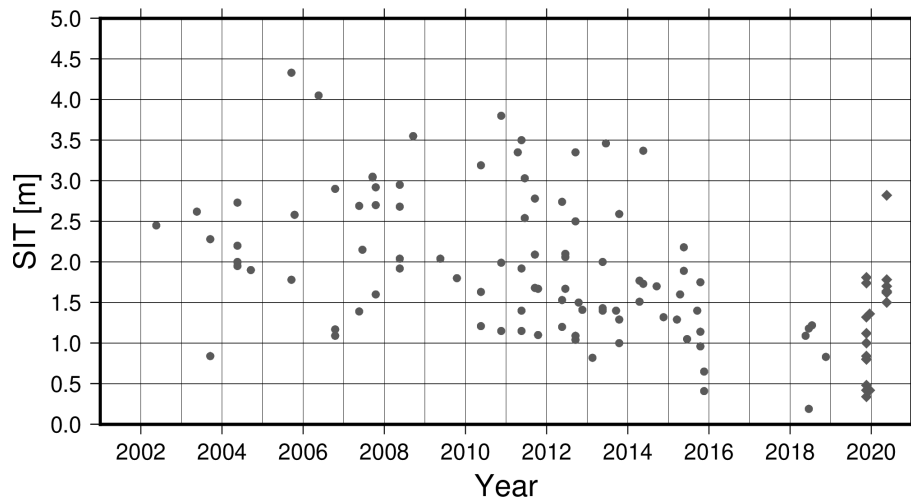


**Figure 3.** Initial thickness for the [87-92 IMB-CRREL \(dots\)](#) and [19 SIMBA \(diamonds\)](#) buoys included in this study.

cover (MYI) with initial thicknesses >2 m [prior to 2009](#) to decrease the likelihood of damage to the buoy due to e.g., sea ice deformation events and thereby prolonging its potential life span. Buoys deployed in MYI do not capture the seasonal cycle (Polashenski et al., 2011). Post-2009, more buoys are deployed in ice with an initial thickness <2 m ([39 out of 5844 out of 63](#)) with a minimum initial thickness of [0.41-0.19 m \(2015H2018D\)](#), i.e., in the seasonal ice cover (FYI). This is consistent with the design of the first IMBs to be adapted and well-suited for deployments in MYI (Richter-Menge et al., 2006b). An optimized buoy design to better fit deployments in [the](#)-seasonal ice zones was first tested in 2009 according to Polashenski et al. (2011). [Basically, all 19 SIMBA buoys \(except 2019T79\) were deployed in ice with initial thickness <2 m.](#)

Snow depth buoys (SB) measure relative changes in snow height, that [is are](#) the accumulation of snow since deployment. These are then calibrated against the initial snow depths measured during deployment in order to retrieve the absolute snow depth values. In the Alfred Wegener Institute snow depth buoys (SB-AWI) (Nicolaus et al., 2017), the measurements are made with four ultrasonic snow depth sensors that are installed on a mast-attached platform. SB-AWI measurements are available for both hemispheres. The data transmission interval for SB-AWI is approximately once per hour [resulting in similar](#), [resulting in](#) spatial and temporal characteristics [similar](#) to IMB-CRREL. [We were not able to identify validation studies where the derived snow depths were inter-compared with in situ data or reported, however the SB is consistently deployed by AWI in both hemispheres, and has shown reasonable accumulation rates \(e.g., Nicolaus and Katlein, 2017; Nicolaus et al., 2021; Arndt et al., 2024\)](#)

## 2.4 Ships

Collected and archived ship-based observations are provided via the Ice Watch program (Hutchings et al., 2018) for the NH. These are visual observations, that are recorded with the ASSIST (Arctic Shipborne Sea Ice Standardization Tool) following an established Ice Watch protocol. Reported observations may include e.g. sea ice concentration and thickness, stage of growth or

melt, state of the snow cover and surface roughness, and may be inconsistent in which variables are recorded within a particular observation and at what quality depending on the experience and qualifications of the observer (find a brief description of Ice Watch instructions for observers in Section 3.1.1). We are not aware of any specific validation practices that compare visual ship observations with other complementary data. However, new techniques are emerging such as the Sea Ice Monitoring System (SIMS, von Abedyll et al. (2024)) and downward looking cameras mounted on ships. ASSIST data is available from 2006–2021 and contains data from 61 voyages. The Southern Hemisphere has a corresponding program called ASPeCt (Antarctic Sea Ice Process and Climate), which was established in 1997 by the Scientific Committee on Antarctic Research. Data until 2005 is available from the ASPeCt data archive and contains data from 83 voyages and 2 helicopter flights for the period 1980–2005. More recent additions (2002–2019) to the dataset have been processed and are publicly available (Kern, 2020). Links to data sources for ASPeCt and ASSIST are available from Table 2. Ship observations are, in a similar manner as the airborne campaigns, dedicated to individual cruises with a duration of 1–2 months. Many of the observations in SH are made from supply ships, which primarily take place during the Austral summers and tend to navigate thin or less consolidated ice. In general, ships, whenever possible, tend to avoid ~~well-consolidated~~well-consolidated and deformed ice to limit risks, which impacts the ice observations.

## 2.5 Submarines

The submarine dataset ~~provide~~provides ULS SIDs, similarly to stationary moorings, except that the measurements are taken along trajectories and thus have a larger regional coverage. However, the data is collected only during dedicated cruises of 1–3 months duration. The submarine cruises are primarily military operations, which can imply that the data distribution to the common sea ice community can take several years due to restrictions on data sharing. The data included here were collected by the U.S. Navy and Royal Navy and are available for the Arctic Ocean. The temporal span of the data is from the 1st of February 1960 to the 30th of November 2005, along with data available in 2011 and 2014. Data from several other years (2012, 2016, 2018 and 2020) are currently being processed and evaluated for releasability. Examination of SCICEX data from the 2014 New Mexico cruise reveals anomalous behavior when compared to data from other years. Additionally, according to the SCICEX data product user manual (SCICEX, 2009, 2014), the 2014 New Mexico dataset has undergone an unspecified level of processing. Given these issues, the 2014 data has been excluded from the analysis, as it is likely not comparable with the other submarine measurements.

## 3 Processing of RRDP reference measurements

~~Averaging of the reference data was performed using the Equal-Area Scalable Earth Grid in version 2 (EASE2) provided by the National Snow and Ice Data Center (NSIDC). EASE2 is based on a polar aspect spherical Lambert Azimuthal equal-area projection Brodzik et al. (2012) and the WGS-84 ellipsoid. The NH grid dimension is 5400 km x 5400 km with a spatial resolution of 25 km, resulting in a grid consisting of 432 x 432 grid-cells, whereas the SH grid has a spatial resolution of 50 km, resulting in a grid consisting of 216 x 216 grid-cells. The grid is centered on the geographic pole, meaning that the~~

Timeline of all data included in the CCI SIT RRDP. The CDR observations are color-coded according to project as shown in the legend, whereas the colors of the RRDP reflect the type of reference observations as defined in Figure 5.

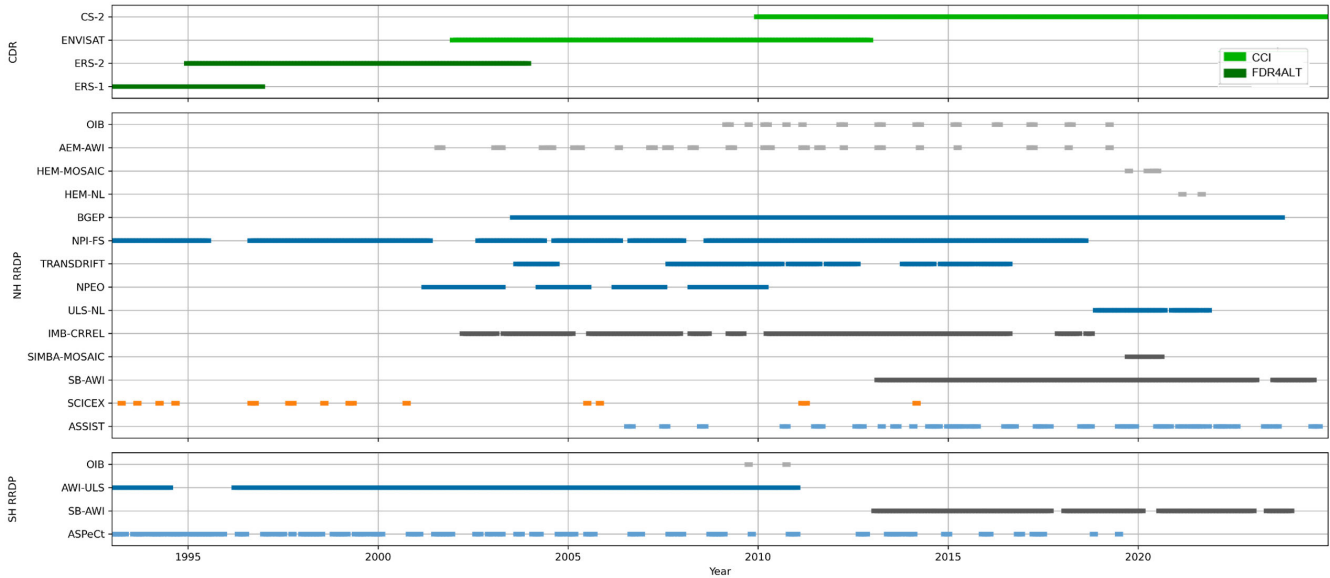


**Figure 4.** Timeline of all data included in the CCI SIT RRDP. The CDR observations are color-coded according to project as shown in the legend, whereas the colors of the RRDP reflect the type of reference observations as defined in Fig. 5.

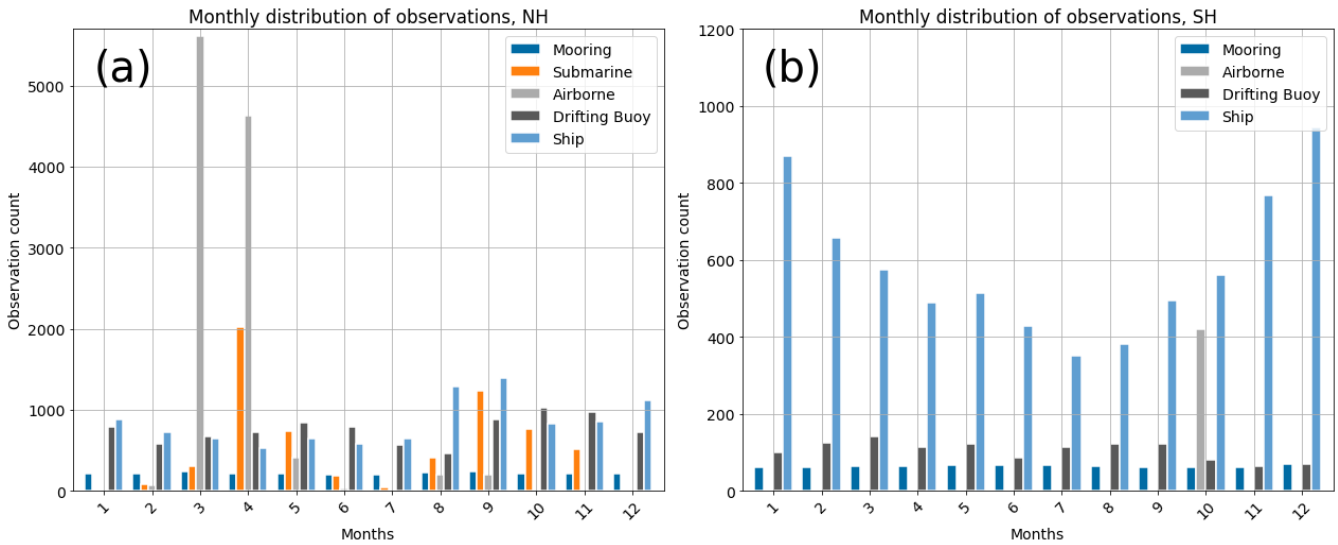


**Figure 5.** Seasonal distribution of reference data in CCI SIT RRDP; (a) NH and (b) SH categorised based on sensor type.

460 pole is located at the intersection of center cells. A temporal resolution of 30 days and a spatial resolution of 25 km for the Northern Hemisphere and 50 km for the Southern Hemisphere is used. Data obtained from stationary moorings, have only been temporally averaged, as these are fixed in space. The output data was subsequently temporally sorted and processed to fit into a standardized text format, as shown in Table 3. Since most campaigns only record some of the information in the standardized format, missing information was filled with NaN.

### 3.1 Pre-processing of reference data

465 All of the collected reference data underwent some degree of processing ~~procedures prior to using Ease-Grid 2.0~~prior to converting into the spatial and temporal scales for comparison with satellite-altimetry-derived composites. In most cases, the necessary pre-processing steps involved converting the date and coordinate formats to the desired output format and/or automatically extracting location and/or date information from the file header. ~~These pre-processing steps are~~, which are all considered standard procedures. Additionally, observations were filtered to exclude data points that potentially represent  
470 outliers. Specifically, measurements were removed if SIT exceeded 10m, SD exceeded 2m, SID exceeded 8m, FRB exceeded 2 m, or if any variable had values below 0 m. In addition, several reference data subsets needed additional pre-processing steps due to, e.g., incomplete information of time and/or position. As a result, a pre-processing (pp) flag is included in the final data file, indicating ~~if the file required supplementary~~whether the data required additional pre-processing steps, which could be associated with higher uncertainties. As the required level of additional pre-processing varies ~~the~~for the different types of  
475 reference measurements, an overview of the use of the pre-processing flag is ~~categorized into the following~~presented in Table 4. It should be noted that because the data are subsequently averaged into monthly means on a 25 km grid for the Northern Hemisphere (NH) and a 50km grid for the Southern Hemisphere (SH), temporal uncertainties of up to 24 hours are expected to have minimal impact. Discussions of temporal and spatial representativeness is presented in sections 4, 7.6 and 7.7. In the following sub-sections, specific major processing steps are further detailed.

#### 480 3.1.1 AEM-AWI

Files within AEM-AWI either contain measurements of total FRB or total thickness (in combination with SD for files in 2017 and 2019). It was therefore decided to split the final product into two files, one with all the measurements of total ice thickness and one with all measurements of total freeboard (see appendix in Olsen and Skourup (2024a) for a filewise overview).

### 3.2 Pre-processing of NPI

485 ~~Stationary mooring data from NPI is given a pp-flag of category 1, due to the raw data already being processed into monthly means by the data source (see Table 7). This means that no standard deviation or information about the number of measurements used for each average value is available from the dataset. However, an updated version of the data (Sumata, 2022) contains an estimate of the number of samples per observation given as in the order of  $10^4$  for data obtained with the ES300 instruments~~

**Table 3.** Description of reference data structure in CCI SIT RRDp.

<b>SIT, SD and FRB reference data files</b>										
<b>obsID</b>	Observation Identifier	<b>date</b>	Median of dates in gridcell	<b>lat</b>	Latitude of grid center	<b>lon</b>	Longitude of grid center			
<b>SD</b>	Median SD in gridcell	<b>SDstd</b>	Robust standard deviation of SD in gridcell	<b>SDIn</b>	Number of SDs in average	<b>SDunc</b>	Uncertainty of gridcell SD (*)			
<b>SIT</b>	Median SIT in gridcell	<b>SITstd</b>	Robust standard deviation of SIT in gridcell	<b>SITIn</b>	Number of SITs in average	<b>SITunc</b>	Uncertainty of gridcell SIT (*)			
<b>FRB</b>	Median FRB in gridcell	<b>FRBstd</b>	Robust standard deviation of FRB in gridcell	<b>FRBIn</b>	Number of FRBs in average	<b>FRBunc</b>	Uncertainty of gridcell FRB (*)			
<b>Tsur</b>	Median Surface temperature	<b>Tair</b>	Median Air temperature	<b>wSD</b>	Warren Snow Depth (**)	<b>w-rho</b>	Warren Snow Density (**)			
<b>pp-flag</b>	Pre-processing flag (*)	<b>unc-flag</b>	Uncertainty flag (*)	<b>QFT</b>	Temporal representativeness quality flag (***)	<b>QFS</b>	Spatial representativeness quality flag (***)			
<b>SID reference data files</b>										
<b>obsID</b>	Same as above	<b>date</b>	Same as above	<b>lat</b>	Same as above	<b>lon</b>	Same as above			
<b>SID</b>	Median SID in gridcell	<b>SIDstd</b>	Robust standard deviation of SID in gridcell	<b>SIDIn</b>	Number of SIDs in average	<b>SIDunc</b>	Uncertainty of gridcell SID (*)			
<b>wSD</b>	Same as above	<b>w-rho</b>	Same as above	<b>pp-flag</b>	Same as above	<b>unc-flag</b>	Same as above			
<b>QFT</b>	Same as above	<b>QFS</b>	Same as above							

(\*) see sec. 5 for a description of how uncertainties are determined for each campaign (\*\*\*) from Warren et al. (1999), (\*\*\*\*) see section 4

Information is available on SD+SIT (file A), position (file B), air temperature (file C), and ice surface temperature (file D), but the measurements do not coincide directly in time. Data is collocated to file A format using the smallest time difference.

2.

**Minor pre-processing:** Includes temporal approximations of up to 24 hours, along with additional calculations performed on raw data

IMB CRELL

If the difference in time between observations from the different files (A-D) exceeds 12 hours.

AEM-AWI required additional pre-processing due to missing time information, see data

Missing time of day information (several AEM-AWI files see an overview in Olsen and Skourup (2024a) for a file-wise overview. For files with missing time information, where the output date-time is given as the date plus an date + arbitrary time stamp of 00:00:00 of the respective day. These files are marked by a pp-flag of category 1-00.

SCICEX

Geographical coordinates (lat,lon) are found based on start and end positions + distance traveled by the submarine. No time of day is provided, only the date

(until Sep 2006) and in the order of  $10^6$  for data obtained with the IPS4/5 instruments. This information has been added to the CCI SIT RRD, but users should be aware that the number is an approximation.

## 3.2 Pre-processing of IMB-CRREL

IMB-CRREL data is structured so that it contains a mass balance file, a position file, a file with meteorological data and a file with ice temperature data. SD and SIT information is available from the mass balance file, coordinates from the position file, air temperature from the meteorological data file and ice surface temperature from the temperature data file. However, these files have different date arrays and do therefore not generally coincide in time, signifying that they cannot be automatically combined. To combine information from these files, a starting point is taken in the mass balance data, as this is the most important data for this study. Therefore, data from the other files are co-located to this by assigning data with the smallest time difference. As data does not overlap perfectly in time, a pp-flag of category 1 is given as default. If the time difference between the position data and the mass balance data is more than 12 hours for any value used in a grid point, then this grid point is given a pp-flag of category 2. IMB SD data is recorded as a change in snow depth compared to an initial measurement. However, some data lacks records of initial snow depth. This data is given a pp-flag of category 3 and should be used with care.

## 3.2 Pre-processing of ship measurements

### 3.1.1 Ship measurements

The IceWatch manual provides guidelines for [how to observe](#) [observing](#) SIT and SD from the ships. The standard procedure [for an ice watch is to make](#) [requires making](#) observations every hour while the ship is in motion. The ice is observed, depending on actual visibility conditions, up to a mile from the ship during a 10-minute observation period, which is usually performed on the bridge of the ship. [Recent instructions](#) ([https://aspectsouth.org/wp-content/uploads/2024/06/sea-ice-cards\\_LOGODOI.pdf](https://aspectsouth.org/wp-content/uploads/2024/06/sea-ice-cards_LOGODOI.pdf), [last accessed 2025-05-23](#)) reiterate that observations should be made every hour, and recorded on the hour. Observers are required to document the sea ice types/classes and estimate their area coverage within a 1 km radius of the ship, estimated from the radar display on the bridge of the ship. SIT estimates are made by visually assessing overturned sea ice viewed from the bridge referenced to a 55 cm diameter buoy on the side of the ship, or a ruler/stick sticking out. Rafted ice is included in the thickness estimate, whereas ridged ice is excluded. The same measurement methodology is applied for SD, which is differentiated from ice by color. The manual did not mention any specific validation approaches to ensure consistency or quality of the visual observations.

The aim is to classify up to three prevalent ice types/classes that combined cover the most area. Of these, the thickest is the *primary* ice type, and the thinnest is the *tertiary* ice type. The area of *primary*, *secondary*, and *tertiary* ice should sum to the total ice concentration (Hutchings et al., 2018).

Due to [this](#) [the](#) acquisition method, data from ASSIST and ASPeCt must undergo pre-processing to combine the observations of the individual ice types into one. The thickness and partial concentration of each ice type are used to make a weighted average of the mean sea ice thickness within the observed area (1 nautical mile  $\approx$  1.85 km according to Hutchings et al. (2018)). The

following formulas show the computation of such averaged sea ice thickness estimates:

$$\text{SIT}_{\text{EP}} = \frac{C_{\text{P}}}{C_{\text{tot}}} \cdot \text{SIT}_{\text{P}}, \quad (1)$$

$$\text{SIT}_{\text{ES}} = \frac{C_{\text{S}}}{C_{\text{tot}}} \cdot \text{SIT}_{\text{S}}, \quad (2)$$

525

$$\text{SIT}_{\text{ET}} = \frac{C_{\text{T}}}{C_{\text{tot}}} \cdot \text{SIT}_{\text{T}}, \quad (3)$$

$$\text{SIT} = \text{SIT}_{\text{EP}} + \text{SIT}_{\text{ES}} + \text{SIT}_{\text{ET}} \quad (4)$$

Here, P, S and T stand for *primary*, *secondary* and *tertiary*, respectively.  $C_{\text{tot}}$  is the total ice concentration, and  $C_{\text{P, S, or T}}$  denote  
530 the ice concentration of the particular ice type. The combined SD is derived using the same weighting principle.

Reference data is used if the sum of the partial concentration adds up to the total concentration and at least one of the partial concentrations belonging to SIT/SD is defined (e.g. is not NaN). ~~The calculation method only considers the average SIT/SD of areas covered by sea ice. Thus, the estimates do not take into account whether the ship is primarily surrounded by water or ice. This can bias the estimates towards higher sea ice thickness and snow depth when compared to satellite measurements since it is not weighted by information of open water coverage. However, as will be shown and discussed in Section 7, comparisons between ship-based reference data and satellite products tend to show the opposite trend, with higher values of satellite products than reference data from ships. If the total sea ice concentration is recorded as 0, the corresponding SIT and SD are also set to 0. Due to these processing steps, all ASSIST and ASPeCt observations are marked by a pp-flag of category 2.~~  
535

## 3.2 Pre-processing of submarine measurements

### 540 3.1.1 Submarine measurements

SCICEX submarine measurements are obtained over a long time span period (1960-2014). During this time period, the information provided in the data acquisition files ~~are not consistent~~ is not consistent, and post-processing of different parts of the data ~~have has~~ been treated by different institutions, which results in ~~reference observation~~ inconsistencies between different cruises. Nevertheless, as all SCICEX data are subject to some level of interpolation, due to a lack of continuous measurements  
545 of time and position, all the data is given pp-flags in categories ~~1 to 3~~ 2 or 3 (see Table 4).

Parts of the SCICEX data are known as the "analog subset" because it was derived from traces on paper rolls (SCICEX (2009, 2014), see General resources *Documentation for G01360 Analog Subset*). Each file in the analog subset contains sea ice drafts of one line segment and provides only the start and end coordinates, along with date information including the year, month and the segment of the month in which measurements were obtained, given as the first, second or third part of the month.  
550 We are using the following date-time conversion for converting the segment of the month into a date containing day and time:

- 1st third = Day 5 at 00:00:00
- 2nd third = Day 15 at 00:00:00
- 3rd third = Day 26 at 00:00:00

Other files within SCICEX provide a specific day of the month and for these, we use the specified day and an arbitrary time at  
555 00:00:00.

Spatial interpolation to obtain positions of each reference measurement is done using the inverse haversine formula from the Python package haversine 2.8.0 (released Feb 28 2023). Here the coordinates  $(\phi, \lambda)$  are calculated iteratively by using the provided distances  $(\delta d)$  between observations when available and the bearing  $(\theta)$  between ~~neighbouring~~ neighboring points. When these are not available, equal distance is assumed between subsequent measurements using the start and end positions.

### 560 3.2 Transformation into composites for comparison with satellites

The reference measurements were averaged to the Equal-Area Scalable Earth Grid in version 2 (EASE2) provided by the National Snow and Ice Data Center (NSIDC). For each gridcell, the median was used to compute the average value, accompanied by the corresponding robust standard deviation (see Eq. 5). The date assigned to each gridcell corresponds to the median date of all observations within that gridcell. EASE2 is based on a polar aspect spherical Lambert Azimuthal equal-area projection  
565 Brodzik et al. (2012) and the WGS-84 reference ellipsoid. The NH grid dimension is 5400 km x 5400 km with a spatial resolution of 25 km, resulting in a grid consisting of 432 x 432 grid cells, whereas the SH grid has a spatial resolution of 50 km, resulting in a grid consisting of 216 x 216 grid cells. The grid is centered on the geographic pole, meaning that the pole is located at the intersection of center cells. A temporal resolution of 30 days is used for both hemispheres. Data obtained from stationary moorings have only been temporally averaged, as these are fixed in space. The output data was subsequently sorted  
570 temporally and processed to fit a standardized text format, as shown in Table 3. Since most campaigns only record some of the information required by the standardized format, missing values were filed as NaNs.

$$\sigma_{\text{robust}} = 1.4826 \cdot \text{median}(|x_i - \text{median}(x)|) \quad (5)$$

## 4 Representativeness in space and time

We further flag ("quality-flag" or QF) data with temporal or spatial representativeness issues. This is achieved by separating the flag into two categories: a temporal representativeness flag (QFT) and a spatial representativeness flag (QFS), see Table  
575 5 for specifications. Spatial representativeness (QFS) is difficult to assess, particularly given the different nature of the reference measurements. To address this, the reference data are split into categories based on how they are measured. Airborne measurements (OIB, AEM-AWI and parts of the MOSAiC and Nansen Legacy) and submarine measurements (SCICEX) move above/below the ice and have a particular footprint size. Therefore, the number of observations within a grid cell scales with the area covered.

**Table 5.** Quality flags to deduce representativeness of the reference measurements. Note that QFT thresholds are based on the monthly temporal resolution produced within the RRDP, and would need to be updated for users that utilise a different spatial resolution when processing with this set-up.

<u>Abbreviation</u>	<u>Flag name</u>	<u>Flag value</u>	<u>Description</u>
<u>QFT</u>	<u>Quality Flag Temporal</u>	<u>0</u>	<u>Data within cell spans &gt; 15 days</u>
		<u>1</u>	<u>Data within grid cell spans 5 &lt; days &lt; 15</u>
		<u>2</u>	<u>Data within grid cell spans 1 &lt; days &lt; 5</u>
		<u>3</u>	<u>Data within grid cell spans &lt; 1 day</u>
<u>QFS</u>	<u>Quality Flag Spatial</u>	<u>0</u>	<u>Airborne: The number of observations in a cell is above Q3</u> <u>Moorings: Data in grid cell spans &gt; 15 days</u>
		<u>1</u>	<u>Airborne: The number of observations in a cell is between Q2 and Q3</u>
		<u>2</u>	<u>Airborne: The number of observations in a cell between Q1 and Q2</u> <u>Airborne: The number of observations in a cell is below Q1</u>
		<u>3</u>	<u>Moorings: Data in grid cell spans &lt; 15 days</u> <u>Buoys &amp; Ship: Data has known representativeness issues</u>

580 Due to the very different footprint sizes of particularly airborne and submarine measurements the spatial representativeness is  
estimated by the number of measurements within a grid cell. Four flag values are used based on the 25% (Q1), 50% (Q2) and  
75% (Q3) quartiles of the total number of observations across the dataset. These spatial flags provide a relative indication of  
the extent of area coverage compared to the overall data distribution. In contrast, buoys placed on the ice have an inherent issue  
with temporal representativeness due to their fixed location on the ice floe. Thus, by definition, these have limitations regarding  
585 high spatial representativeness. Similarly, ships navigating in ice tend to choose a route with thinner sea ice and therefore  
exhibit an inherent bias in terms of spatial representativeness. In contrast, moorings, although fixed in position beneath the sea  
ice, can achieve high spatial representativeness due to the drifting ice passing over them, provided that different ice masses  
drift across. As such, their spatial representativeness can be approximated by the number of days with measurements in a given  
month.

## 590 **5 Uncertainties of RRDP reference measurements**

All reference data in the CCI SIT RRDP are related with some degree of uncertainty,; however, except for OIB, they lack  
uncertainty information for individual data points. Instead, uncertainty quantification in the CCI SIT RRDP must rely on  
average errors, accuracies, or uncertainties reported in various studies. These sources are presented in Table 7 along with the  
estimated uncertainty. It is important to note that the amount of uncertainty information varies greatly among the datasets, ~~and~~  
595 ~~several~~. Several uncertainty estimates are based on assumptions (e.g., AEM-AWI), ~~instrument accuracy alone~~ rely solely on

instrument accuracy (e.g., IMB-CRREL), or are only valid within a certain range. Therefore, an uncertainty flag is introduced to indicate situations where the uncertainty may be underestimated, overestimated, based on assumptions, or potentially flawed. ~~Section~~ quantify the level of variability available in the uncertainty estimate (see Table 6). Whereas this flag serves as an indicator of the confidence we have in the uncertainty estimate it does not take into account issues regarding temporal and spatial representation errors. These are quantified in the quality flags described in Section 4 and examples of the impact of the flags are provided in Sections 7.6.

600

Section 5.2.2 provides a description of the uncertainty for each reference dataset, including whether and why an uncertainty flag has been assigned. As the assumptions linked to the uncertainty vary, the uncertainty flag is categorized as:-

1. ~~No uncertainty assumption, individual uncertainties are provided for each measurement~~
2. ~~Uncertainty measures have some degree of distinction based on e.g. thickness, time of year or likewise~~
3. ~~The same uncertainty is assumed for all data~~
4. ~~The same uncertainty is assumed for all data and this uncertainty is linked to incorrect assumptions~~

605

associated with each type of reference measurement, including the assigned uncertainty flag values. An overview of the uncertainty flags is presented in Table 6, and Table 7 lists the uncertainties and corresponding uncertainty flags for all datasets.

610

Another concern is the interchangeable use of terms such as error, uncertainty, and accuracy, despite their distinct statistical meanings. Error represents the absolute deviation between measured and true values, accuracy describes a closeness of the agreement between measured and true values ~~and is a qualitative term only~~, and uncertainty provides a quantification of the doubt of a measurement given as an estimate of the range within which the true value is expected to lie (Taylor, 1939; Bell, 1999). Therefore, while error is calculated based on a known true value, uncertainty is typically described by a confidence interval or standard uncertainty within which the true value is expected to fall. Uncertainty is a measure of the random error in a sample, whereas systematic error is referred to as bias or an offset (Bell, 1999). Based on these definitions, when a paper refers to an error indicated by a  $\pm$  value, it is here interpreted as an uncertainty.

615

## 5.1 Uncertainty propagation in average calculation

620

The propagation of uncertainties in the final CCI SIT RRDP product is based on the principles outlined in Taylor (1939). According to Taylor's theorem, if the uncertainties of the measurements  $x_1$  to  $x_n$  are independent and random, then the uncertainty of the mean is obtained by summing the individual uncertainties in quadrature and dividing by the square root of the number of measurements (N).

$$\delta\bar{x} = \frac{1}{N} \sqrt{\delta x_1^2 + \delta x_2^2 + \dots + \delta x_n^2}. \quad (6)$$

**Table 6.** Uncertainty flag describing the expected quality of the uncertainty estimate (level of variability and whether it seems reasonable). Does not take into account issues with representativeness. This is quantified by the quality flag (see tab 5)

<u>Abbreviation</u>	<u>Flag name</u>	<u>Flag value</u>	<u>Description</u>
<u>unc-flag</u>	<u>Uncertainty flag</u>	<u>0</u>	<u>No uncertainty assumption, individual uncertainties are provided for each measurement</u>
		<u>1</u>	<u>Uncertainty measures have some degree of distinction based on e.g. thickness, time of year or likewise</u>
		<u>2</u>	<u>The same uncertainty is assumed for all data within a given dataset</u>
		<u>3</u>	<u>The same uncertainty is assumed for all data within a given dataset and this uncertainty is expected to be too low</u>

625 The upper bound of the uncertainty is the ordinary sum of the measurement uncertainties:

$$\delta\bar{x} \leq \frac{1}{N}(\delta x_1 + \delta x_2 + \dots + \delta x_n) \quad (7)$$

In this study formula 5 is used for the propagation of uncertainties, hence, the uncertainties are assumed to be independent and random, as we do not have sufficient information to obtain full error covariance matrices. Nevertheless, this is not necessarily the case and it will result in some uncertainties being underestimated. The effect of this is largest for those campaigns where the number of observations per grid cell is large, which is particularly the case for the ULS observations, where several thousand measurements are averaged to obtain the final values in the CCI SIT RRDP. Therefore, we underline that it might be more appropriate to use the upper bound uncertainty in some cases, which is equivalent to the uncertainty estimates shown in Table 7. This is especially true for campaigns/data where we have the same uncertainty estimate for all input data, as is the case for the majority of the campaign data. Table 7 presents a summary of input uncertainty estimates for each campaign, along with a citation to the publication where the uncertainty estimate was originally sourced. In the following sections, we describe in more detail how the uncertainty estimates of each campaign are obtained and the underlying assumptions.

## 5.2 Original uncertainties of data

### 5.2.1 Airborne data

OIB data contain individual uncertainty estimates for FRB, SD and SIT measurements as the only data ~~sources~~ source included in the CCI SIT RRDP. These uncertainties are based on variations in the sea ice properties, instrument, and inter-campaign algorithm changes. ~~Therefore~~ As individual uncertainties are provided, OIB data ~~is~~ has been given an uncertainty flag of category 0.

**Table 7.** Uncertainties related to the products in CCI SIT RRDp.

**Campaign Averaging methodology Uncertainty estimates m Uncertainty source**

OIB (Altimetry) EASE-Grid 2.0 Individual uncertainties available Kurtz et al. (2016); Kurtz et al. (2015) AEM-AWI (AEM) EASE-Grid 2.0  $\pm 0.10$  (SIT);  $\pm 0.10$  (FRB) SIT; Haas et al. (2007); FRB: Jutila et al. (2022a) ASSIST (VO) EASE-Grid 2.0  $\pm 0.20$  Huttings et al. (2018) ASPeCt (VO) EASE-Grid 2.0 10-20% of actual thickness Worby et al. (2008a, 1999) IMB-CRREL (IMB) EASE-Grid 2.0  $\pm 0.01$ \*\*\*; Donald K. Perovich, Richter-Menge et al. (2006a) SB-AWI (SDB) EASE-Grid 2.0  $\pm 0.01$  Personal comm.; Nicolaus et al. (2021) BGEP (ULS) Temporal  $\pm 0.05$ -0.10 Krishfield and Proshutinsky (2006) AWI ULS (ULS) Temporal  $\pm 0.05$  (summer);  $\pm 0.12$  (winter)\*\*\* Behrendt et al. (2013a) TRANSDRIFT (ULS) Temporal  $\pm 0.05$  (ULS);  $\pm 0.96$  (ADCP) Belter et al. (2020), Belter et al. (2021) NPI-FS (ULS) Temporal

$\pm 2.7E-03$  (1990-1991), 1.9E-03 (1991-2003), 1.3E-03 (2003-2006), 0.088E-03 (2007-2018) \* Sumata (2022), supplementary materials table 3 NPEO (ULS) Temporal  $\pm 0.05$  Morison et al. (2016)\*\*\*; SCICEX (ULS) EASE-Grid 2.0 Bias:  $\pm 0.29$ , Unc:  $\pm 0.5$ \*\*\*; Rothrock and Wenshanan (2007); NSIDC (1998, 2006)

Campaign	Averaging methodology	Uncertainty estimates [m]	Uncertainty source	Uncertainty flag
OIB (Altimetry)	EASE-Grid 2.0	Individual uncertainties available	Kurtz et al. (2016); Kurtz et al. (2015)	0
AEM-AWI (AEM)	EASE-Grid 2.0	$\pm 0.10$ (SIT), $\pm 0.10$ (FRB), $\pm 0.10$ (SD)	SIT: Haas et al. (2007), SD: provided in data FRB: Jutila et al. (2022a)	2 for SIT $\leq 3m$ 3 for SIT $> 3m$
MOSAIC-HEM (AEM)	EASE-Grid 2.0	$\pm 0.10$ (SIT)	Haas et al. (2007)	2 for SIT $\leq 3m$ 3 for SIT $> 3m$
Nansen_legacy (AEM)	EASE-Grid 2.0	$\pm 0.10$ (SIT)	Haas et al. (2007)	2 for SIT $\leq 3m$ 3 for SIT $> 3m$
ASSIST (VO)	EASE-Grid 2.0	10-20% of actual thickness	Worby et al. (2008a, 1999)	1
ASPeCt (VO)	EASE-Grid 2.0	10-20% of actual thickness	Worby et al. (2008a, 1999)	1
IMB-CRREL (IMB)	EASE-Grid 2.0	$\pm 0.01$ ****	Perovich et al. (2022) Richter-Menge et al. (2006a)	3
MOSAIC-SIMBA (IMB)	EASE-Grid 2.0	$\pm 0.02$	Lei et al. (2021)	3
SB-AWI (SDB)	EASE-Grid 2.0	$\pm 0.01$	Personal comm.; Nicolaus et al. (2021)	3
Nansen_legacy (ULS)	Temporal	NaN	No source	3
BGEP (ULS)	Temporal	$\pm 0.05$ -0.10	Krishfield and Proshutinsky (2006)	2
AWI-ULS (ULS)	Temporal	$\pm 0.05$ (summer), $\pm 0.12$ (winter)**	Behrendt et al. (2013a)	1; 3 for 206-4 and 227-3 files
TRANSDRIFT (ULS)	Temporal	$\pm 0.05$ (ULS), $\pm 0.96$ (ADCP)	Belter et al. (2020), Belter et al. (2021)	2
NPI-FS (ULS)	Temporal	$\pm 2.7E-03$ (1990-1991), 1.9E-03 (1991-2003), * 1.3E-03 (2003-2006), 0.088E-03 (2007-2018)	Sumata (2022), supplementary materials table 3	1
NPEO (ULS)	Temporal	$\pm 0.05$	Morison et al. (2016)*****	2 for SID $\leq 2$ , 3 for SID $> 2$
SCICEX (ULS)	EASE-Grid 2.0	Bias: $\pm 0.29$ , Unc: $\pm 0.5$ **	Rothrock and Wenshanan (2007); NSIDC (1998, 2006)	2

VO: Visual Observation

\*: Uncertainty of the monthly means Supplementary materials table 3

\*\*; uncertainty based on 2-std

\*\*\*: default: line correction for sound speed model;  $\pm 0.23$

\*\*\*\*: 0.01 m accuracy in usual conditions 0.02 m if it is very cold the sensors do not work well during the melting season

\*\*\*\*\*: uncertainty estimate available from metadata

A detailed overview of how uncertainties are calculated is presented in Kurtz et al. (2013). A central concern by this approach is the substantial variation in both the magnitude and interannual variability of snow depths among different OIB-derived datasets see Section 2.1.2. In particular the OIB QLs are prone to bias -4.5 to -6.7 cm low depending on sea ice type and settings (i.e. deformed vs level) (Kwok et al., 2017; King et al., 2015; Petty et al., 2023). These magnitudes might exceed the uncertainties provided in the OIB data products which complicates our efforts in establishing a consistent uncertainty estimate based on the uncertainties provided in the products.

The uncertainty of AEM/HEM (AEM-AWI, MOSAiC and Nansen Legacy) measurements depends on the SIT. For a single helicopter-borne EM measurement, the uncertainty is sea ice conditions i.e., whether the ice is level or deformed, as described in Section 2.1.3. For airborne EM measurement we here adopt a constant uncertainty of  $\pm 0.1$  m over level ice. However, since this uncertainty is inaccurate for deformed ice, as deformed ice thickness can be strongly underestimated due to the footprint of EM measurements over those 3D structures, and due to e.g., air pockets between the ice floes that have been pushed together (Haas et al., 2009; Mahoney et al., 2015). However, and, to our knowledge, no uncertainty quantification for thicker sea ice has been made and therefore has been estimated for it, further analysis is needed. Here, we introduce an uncertainty flag of category 3 for average sea ice thicknesses of more greater than 3 m are given an uncertainty flag of category, while sea ice thinner than 3, whereas sea ice m is assigned a category 2 uncertainty flag. In principle, level ice can exceed 3 m, and deformed first-year ice can be thinner than 3 m are given an uncertainty flag of category 2. Measurements of total FRB are related with. Therefore, using this threshold may introduce some erroneous assumptions affecting the results. However, since we lack detailed information whether the ice is level or deformed, this represents a first approach to flag the data based on these parameters. The total FRB measurements are related to an overall uncertainty of  $\pm 0.1$  m (Haas et al., 2007) and are given an uncertainty flag of category 2. Snow depth measurements are also linked to a fixed uncertainty of  $\pm 0.1$  m, which is provided in the input data.

## 5.2.2 Stationary moorings

Although individual moorings have their own uncertainty estimates, the cause of uncertainty for observations obtained by similar measurands tend tends to be similar. Raw ULS measurements can be linked to significant biases caused by measuring the first return that comes from the ice closest to the sonar, which can cause draft values for deformed ice to be overestimated. They are also prone to uncertainties linked to, e.g. corrections for variations in local atmospheric pressure, instrument tilts, and variations in the speed of sound in the water column (BGEP, 2003). However, all mooring data used in this validation study has have undergone some level of correction to decrease the uncertainties and biases.

BGEP, TRANSDRIFT, and NPI and TRANSDRIFT data have undergone significant processing, resulting in no expected bias and an uncertainty in the range of  $\pm 5$ – $10$  cm for BGEP, and  $\pm 5$  cm for ULS data from TRANSDRIFT.

As previously mentioned NPI data was already processed into monthly means and therefore the uncertainty used in this dataset is based on the uncertainties of the monthly mean sea ice thickness product, which was created based on the monthly mean sea ice drafts see (Sumata, 2022), see Sumata (2022). In the supplementary materials of this publication (table Table 3) are listed four categories of uncertainties based on a mix of instrument type (ES300 or IPS4/5) and on the year. The uncertainties

vary between  $\pm 2.7\text{E-}03$  and  $\pm 0.088\text{E-}03$ . ~~For raw NPI data the uncertainty is expected to be between  $\pm 10$  cm for NPI data based on ice profiling sonars (IPS4/5 (from 2006)) and  $\pm 20$  cm based on upward looking sonar (ES300) Hansen et al. (2013) -As NPI uncertainty estimates contain some level of variation based on sensor type and age of instrument, an uncertainty flag of 1 is assigned.~~ Upward-looking ADCP data from TRANSDRIFT has a significantly larger uncertainty of  $\pm 96$  cm, which is  
680 a consequence of ADCP's general instrument setup being designed to measure velocity fields within the water column rather than to derive sea ice draft (Belter et al., 2021). NPEO has also undergone corrections resulting in an estimated uncertainty of  $\pm 5$  cm for level and gently undulating ice, but no additional correction has been made to correct for the first return. Therefore, sea ice drafts for ~~rough deformed~~ sea ice may tend to be biased high. To account for this, data points with an average sea ice draft of more than 2 meters are given an uncertainty flag of category ~~3, as thicker ice tends to be rougher (Tucker et al., 1992)~~  
685 ~~-3. SID from ADCP's from the Nansen Legacy has no quantified uncertainty. Furthermore, the provided uncertainty for the TRANSDRIFT ADCP's cannot be used, as a major contributor to the TRANSDRIFT ADCP's uncertainty is the lack of reliable measurements of pressure, which is not the case for Nansen Legacy ADCP's. Due to this, the Nansen Legacy SID measurements are given an uncertainty of NaN and an uncertainty flag of 3.~~

The mooring data for the ~~Antarctic SH~~ from the AWI-ULS dataset ~~has have~~ undergone varying levels of processing, and the  
690 estimated uncertainty depends on both the time of the year and the applied corrections. Based on Behrendt et al. (2013a), drafts corrected by zero-line correction have an estimated uncertainty of  $\pm 5$  cm in summer (~~November to May~~) and  $\pm 12$  cm in winter (~~June to October~~). When using the sound-speed model instead of zero-line correction, the estimated uncertainty is  $\pm 23$  cm. Here we decide to use the zero-line correction result when available, as Behrendt et al. (2013a) found only a few cases where the sound-speed model performed better than the zero-line correction. SID data from moorings 206-4 and 227-3 are given an  
695 uncertainty flag of category 3, as Behrendt et al. (2013a) states that these moorings have problems with the pressure sensor, signifying that they have undergone a simpler and likely less accurate correction. ~~This is especially visible in the data for mooring 206-4, where some SID values in the final product have a standard deviation of more than 10 m. This data should therefore be used with care.~~

Behrendt et al. (2013a) also find significant biases for AWI-ULS drafts, as the measured drafts are consistently overestimated,  
700 except when measuring on completely level ice. The bias depends on the draft depth and ice type, with MYI summer having smaller biases of around 30 cm, whereas FYI winter has the largest biases, ranging from 42 cm for ULS depth of up to 100 cm and 68 cm for ULS depth up to 180 cm. However, these biases were computed for the Arctic, and since sea ice in the Antarctic is generally younger and thinner due to e.g., differences in ocean heat flux and thermal insulation by a thicker snow cover in the Antarctic (Maksym et al., 2012; Haas, 2016), they may not be accurate. ~~Nevertheless, by the lack of more certain estimates, the biases presented in Behrendt et al. (2013a) (their Table 4) are used to correct the AWI-ULS SID measurements, however a dataset is also provided without the added bias correction. As the majority of Antarctic sea ice melts during summer (Haas, 2016), it is assumed here that all Antarctic sea ice is FYI, although this is not exclusively the case with especially the Weddell Sea having a larger extent of MYI (Wang et al., 2023).~~

### 5.2.3 Drifting buoys

710 IMB-CRREL drifting buoys lack information regarding the uncertainty of the data after processing. However, information about the estimated accuracy of the acoustic rangefinder sounders, used for the measurements, is provided. Therefore, this information is utilized as the uncertainty for each measurement. According to Richter-Menge et al. (2006a), the acoustic rangefinder sounders, which are located above and below the ice surface, have an accuracy of 5 mm, resulting in a combined uncertainty of 0.01 m, when summed. However, this value is likely underestimated when compared to satellite measurements,  
715 as IMB-CRREL buoys provide localized data. Although the standard deviation of the final measurements in CCI SIT RRDP accounts for some variability, each buoy is positioned and follows its own drifting ice floe, and thus the impact of the overall variability of the ice in the area is expected to be largely unaccounted for, unless an array of buoys have been deployed which are representative of the ice on the satellite scales. Additionally, no specific uncertainty for SD versus SIT is provided, resulting in the acoustic rangefinder sounders' accuracy being used as the uncertainty for both SD and SIT. Lastly, the initial  
720 SD measurement is expected to be one of the major sources of uncertainty, but no estimate of this uncertainty is available. Due to these concerns, the uncertainty estimates of IMB-CRREL are assigned an uncertainty flag of category 3. SIMBA drifting buoys have recorded an overall uncertainty of 0.02m for both the snow depth and the ice thickness. As both IMB-CRREL and SIMBA consist of IMB's this uncertainty could be an alternative to the uncertainty of 0.01m. Nevertheless, neither of the uncertainties take into account issues of representativeness, which are instead addressed by the use of quality flags (see section  
725 4).

Uncertainty measurements are also not provided for SB-AWI. However, a study by Nicolaus and Katlein (2017) mentions that the largest source of uncertainty originates from the initial snow depth measurement, which remains unquantified. The sensor uncertainty is reported to be on a millimeter scale, with each of the four sensors linked to the snow depth buoy having an uncertainty of 1 mm according to information from Meereisportalen (<https://www.meereisportal.de/en/>, last accessed on  
730 May 2, 2024). Lee et al. (2015) investigated the uncertainty of SD measurements performed with ultrasonic sensors and found that each of the three different ultrasonic sensors had an uncertainty in the range of 0.0187 to 0.0217 m. However, this study was conducted on terrestrial snow, and none of the sensors used were consistent with the one used for SB-AWI. Nevertheless, an uncertainty of 0.02 m is utilized here, as it is considered more realistic than the alternative of 1 mm. In Lee et al. (2015), a comparison to manual snow depth measurements was also performed, revealing biases between 0.005 m and 0.1 m.

735 Consequently, the uncertainty estimate is based on several assumptions and does not account for time, space, or thickness variability. Therefore, SB-AWI is assigned an uncertainty flag of category 3.

### 5.2.4 Ship data

The data acquisition of ship observations from NH (collected in ASSIST) and SH (collected in ASPeCt) follow the same guidelines. Nevertheless, the uncertainty of the visual observations is-are not recorded as being the same. For ASSIST, the only  
740 information about uncertainty provided is the expected precision of the visual observations. The precision of estimating snow depth is not explicitly stated, but as the method for observing SIT and SD is the same, it is expected that the uncertainties will

range close to the same intervals. Based on Hutchings et al. (2018), the precision of this estimate is 0.2 m for an experienced observer. ASPeCt ~~denote~~ denotes that the error, when compared to drilled measurements, depends on the thickness of the ice floe (Worby et al., 2008a). For sea ice <0.1 m thick, the estimated error is  $\pm 50\%$ ; for ice between 0.1 and 0.3 m, the error is  $\pm 30\%$ ; and for level ice >0.30 m, the error is  $\pm 20\%$ . Here, it is also stated that similar error estimates apply to snow of the same thickness. As these estimates provide a quantified uncertainty estimate, and as the data acquisition method for ASSIST and ASPeCt is the same, it is decided to use the uncertainty measures from (Worby et al., 2008a) for both. These uncertainty estimates provide some degree of variation due to the sea ice thickness dependency. Therefore, ASSIST and ASPeCt are given an uncertainty flag of category 1. However, we acknowledge that this does not take into account human error, such as the use of a non experienced observer.

### 5.2.5 Submarine data

Bias and standard deviation of SCICEX submarine data are based on a paper by Rothrock and Wensnahan (2007) addressing the accuracy of US NAVY submarine measurements, which are a part of the SCICEX data, using all available data from 1975 to 2000. The combined estimated bias is +0.29 m when compared to the reference obtained from ice drillings, and the combined standard deviation among submarine measurements due to seven error sources is 0.25 m (see Rothrock and Wensnahan (2007) for further information). To convert this into a 95 % confidence interval, an uncertainty of twice the standard deviation is used, giving a  $\pm 0.50$  m uncertainty for each data point. Furthermore, the 0.29 m bias is subtracted. As the uncertainty is assumed to be the same for all data points, SCICEX data is given an uncertainty flag of category 2.

## 6 Satellite Validation and inter-comparison with satellite SIT CDRs as an example

To illustrate the use of the CCI SIT RRDp reference measurements, the data has been collocated with CCI SIT CDRs v3.0 from CryoSat-2 and Envisat for both NH and SH. The satellite datasets are available from the ESA CCI open data portal (last accessed on August 8, 2024):

- CryoSat-2 (NH): <https://catalogue.ceda.ac.uk/uuid/c6504378f78c4ecd9f839b0434023eff>
- CryoSat-2 (SH): <https://catalogue.ceda.ac.uk/uuid/861ad3c7f3a34ebd8be6f618a92bd8e3>
- Envisat (NH): <https://catalogue.ceda.ac.uk/uuid/92eb2ba942074bec804af6a8b5436bee>
- Envisat (SH): <https://catalogue.ceda.ac.uk/uuid/af96a1ec493f49caa39dc912d15f2b17>

CryoSat-2 in the CCI CDR data set is available from 2010–2021 for both NH and SH, with 2010 having only data from November, December and the following years having data from October through April in the NH, and for all months in the SH. Envisat data is available from 2002–2012 for similar months as CryoSat-2.

## 770 6.1 Algorithm description

The method for extracting sea ice freeboard and thickness from radar altimetry data follows work of Laxon et al. (2003) and Tilling et al. (2018), where some of the key steps include distinguishing the sea ice (floes) and sea surface (leads) radar echoes, correcting for slower wave propagation speed, and calculating the sea ice thickness assuming hydrostatic equilibrium. To derive sea ice elevation estimates (and freeboards), one needs a dataset containing radar echo waveforms for range retrieval and other relevant variables such as altitude, atmospheric and geophysical corrections, in addition to auxiliary data of mean sea surface height, sea ice type, SD, snow density and sea ice density. The CCI CryoSat-2 sea ice processing uses the Baseline D Level 1b SAR and SARIn orbit data files from November 2010 until April 2021. For Envisat, the version 3.0 of the Envisat SGDR (Sensor and Geophysical Data Record) data has been used. The auxiliary data common to both Arctic and Antarctic sea ice processing contain the DTU21 mean sea surface product (Andersen et al., 2023) and the Copernicus Climate Change Service (C3S) CDR for sea ice concentration. For sea ice type in the Arctic, the C3S CDR is used, and for the Antarctic, the ice is considered to be of a single type, i.e. FYI. Snow is handled for the Arctic by using the merged monthly Warren et al. (1999)-AMSR2 snow depth climatology interpolated to daily values (more in Paul et al., 2021) with the snow density modifications suggested by Mallett et al. (2020). In the SH, a revised version of the approach described by Cavalieri et al. (2014) are is used. Here, the daily estimated AMSR-E/2 snow depths are averaged for each calendar day of the year to form a daily climatology used together with a fixed climatological value for snow density (Paul et al., 2021).

For CryoSat-2, the sea ice freeboard and thickness processing is done conventionally, classifying the surface type with multi-parameter approach (using the following waveform parameters: backscatter, leading edge width and pulse peakiness), and using the Threshold First Maximum Retracker Algorithm (TFMRA) with a 50% threshold from the first maximum peak power for range retrieval (find more details in Paul et al., 2021). To achieve a consistent time-series accounting for the different types CryoSat-2 and Envisat radar altimeters, the CCI SIT CDR v3.0 Envisat product makes use of orbit crossovers and orbital overlap during coincident mission periods with CryoSat-2 during winter months between October 2010 and March 2012. This data is used to retrieve optimal retracker parameters for calibration of Envisat, while using CryoSat-2 freeboard estimates as a reference which is applied to the full Envisat period (Paul et al., 2021, 2022). The satellite data is available in two formats; a L3 gridded product and a L2 trajectory product. Here, the L2-trajectory product was used to ensure that the spatial overlap between satellite and reference data was as close as possible. The L2 product consist of daily satellite trajectories and contain information including radar freeboard, sea ice freeboard (radar freeboard corrected for the slower radar wave propagation speed in snow), sea ice thickness and auxiliary snow depth with related uncertainties.

In addition, radar freeboards from ERS-1/2 are available within the ESA FDR4ALT project (Bocquet et al., 2023) in a gridded format for both NH and SH. As the ERS-1/2 products only include radar freeboards in its current form with no additional information of snow depth, snow and ice densities nor sea ice types, which are needed in the radar-freeboard-to-sea-ice freeboard and sea-ice-freeboard-to-sea-ice-thickness conversions, we only use the FDR4ALT dataset to demonstrate the availability of overlapping satellite and reference measurements during the ERS-1/2 satellite period. We note, that FDR4ALT also provides freeboards from Envisat and CryoSat-2 having, through an application of neural-networks, aimed to account for

inter-satellite-mission biases caused by different acquisition modes (Bocquet et al., 2023) and thus provides a full time-series  
805 ranging back to 1994 of radar freeboards.

## 7 ~~Comparability and collocation of RRDP and CDR~~

### 6.1 Comparability and collocation of RRDP and CDR

It is imperative to ensure that we compare the same measurand of the reference measurements within the CCI SIT RRDP and the satellite altimetry derived CCI SIT CDR. From a metrological approach, the aim is to ensure that the reference measurement  
810 and the measurand of the satellite product, whether being the total FRB, sea ice FRB, SIT, SID or SD, are comparable (Da Silva et al., 2023). Here, we aim to ensure this by, in most cases, keeping the reference measurand in its most original form and adapting the CCI SIT CDR measurand accordingly. As an example, when we compare the CCI SIT CDR with SID from ULS, we convert the satellite-derived SIT into SID by subtracting the sea ice FRB from SIT, as the ULS does not provide any information about the ice above the local sea level, following:

$$815 \text{SID}_{\text{CDR}} = \text{SIT}_{\text{CDR}} - \text{FRB}_{\text{CDR, sea ice}} \quad (8)$$

In addition, for NH OIB, we have coincident reference measurements of total FBR and SD, thus we compare the OIB derived sea ice FRB by subtracting the measured SD from the total FRB directly with the satellite derived sea ice freeboard, provided in the CCI SIT CDR, following:

$$\text{FRB}_{\text{OIB NH, sea ice}} = \text{FRB}_{\text{OIB NH, total}} - \text{SD}_{\text{OIB NH}} \quad (9)$$

820 Additionally, we compare the OIB SD directly with the auxiliary SD product in the satellite CCI SIT CDR. By using this approach, we avoid introducing additional auxiliary products (e.g., snow depths) which is not already used, and reduce errors from introducing new products. For SH OIB, we do not have any SD measurements and the same is the case for FRB measurements from AEM-AWI. Therefore, the comparison is made by adding the auxiliary SD to the satellite derived sea ice freeboard in the CCI SIT CDR, following:

$$825 \text{FRB}_{\text{CDR, total}} = \text{FRB}_{\text{CDR, sea ice}} + \text{SD}_{\text{CDR}} \quad (10)$$

Similarly, the SIT measured by AEM-AWI is the total thickness (snow + ice). Hence, to compare this measurand to the satellite observations, we add the auxiliary SD product in the satellite CCI SIT CDR to the SIT in the CCI SIT CDR, following:

$$\text{SIT}_{\text{CDR, AEM-AWI}} = \text{SIT}_{\text{CDR}} + \text{SD}_{\text{CDR}} \quad (11)$$

Collocation is performed by finding all satellite data points obtained within  $\pm 15$  days from the date of the reference data,  
830 and within the 25 km (50 km for SH) grid cell of the reference coordinates. The ~~average (arithmetic mean~~ median (arithmetic median) of these satellite points are subsequently allocated to the reference data.

## 7 Results and discussions

We present the comparison between CCI SIT RRDP and CDRs for each of the NH and SH sea ice variables (FRB, SIT, SID and SD) in Fig. 6–9, with the location of SH CryoSat-2 and Envisat collocated observations in Fig. 10a. The ~~figure visualizes figures~~ ~~visualize~~ the geographical distribution of the CCI SIT RRDP reference measurements collocated to CCI SIT CDRs of CryoSat-2 and Envisat, respectively, together with associated scatterplots and histograms. Linear best fits are added to the scatter plots for both individual campaigns and for the combined data available for each sea ice variable. Linear fits are obtained by using an Orthogonal Distance Regression (ODR), which involves calculating the orthogonal distance of the points with respect to a linear fit and allows taking into account the errors in measurements for both independent and dependent variables (Boggs and Rogers, 1990). Hereby, the linear fits are weighted by the individual uncertainties in both the CCI SIT CDRs and the CCI SIT RRDP. The pearson correlation coefficient (R) of each fit are shown in the scatter plots and additional statistical information can be found in Tables B1 (CryoSat-2) and B2 (Envisat) in Appendix B. Histograms show the distribution of reference measurements in blue and collocated CryoSat-2 or Envisat in orange with red and black vertical lines indicating the mean of satellite and reference data, respectively. For SIT and SID a bin size of 10 cm is used, whereas 3 cm is used for SD and FRB. Data from the SH is marked by a black outline around the histogram bins. The geographical representation of both the SH sea ice variables collocated to CCI SIT CDRs of CryoSat-2 and Envisat and the NH and SH sea ice variables collocated to FDR4ALT dataset of ERS-1/2, is highly limited. Therefore, only the data locations from the variables are presented in Fig. 10; ~~and the statistics of CryoSat-2/Envisat comparisons with reference observations are provided in Fig. 6-9.~~ As the ERS-1/2 product only included radar freeboard at the time that this research was conducted, there has not been made any comparisons with scatter plots and histograms.

~~SD satellite and reference observation comparison for CryoSat-2 (a-e) and Envisat (d-f). Maps of overlap data are shown for NH in (a,d), associated scatterplots with uncertainty weighted linear fits and associated correlation coefficients in the legend in (b,e) and histograms in (c,f). In the histograms the reference observations and satellite CDRs are marked with blue and orange, respectively, with associated average as black and red vertical lines. A black outline around the histogram bins are added to data from the SH~~

When examining Fig. 6–9, it is important to note that the main objective of this paper is not to conduct an inter-comparison study but rather to present the applications of the CCI SIT RRDP. Therefore, we focus on demonstrating how the database can be utilized to validate satellite products by highlighting the advantages and limitations of the different types of reference observations. Furthermore, we discuss the availability of reference measurements for validating the four primary variables (FRB, SIT, SID and SD) for CryoSat-2, Envisat and ERS-1/2, respectively.

### 7.1 Freeboards (FRB)

The amount of reference observations for freeboard validation are limited to airborne campaign data, which is primarily collected in March/April in NH ([See Section 2.1](#), Fig. 5a). Nevertheless, the airborne reference data show a good geographic representation in the western Arctic i.e., the Beaufort Sea, the Canadian Archipelago, as well as the Lincoln and Wandel

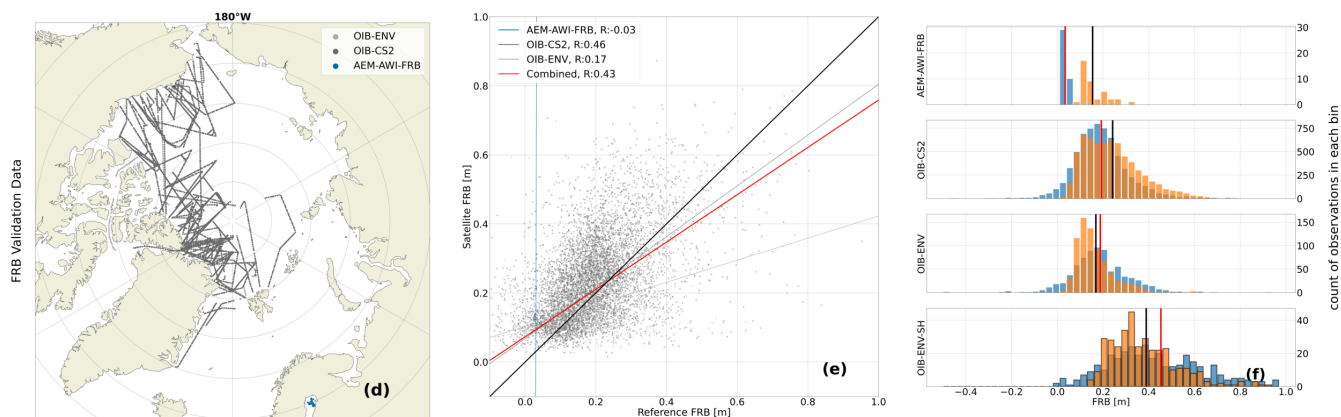


**Figure 6.** FRB satellite and reference observation comparison for CryoSat-2 (CS2) and Envisat (ENV) combined. The campaign names are followed by the satellite abbreviation, to highlight which satellite the reference data has been collocated to. (a) map of available overlap data for NH, (b) scatterplot with NH data with uncertainty weighted linear fits and associated correlation coefficients in the legend and (c) histograms with the reference observations and satellite CDRs marked with blue and orange, respectively, with associated average as red and black vertical lines. A black outline around the histogram bins are added to data from the SH.

865 Seas north of Greenland, and to a less degree the Fram Strait with CryoSat-2 and a reasonable overlap with Envisat (Fig. 6). However, no data is available from eastern Arctic including the East Siberian, Laptev, Kara and Barents Seas due to logistical challenges operating in these regions. For the SH, FRB measurements are currently limited to OIB campaign data from October 2009 and 2010 (See Section 2.1, Fig. 5b) collected in the Weddell, Bellingshausen and Amundsen Seas (Fig. 10a). Thus, no FRB reference data is available for CryoSat-2 in SH. ~~The FRB reference measurements, in particular those measuring the sea ice FRB, such as OIB NH, are in principle directly comparable to the sea ice FRBs from the satellite altimeter measurements. They can be used to directly evaluate the penetration depth by the radar signal and errors introduced by the reduced radar propagation speed in the snow (Section 1), assuming proper considerations regarding snow depth estimates from conversion of radar FRB to sea ice FRB, and from total FRB to sea ice FRB has been accounted for.~~ The associated histograms in Fig. 6c show similar distributions for NH OIB and CryoSat-2 FRB with ~~only -0.02~~ -0.03 m mean difference (Table B1). Envisat is over-represented in thin sea ice thicknesses (FRB < 0.20 m NH) and has, in general, a narrower distribution when compared to OIB FRB in NH, which is not reflected in the mean difference of ~~0.03~~ 0.02 m (Table B2).

Reference data from AEM-AWI NH and OIB SH presents total FRB. Therefore, they are compared to the collocated satellite-derived sea ice FRB plus SD from the auxiliary snow depth information as provided in the CCI SIT CDR (Section 6.1) using Equation 10. AEM-AWI FRB only includes data from the Baltic Sea, which is reflected in the low total FRB heights (< 0.3 m) representative for FYI. The limited geographical extent and the limited data amount of the AEM-AWI total FRB is expected to be one of the causes of the negative correlation coefficient ( ~~$R = -0.41$~~   $R = -0.03$ ) as seen in Fig. 6b. Additionally, we do not know how well Envisat performs in the Baltic Sea, which is an area with only FYI and confined by land with many small Islands, which may impact the relatively large footprint size of Envisat. The over-representation of Envisat total FRB

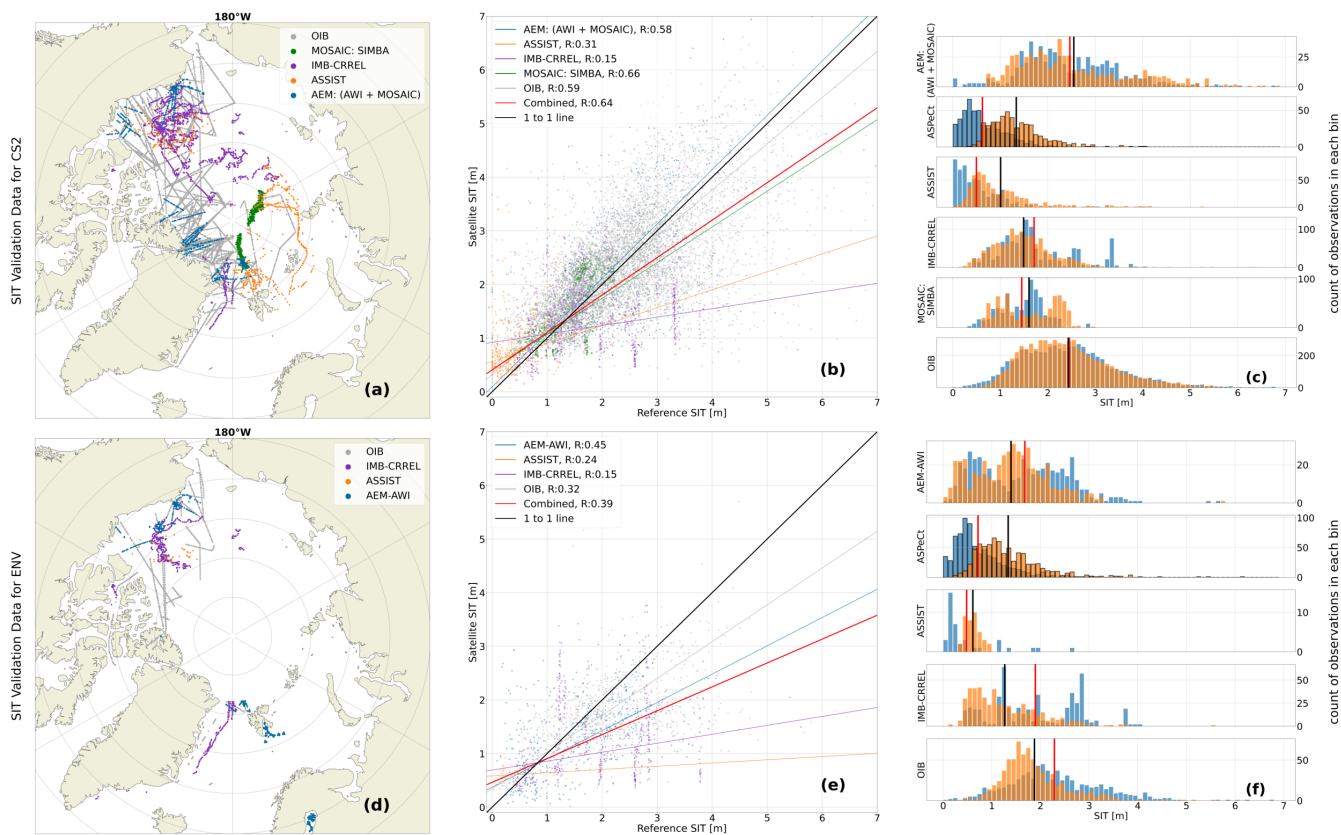


**Figure 7.** SIT satellite and reference observation comparison for CryoSat-2 (a-c) and Envisat (d-f). Maps of overlap data are shown for NH in (a,d), associated scatterplots with uncertainty weighted linear fits and associated correlation coefficients in the legend in (b,e) and histograms in (c,f). In the histograms the reference observations and satellite CDRs are marked with blue and orange, respectively, with associated average as black and red vertical lines. A black outline around the histogram bins are added to data from the SH

for thinner ice is also present in the SH when compared to OIB. The over-estimation of thin sea ice and a more narrow distribution is presumed to be a consequence of the different footprints of Envisat and CryoSat-2, and not caused by the reference measurements.

## 7.2 Thicknesses (SIT)

The amount of NH SIT reference measurements are more substantial than is the case for FRB and include observations from airborne campaigns, ships, and ice mass balance buoys, which complement each other in terms of spatial and temporal coverage. For CryoSat-2 (Fig. 7a) reference measurements are well covered in the western Arctic region and also include some reference measurements in the eastern Arctic north of  $80^{\circ}\text{N}$ . However, most of the reference measurements in the eastern Arctic is-are based on visual ship observations. The reference measurements overlapping with Envisat are sparse and limited to

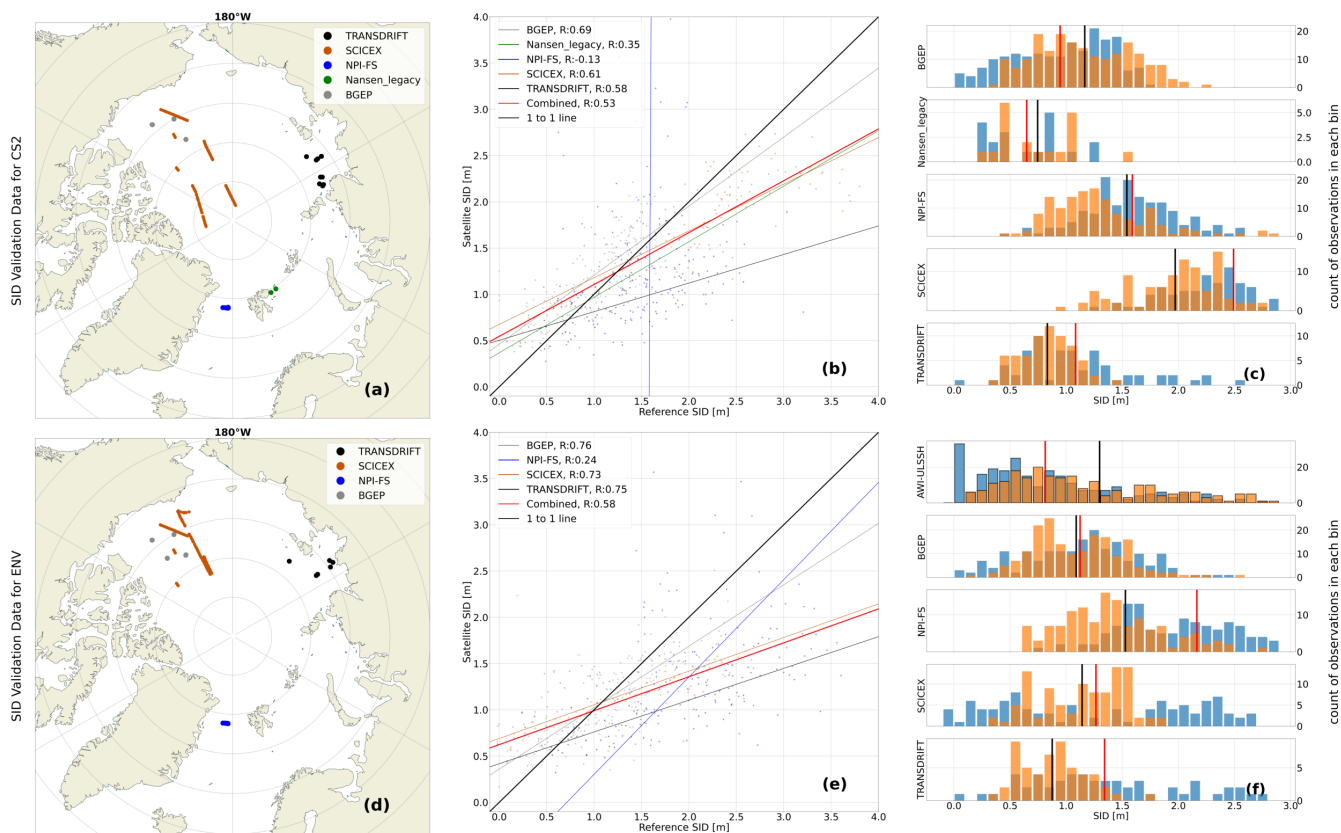


**Figure 8.** SID satellite and reference observation comparison for CryoSat-2 (a-c) and Envisat (d-f). Maps of overlap data are shown for NH in (a,d), associated scatterplots with uncertainty weighted linear fits and associated correlation coefficients in the legend in (b,e) and histograms in (c,f). In the histograms the reference observations and satellite CDRs are marked with blue and orange, respectively, with associated average as black and red vertical lines. A black outline around the histogram bins are added to data from the SH

few drifting buoys and airborne campaigns in Beaufort Sea and Fram Strait (Fig. 7d). SIT reference measurements to compare with ERS-1/2 are limited to some AEM-AWI airborne observations around Svalbard in the NH (Fig. 10b). In SH, SIT reference data is limited to visual ship observations from ASPeCt (Fig. 10a and 10c).

A reasonable overlap is found between the distribution of IMB and CryoSat-2 SIT (Fig. 7c) with an overall bias of 0.23 a mean difference of 0.22 m, where IMB SIT is thicker than CryoSat-2 SIT. Nevertheless, the linear relationship between the two datasets is nonexistent, as evidenced by the low correlation coefficient (Fig. 7b) and the  $R^2 \approx 0$  value (Table B1). This is mainly expected to be due to the acquisition method of the ice mass balance buoys, where, as mentioned in section 4 resulting in a QFS of 3 for buoys, as each buoy is measuring the temporal evolution of the same ice floe. Hereby, the measurements are local and do not capture variations in the surrounding ice as measured on satellite scales e.g, the growth of new ice and thicker ice, and deformation caused by the divergent and convergent motion of sea ice. As the ice mass balance buoys must be placed on a stable ice floe, this also mean that, the buoys tend to be slightly biased towards thicker ice, resulting from the

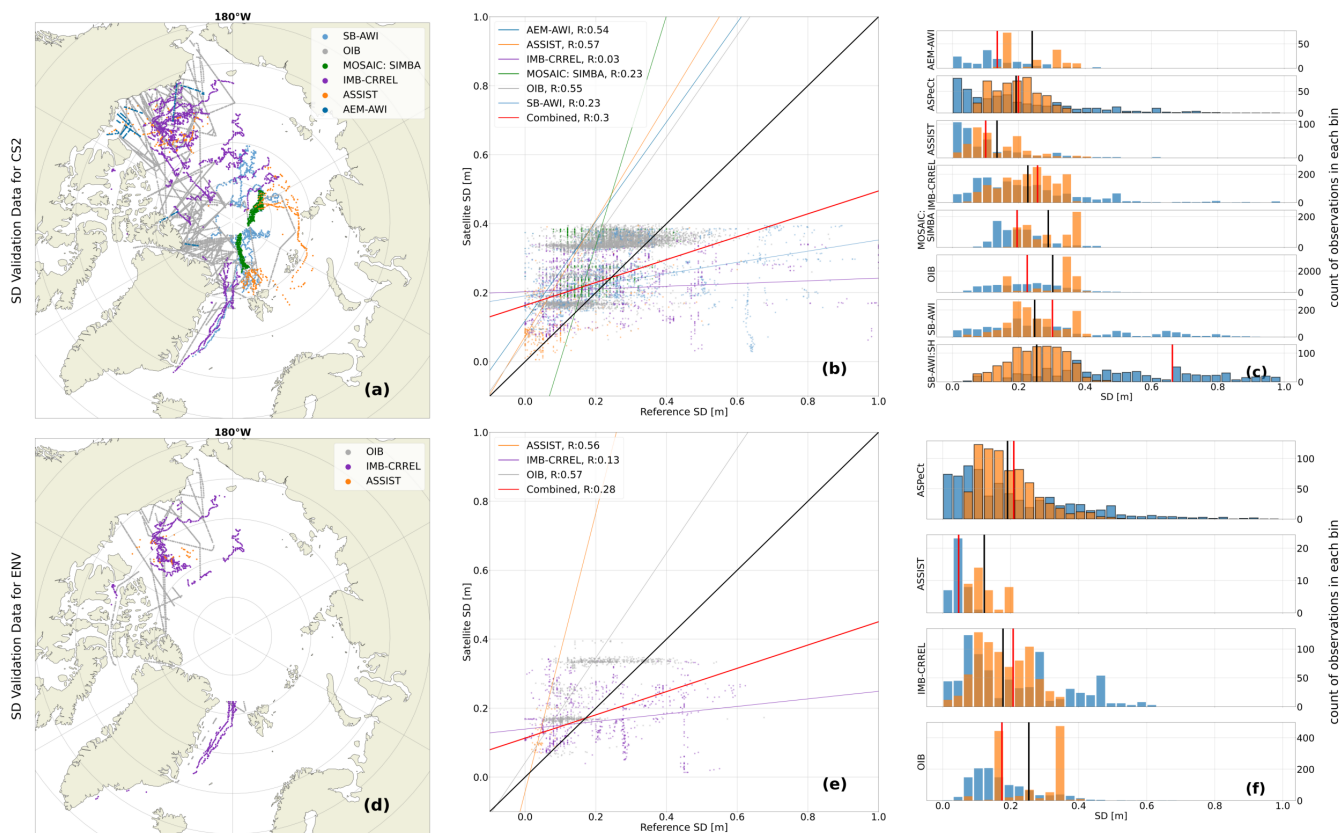


**Figure 9.** SD satellite and reference observation comparison for CryoSat-2 (a-c) and Envisat (d-f). Maps of overlap data are shown for NH in (a,d), associated scatterplots with uncertainty weighted linear fits and associated correlation coefficients in the legend in (b,e) and histograms in (c,f). In the histograms the reference observations and satellite CDRs are marked with blue and orange, respectively, with associated average as black and red vertical lines. A black outline around the histogram bins are added to data from the SH

need to ensure that the ice floe does not melt or deform in a manner that cause damage and premature loss of the buoy. On the other hand, the satellites measures a much larger area, which is likely why the linear relationship between the two is weak. Contrary to IMB-CRREL buoys, MOSAIC-SIMBA buoys has a high correlation ( $R = 0.66$ ), which is likely due to MOSAIC SIMBA bouys being a part of a distributed network. Nevertheless, as will be shown in section 7.6 the low correlation between IMB-CRREL and CS2 and ENV is also highly linked to the method of comparison, where other methods than the one presented in Fig. 7 are more suitable.

The use of the visual ship observations, as reference measurements for SIT, is dubious, as is also reflected in the assigned QFS of 3 (see section 4). First, visual ship observations are dependent on human interpretation, which introduce a larger uncertainty on the individual measurements in particular if the "IceWatch" manual (Hutchings et al., 2018) is not followed in detail and thus, is subjective. In the future, more systematic methods which decreases the influence of the observer should be

~~investigated allowing for more standardized observations.~~ Additionally, as stated in U.S.Fleet (2007, Chapt. 7), ~~icebreakers~~  
915 ~~ships~~ tend to choose the fastest and most economical route, which usually means avoiding ice to the highest degree possible by  
navigating in areas with thin ice, in leads or where there is low concentration. Additionally, Hutchings et al. (2018) states that  
only level ice should be recorded due to the likelihood of thicker ice not fully overturning. ~~The two~~ These factors combined  
suggests that observations from ships tend to have a larger representation of thin ice in the SIT distribution.

This tendency is clearly reflected in the ASSIST and ASPeCt SIT distributions when compared both to CryoSat-2 and  
920 Envisat (Figs. 7c and 7f). This results in large negative biases of ~~-0.47~~ -0.51 m and ~~-0.77~~ -0.71 m, when comparing ASSIST  
and ASPeCt SIT to CryoSat-2 SIT. Similar large negative bias of ~~-0.63~~ -0.62 m is found between ASPeCt and Envisat SIT,  
whereas the bias is smaller for ASSIST (~~-0.17~~ -0.13 m). This is expected to be partly due to the limited amount of available  
ASSIST reference data overlapping with Envisat (Fig. 7d). As shown in Table B2 ~~96~~ 39 data points are available in the CCI  
SIT RRDP after averaging. In general, few ship observations are averaged for each value in the CCI SIT RRDP, as a result of  
925 limited data availability for each 25 km (50 km) grid cell for NH (SH). As a reference, 1.1 observations are used per average  
for the ASSIST measurements coinciding with Envisat and 1.95 for CryoSat-2. This means that the ~~96~~ 39 available reference  
data points from ASSIST to Envisat represent a limited amount of information, and is thus related with a larger uncertainty in  
the reference measurements.

In section 7.6 and in particularly in Fig. 11 an example of applying a filter of  $QFS < 3$  is presented, showing that the  
930 correlation between CS2 and SIT reference observations can be vastly improved by filtering out observations from buoys and  
ships.

### 7.3 Sea ice draft (SID)

SID data has a very limited geographical representation, as seen in Fig. 8a for CryoSat-2 and Fig. 8d for Envisat, and Fig. 10b  
for ERS-1/2 in NH, as most of SID data (except for SCICEX) is obtained from stationary moorings. However, the moorings  
935 represent a time-averaged SID and thus represent a larger sample of sea ice due to the sea ice drift (See Section 2.2), and  
have been used extensively to validate satellite-derived sea ice thicknesses (e.g. Sallila et al., 2019; Quartly et al., 2019).  
A good-reasonable agreement are seen in the distributions (Fig. 8c) between CryoSat-2 and SID data from SCICEX, NPI,  
Nansen legacy and BGEP.

The TRANSDRIFT data is the only sea ice reference measurement available for the Seas north of Russia, and represents  
940 data over assumed fairly level FYI (the ideal sensing scenario for CryoSat-2). ~~Nevertheless, the difference in the distributions~~  
~~between CryoSat-2 and TRANSDRIFT SID is larger than those of SCICEX, NPI and BGEP.~~ In Belter et al. (2020) they find  
a correlation coefficient ( $R = 0.47$ ) and a mean difference (0.28 m) using orbit information from CryoSat-2 similar to our  
approach. These values are similar to those found in this study ( ~~$R = 0.52$~~   $R = 0.58$ ) and mean difference of (~~0.33~~ 0.25 m).  
Their findings of a general tendency of the satellite CDRs to overestimate SID  $< 0.7$  m and underestimate SID  $> 1.3$  m are  
945 in agreement with our findings. The SID distributions for Envisat and reference measurements in NH (Fig. 8f) are similar  
to those discussed for Envisat in SIT See Section 7.2, where Envisat tend to be over-represented in the thinner ice and vice  
versa for thicker ice. This is most pronounced for the comparison with SCICEX and TRANSDRIFT SID, where the reference

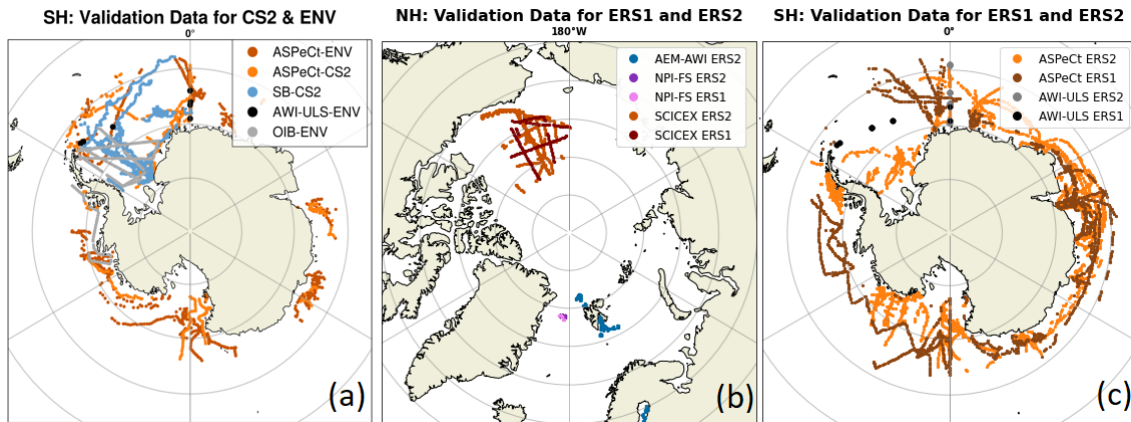


**Figure 10.** Maps showing the geographical representation of; (a) SH reference measurements collocated with CryoSat-2 and Envisat data, (b) NH reference measurements collocated with ERS-1/2 and (c) SH reference measurements collocated with ERS-1/2.

observations have SID up to 3 m and Envisat SID < 1.8 m. Nevertheless, a good agreement is seen when comparing the Envisat and BGEP distributions, which is also reflected in the small mean difference of 0.03 m. Furthermore, high correlation coefficients are observed for all data except for NPI, ranging between  $R = 0.73$  and  $R = 0.76$ . SID data from NPEO is also available in the CCI SIT RRDP, but this data is located at the north pole and is, therefore, within the polar gap of the existing satellites. Nonetheless, the data has been included to validate future satellite products which may cover the polar gap by the implementation of different interpolation techniques. The strength of the SID reference measurement record is that NH NPI-ULS and SCICEX covers both CryoSat-2, Envisat and ERS-1/2.

The representation of SID data for SH (Fig. 10a and 10c) is limited to moorings in the Weddell Sea and Lazarev Sea, which only overlaps with Envisat and ERS-1/2. This data shows a reasonable overlap in the distributions with AWI-ULS SID, except for a larger spike in SID measurements close 0 m caused by AWI-ULS measuring many leads (Fig. 8f) being on average 0.21 m higher. AWI-ULS SID is on average 0.47 m lower when compared to Envisat SID if no bias correction is applied, whereas application of a bias correction results in an average bias of Envisat SID being 0.06 m higher than AWI-ULS SID. However, Moreover, no significant trend ( $R^2 \sim 0$ ) is seen between Envisat SID and AWI-ULS SID (Table B1B2).

#### 7.4 Snow depth (SD)

A quite extensive amount of SD reference observations are available for the NH in particular overlapping with CryoSat-2 (Fig. 9a), and to a lesser extent Envisat (Fig. 9d), including airborne, buoy and ship data. The geographic distribution of data is similar to the SIT data presented in [Seet. Section 7.2](#). For SH, ASPeCt ship observations are available as presented in Fig. 10a for CryoSat-2 and Envisat, and in Fig. 10c for ERS-1/2. Snow depth measurements from buoys (SB-AWI-SH) are only available for CryoSat-2.

The comparison of the distributions presented in Figs. 9c and 9f show large variability, where the CCI SIT CDRs auxiliary snow depth climatologies tend to have a narrower distribution when compared to the different reference observations. This indicates that the auxiliary snow depth climatologies provided in the CCI SIT CDRs (described in [Sect. Section 6.1](#)) fail to  
970 quantify sufficient variability in the snow depth distribution, when compared to reference data, ~~even particularly~~ for the SH snow depth climatology, which is based on daily satellite radiometer observations. This is a fair assumption, as climatologies are averages and do not provide inter-annual variations. However, the variability may also be caused by the reference data having too high variability, which may not signify the larger scale variability of satellite products. This was also discussed in ~~?~~  
[Stroeve et al. \(2020a\)](#) for drifting buoy observations of snow depths compared to models of similar spatial resolution (25 km)  
975 as for the CCI SIT CDRs in NH. Further work should be prioritized to improve this.

Nevertheless, reasonably high correlation ( $R > 0.45$ , Figs. 9b and 9e) coefficients are obtained for several reference data sources such as, ASSIST, [AEM-AWI](#) and OIB. Therefore, although the distributions do not show strong agreement, some degree of linear correlation is observed between the satellite SD product ~~and certain~~[for some](#), but not all, sources of reference observations.

980

## 7.5 Uncertainty quantification

Accurate uncertainty quantification is crucial to obtain the full potential of reference observations. However, this requires individual uncertainty measurements, that are ideally propagated all the way from the raw measurements through the processing chain to the final estimates. In this study uncertainties have been assumed to be independent, although this is likely not the  
985 case, and is expected to result in an underestimation of the uncertainties for the CCI SIT RRDP. However, in lack of more accurate estimates these values provide a first assessment of uncertainties and can be used as an alternative to the uncertainty values provided in Table 7. In the future, all reference measurements (buoy, airborne, submarine and ship) should be quantified with individual uncertainty measurements or provided with uncertainty estimates that take into account some degree of seasonal/spatial variation.

990 An additional uncertainty source in the CCI SIT RRDP arises from the representativeness of the reference data for a 25/50 km grid cell for a monthly period. An attempt has been made to provide an estimate of this by providing the standard deviations and number of entries for each grid cell. However, differences in spatial and temporal coverage between reference data sources and between satellite products within a 25/50 km grid cell for a monthly period might result in temporal and spatial biases, which are not accounted for here. However, this study provides an initial assessment and steps towards a unified uncertainty  
995 estimate for SIT reference observations, which requires future iterations and additional information to be fully described.  
[Further discussion of this is provided in Section 7.7.](#)

## 7.6 Filtering ~~, representativeness and stability~~[flagging](#)

~~Input data to~~ [Global filters have been applied in](#) the CCI SIT RRDP ~~has not been filtered and therefore data shown in this paper~~, [where all observations with values below 0 have been replaced with NaN, along with SIT > 10m, SID > 8m, SD > 2m and](#)

1000 FRB>2m. Apart from these filters, the only additional filtering has included removing clearly erroneous data, such as data from  
IMB-CRREL in 2017 (see Section 5.2.3). As was mentioned in Section 6.1 both satellite and reference observations have been  
gridded using median and robust standard deviation, which makes the dataset less sensitive to outliers. Nevertheless, data in the  
CCI SIT RRDP include observations with high-potentially high robust standard deviations and/or observations based on very  
1005 ~~very-high standard deviations or very few input measurements.~~ If the standard deviation is very-high, the data either contains  
outliers that could be faulty or the variation of the reference data within the grid cell is very-high, reflecting a complex ice  
topography within the grid cell or conditions where the sea ice (or snow depth) have undergone large variations within the  
time-span of the reference observation (up to a month) within-in the grid cell e.g., caused by deformation or redistribution. On  
the other hand, very-a few reference measurements included in-the-within one grid cell estimate could-might indicate that the  
1010 reference data will-not-be-is not representative of the whole area and/or time period.

Nevertheless, these considerations are ~~highly linked to measurement and method as the number of e.g., airborne measurements~~  
~~are typically high although the data is typically limited~~ closely linked to the nature of the measurements and the applied  
methodology. For example, airborne campaigns often yield a high number of observations, but these are typically confined to  
a few days ~~in~~ within a specific region, ~~which~~. When such limited temporal and spatial coverage is compared to a monthly  
1015 ~~CDR mean value, questioning the representativeness.~~ However, when comparing CryoSat-2-NH observations with OIB sea  
ice FRB ( $R=0.47$ , Fig. 6b), AEM-AWI total SIT ( $R=0.59$ , Fig. 7b), OIB derived SIT ( $R=0.56$ , Fig. 7b) and OIBSD  
( $R=0.57$ , Fig. 9b) we find relatively high correlation coefficients, which are similar to other comparison studies using airborne  
campaign data for monthly satellite evaluations (e.g. Quartly et al., 2019; Sallila et al., 2019). ~~mean from the CDR, questions~~  
~~arise regarding the representativeness of the comparison. A more detailed analysis of this issue is provided in Section 7.7.~~

1020 To maximize the usability of the CCI SIT RRDP, a quality flag is provided for the data (Section 4). The temporal quality  
flag (QFT) describes how temporally representative the data is, whereas the spatial quality flag (QFS) aims at describing how  
spatially representative the data is. An example of filtering CS2 data using  $QFS < 3$  is shown in Fig. 11. As seen, this removes  
all of the IMB and the ASSIST data due to their known limitations in terms of spatial representativeness. For airborne data  
(AEM and OIB), this removes datapoints where the number of observations is below the 25% quartile of the respective data  
1025 source. For the remaining data, we see a high overlap in both distributions of the data, with low median differences 0.04 m and  
-0.10 m, a relatively high combined correlation  $R=0.59$ , and an ODR regression line close to the 1 to 1 line.

Other methods, such as matching the satellite SIT CDRs and reference measurements from drifting buoys and stations in a  
Lagrangian framework, i.e., following the buoys, might be a more suitable methodology for future comparisons. This approach  
was successfully demonstrated by ~~(?)~~ Stroeve et al. (2020a), where they compare snow depths from the CRREL-IMBs and  
1030 snow depth buoys to a snow depth model at-of similar spatial scales ~~to-as~~ NH satellite products in our study. However, as  
an alternative and inspired by former studies (e.g., Guerreiro et al., 2016), the buoy data have also been compared in terms  
of time-series relative to the satellite CDR time-series rather than comparing only absolute measurements. An example is  
presented in Fig. 12. Here we observe that although issues in spatial representativeness make the satellite observations and  
buoy observations less comparable, the overall accumulation during the period of the data is generally captured by both CS2

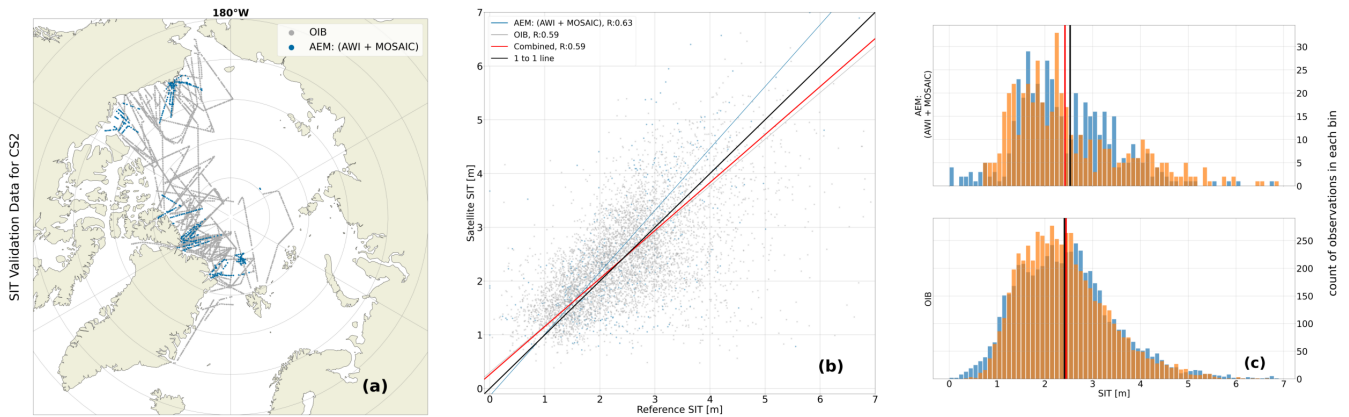


**Figure 11.** Similar to Fig. 7 (a-c), but after applying the spatial representativeness quality flags ( $QFT < 3$ ) to filter the reference measurements.

1035 and reference observations, and overall becomes more comparable when filtering by the temporal flag ( $QFT$ ). An example  
of filtering with  $QFT$  is presented in Fig. 12b+d, where an overall increase in correlation is observed when filtering with a  
high temporal representativeness ( $QFT < 1$ ), where MOSAIC SIMBA  $R$  increases of 0.78 to 0.82 with similar bias of RMSE  
for snow depth, whereas IMBs  $R$  changes from -0.47 to 0.15, but the bias decreases of 0.05 m to -0.03 m and RMSE from  
0.24 m to 0.09 m. Most strikingly for SD is the change of SB-AWI with a change in  $R$  from 0.46 to 0.61, a reduction of bias  
1040 by 0.05 m and RMSE by 0.04 m, respectively. SIT for MOSAIC SIMBA shows highly favorable statistics with a  $R$  of 0.94  
(to 0.97 with  $QFT$  applied), bias of -0.10 m to -0.05 m, and a RMSE of 0.26 m reduced to 0.16 m. We hypothesize that the  
favorable statistics of MOSAIC SIMBA relate to the fact that the MOSAIC SIMBA buoys were part of a distributed network,  
and therefore better represent the spatial conditions observable by the satellite. However, this aspect is currently not included  
in the spatial flag, which, for the buoys, is based on the assumption that the conditions of only one floe are represented. An  
1045 update to the flag could include identifying whether multiple buoys from different floes are present within a single grid cell  
and, similar to airborne data, computing the spatial extent covered by such buoys. An interesting change when applying the  
 $QFT$  flag is observed for IMB (Fig. 12c, d), where the correlation decreases from 0.81 to 0.56, the bias increases from -0.01  
m to -0.17 m, and RMSE increases by 0.15 m. Qualitatively, it shows that the winter of 2010/2011 for the IMB presents an  
opposite relationship (thinning of the ice during the winter season). Exploring it further, only 59 out of 183 (~32%) IMB  
1050 observations would be included for that winter period if the  $QFT < 1$  was applied. The insets of Fig. 12c+d (point observations  
in red) shows the buoy tracks of the 2010/2011 winter season and illustrates how the entire track of the Fram Strait (likely  
due to the high drift speeds) is discarded, and the high thickness observations of the timeseries appear linked with the two  
buoys located in the fast ice area of the Canadian Archipelago which skews the distribution and impacts the monthly derived  
timeseries. One could filter by including information on basins (e.g., Central Arctic Ocean or Barents Sea as examples) to limit  
1055 the potential impact that buoys in landfast ice might introduce. We note that this sensitivity analysis was based on filtering with  
the flags prior to producing the monthly time series. However, this comparison appears more favorable than comparing with

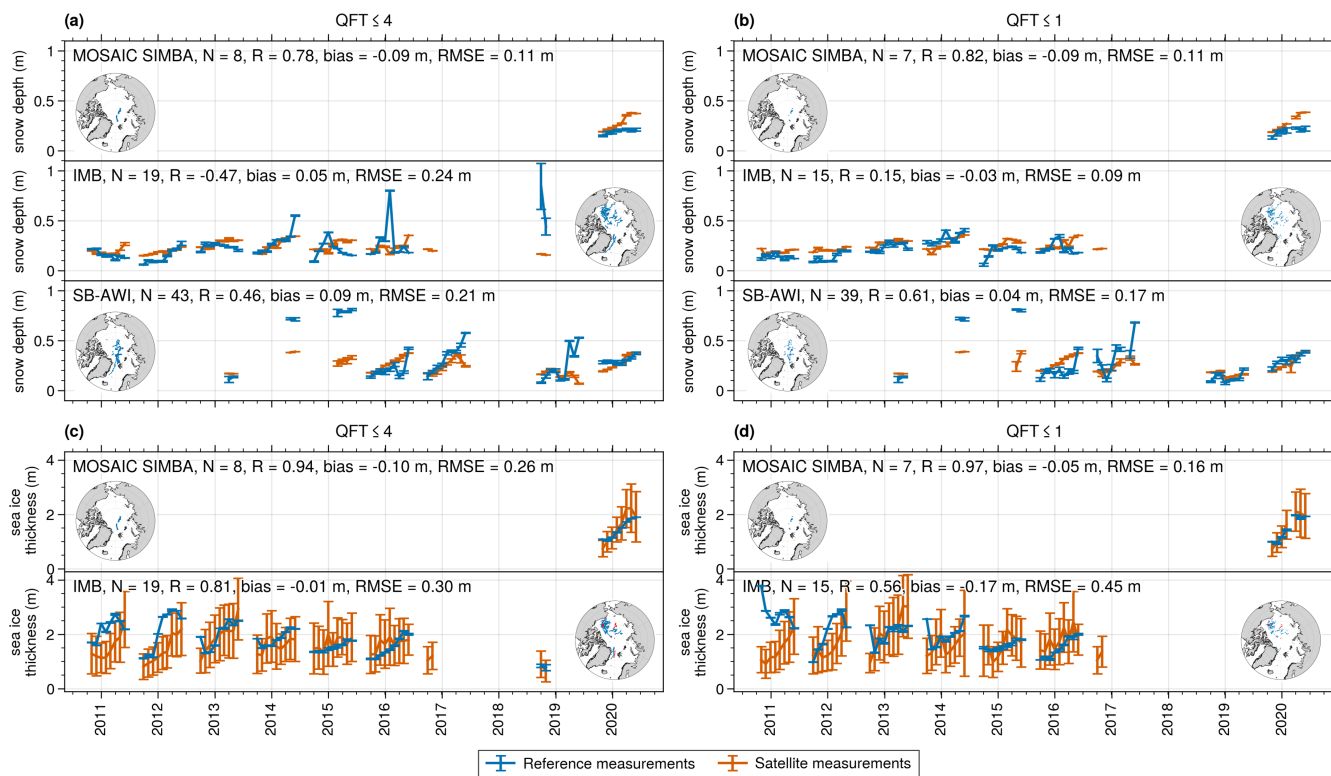


**Figure 12.** Time series of reference measurements from IMB-CRREL, MOSAIC SIMBA and SB-AWI and CS2 satellite observations for collocated data. Each point represents the NH monthly average of all available buoys of a given type and the monthly average of collocated satellite observations, and with the example of utilising the temporal quality flag (QFT) applied (see Table 5 for a description of the flag). Error bars present the averaged standard deviation of the specified variable per grid cell included provided in the data product (see also Table 3 for the RRD data set structure), bias is computed as the satellite measurements subtracted from the reference measurements, and RMSE is the root-mean-square-error. The inset shows the spatial extent of buoy observations included in the monthly time-series (in blue), where in (c) and (d) for IMB, red denotes the observations from winter season 2010/2011 included in the timeseries (dependent on QFT) which is discussed in the text.

absolute observations, and allows for the inclusion of many observations from across the basin to produce one estimate, which minimizes the impact of different type of representation within a grid cell between the two data sources.

To test the

## 1060 7.7 Representativeness and stability

Another important topic is the representativeness of the collocated satellite data when compared to the reference observations. While the spatial and temporal filters help to some degree in quantifying representativeness issues, they are also restrictive and may result in the removal of a significant portion of the reference data if applied too strictly. For instance, the combination

1065 of a QFS<3 and a QFT<3 for SIT would result in almost no reference data (8 observations  $\approx 0.08\%$ ), as the vast majority of  
airborne data would be removed by the temporal representativeness filter. This raises the question of whether using another  
collocation window for satellite measurements would be more appropriate for certain data types. To test this, we have made  
a representation error study using OIB data as the test case. We applied collocation windows varying in temporal sampling  
between 4, 16 and 30 days and in spatial sampling varying between 5, 15 and 25 km. The result of this analysis is shown in Fig.  
1070 14. For the comparison, we consider only the grid cells that contain collocated data across all categories. The analysis shows  
that decreasing the spatial radius of observations tends to reduce the correlation, whereas changing the temporal window has  
little effect.

To further understand these results, we refer to Fig. 13. This figure shows one OIB track (colored by the colorbar, which  
appears black when zoomed out) along with satellite tracks within a 25km radius and a  $\pm 15$  days temporal window. It  
illustrates that the OIB route follows one of the satellite tracks, but for this case not the one closest in time (may not have been  
1075 the target track of the flight campaign). If a small temporal window is chosen, this track would therefore not be included in  
the comparison. Similarly, a smaller spatial window will result in the inclusion of satellite measurements that only cover parts  
of the OIB track. Overall, it also showcases the effect of comparing monthly gridded satellite data, which can cover the grid  
cell more than a one-day OIB track. Furthermore, the footprint sizes illustrate the varying information available from each data  
source, even if they were to fly along the same track. Such issues are inherent to the data itself as the resolution differs, and  
1080 future work should investigate how to further minimise this impact for various data sources.

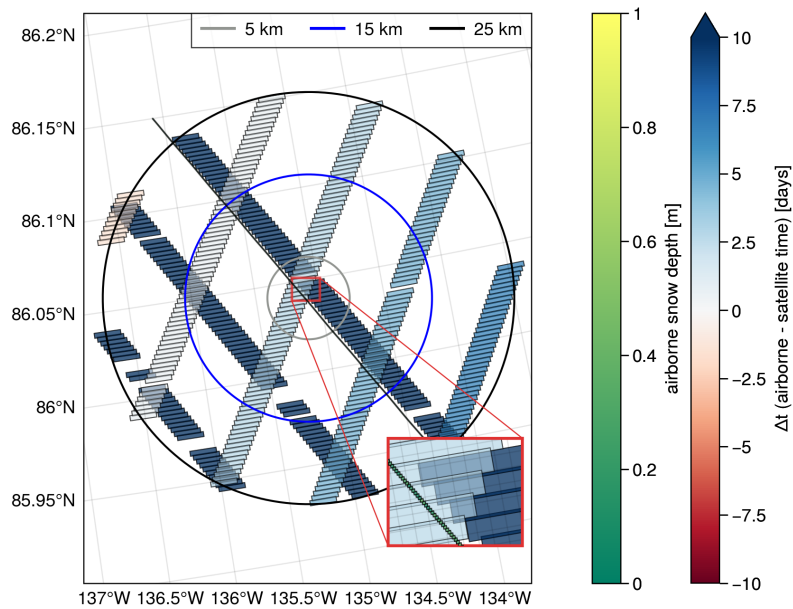


**Figure 13.** Example of spatial representativeness for one grid cell of the EASE2 grid (with center location at 87.38°N and -154.68°E) with an airborne track (OIB-QL, coloured using the snow depth product where fill-values have been given NaN) flown on the 22nd of April 2019 and satellite tracks (CryoSat-2) within the vicinity in time (using a temporal span of maximum  $\pm 15$  days) and space (using search radii of 5 km, 15 km, and 25 km denoted by the circles). Footprints of the different sources are visualised using  $40 \times 40$  m for OIB-QL and  $1600 \times 300$  m for CryoSat-2.  $\Delta t$  describes the temporal difference between the airborne and satellite measurements in days.

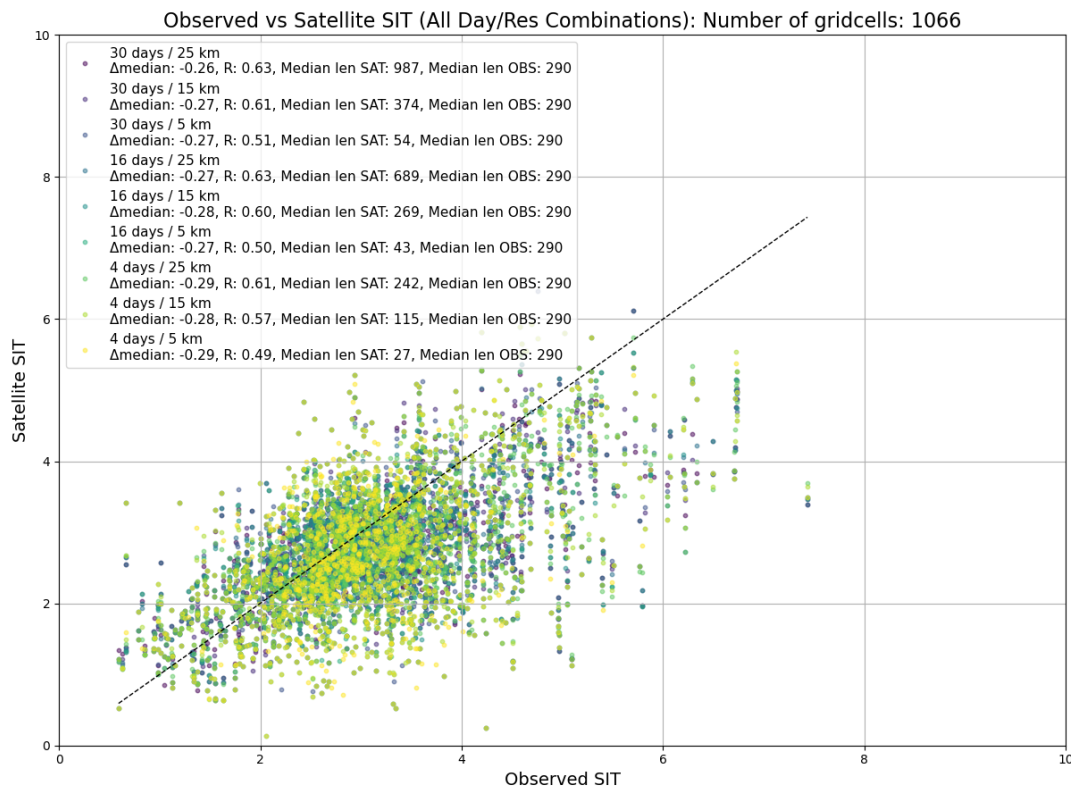


**Figure 14.** Scatterplot of collocated reference observations from OIB and CryoSat-2, when varying temporal sampling windows between 4, 16 and 30 days and spatial sampling windows between 5, 15 and 25 km. Only gridcells that appear when applying the smallest spatial and temporal windows (4 days and 5 km) are included.

To test the stability of the satellite-based SIT CDRs with reference observations, we here recommend using a combination of the long-term monitoring programs, i.e., upward-looking moorings from the Beaufort Gyre Exploitation Project (BGEP), the Fram Strait Arctic Outflow Observatory (NPI-FS) and the Russian-German TRANSDRIFT project (TRANSDRIFT), together with submarine cruises (SCICEX) and airborne EM-campaigns (AEM-AWI) for NH. A similar extensive dataset is not found available for the SH in particular with the biased ASPeCt sea ice thickness observations. To combine the NH measurements into a trend dataset, we need to align the reference measurements and the satellite CDRs to a common measurand, e.g., total SIT or draft. For consistency we shall ensure that a common baseline for auxiliary information of snow depth and densities of sea ice, snow and water are used. Thus, we encourage the community to include the information of all auxiliary data used to support the radar-freeboard-to-sea-ice-freeboard and sea-ice-freeboard-to-thickness conversions to form a consistent baseline. Furthermore, we note that this reference dataset has been prepared to match the format of satellite products provided as monthly, gridded products. However, efforts should also be made to investigate how to utilise available datasets to validate

the lower level (e.g., Level-2) satellite observations, and contribute to the discussion of the formats which validation data should be collected to ensure that satellite data can be deemed fit for purpose and fulfilling of their mission requirements.

## 8 Code and data availability

1095 The CCI SIT RRDP dataset is available at DTU DATA (<https://figshare.com/s/77be0cfd6842d08f1b6b>) (Olsen and Skourup, 2024a) and released under a CC-BY 4.0 license. The final data files are formatted as NetCDF files with not-a-number (NaN) denoting missing data. Apart from the final dataset, all the source code used in the processing steps from the original reference observations to the final CCI SIT RRDP, together with procedures for collocating the CCI SIT RRDP to the satellite measurements from CryoSat-2, Envisat and ERS-1/2, and for creating Figure 3-12 and 14 are available on GitHub through  
1100 (Olsen and Skourup, 2024b). ~~Figure~~ By providing links to the original reference measurements and satellite data (Table 2), this ensures transparency and equips users with the tools and data needed to fully reproduce the final data set. It also allows users to easily redefine their own temporal and spatial scales tailored to their specific needs. In the ReadMe file in GitHub (Olsen and Skourup, 2024b) are specified how the temporal and spatial resolutions can be adjusted in the provided scripts. Fig. 2 (Sankey diagram) was produced using the online tool "VisualParadigmOnline", and adapted in Microsoft Office Power  
1105 Point. ~~Links to the original reference observations and the satellite data are provided in Table 2~~ Fig. 13 has been developed from adapted scripts of Fredensborg Hansen (2024) using intermediate data developed within the framework of the RRDP, which is not provided in the final output version of the data product, and the script to produce this figure is therefore not provided publicly.

## 9 Conclusions

1110 Here, we have presented the CCI SIT RRDP (Olsen and Skourup, 2024a) of available sea ice thickness reference observations covering the polar satellite era 1993–2021 including freeboards (total, radar or derived sea ice), thicknesses (total or sea ice), drafts and snow depths from different sources. The CCI SIT RRDP is suitable for the evaluation of satellite altimeter observations of sea ice freeboard, sea ice thickness and auxiliary snow depth products, but can also be used for evaluation of e.g. models. The reference observations have been prepared to a level where they can be directly compared to satellite altimetry  
1115 temporal (monthly) and spatial (25 km NH; 50 km SH) scales, but these can easily be changed by using the CCI SIT RRDP software package Olsen and Skourup (2024b). We have added uncertainties to the associated reference measurements and flagged these according to their reliability.

As examples of how this data package can be used, we have compared them with the CCI SIT CDRs from CryoSat-2 and Envisat. Here, we generally find good agreement across the different reference observations. Visual observations of sea ice  
1120 thickness and snow depths from ship cruises cannot be used as reference measurements for satellite altimetry in its present form presented in the RRDP, as they are biased low in their distributions. This is expected as ships tend to navigate through the thinnest ice. In addition, the approach used in this study by gridding and time-averaging the reference measurements from

drifting buoys and stations to match satellite scales might not be the most optimal. Other methods, such as matching the satellite SIT CDRs and reference measurements from drifting buoys and stations in a Lagrangian framework might present a more suitable solution in the future. However, existing reference data is scarce in the polar regions, even more pronounced in the Antarctic than in the Arctic. It is therefore necessary to include and use as much data as possible while acknowledging the advantages and limitations of each method. We also note that data prior to 2011 is limited to a few reference measurements - even more so if we remove observations above the polar gap - thus, limiting the comparisons to be made with the ERS-1/2 satellites. Existing reference measurements, which are not included in the CCI SIT RRDP, need to be made publicly available and processed to a level where they can directly be used for inter-comparison to satellite altimetry-derived observations before inclusion into the CCI SIT RRDP. This includes e.g., freeboards from ESA's CryoSat Validation Experiment (CryoVEx) campaigns, as well as OIB Antarctic total freeboards and snow depths. When satellite altimetry-derived sea ice thicknesses are provided in a CDR it is important for comparison and evaluation purposes to include all the auxiliary information used in the intermediate steps in the radar freeboard to sea ice thickness conversion.

For future work, it will be crucial to ensure that reference observations follow the protocols and procedures for fiducial reference measurements (FRMs) i.e., that they are traceable, and fully described with uncertainty diagrams, effects tables and comparability diagrams, see first efforts for altimetry derived sea ice thicknesses in Da Silva et al. (2023). Such comparability diagrams will also aid the design of campaigns to produce measurements which are directly comparable to satellite SIT products. As an example, the AWI IceBird Winter campaigns since 2019 use a sensor combination of EM-Bird, airborne laser scanner and snow radar that allows for a direct retrieval of sea ice thickness, sea ice freeboard and snow depth simultaneously (Juttila et al., 2022a). ~~Snow depths from these campaigns have recently been made available (Juttila et al., 2021) and should be included in future iterations of the CCI SIT RRDP. Additionally, recently published data sources, such as the Nansen Legacy project's snow depth and sea ice thickness dataset in the Barents Sea and Arctic Basin (Divine, 2023a, b), as well as those from the MOSAiC Expedition, will be included in future iterations of the CCI SIT RRDP. These datasets will provide data in areas that are underrepresented in the current version.~~ Updating the data package will be ongoing work to ensure it remains current and comprehensive. The community also urgently need to ensure a consistent network of polar observations for continuous reference measurements of current and future satellite altimeter missions such as Copernicus Polar Ice and Snow Topography Altimeter (CRISTAL) (Kern et al., 2020). There are currently no concrete plans for updating the CCI SIT RRDP beyond 2026, where the project ends. However, we will seek other opportunities for a continuation within frameworks of related databases and projects e.g., St3TART-FO project (<https://frm-datahub.noveltis.fr/>), SIN'XS (<https://sinxs.noveltis.fr/>) or C3S (<https://cis2.eea.europa.eu/about>). Otherwise, the code is readily available, making it easy for users to process and update the database with extensions or additional reference measurements.

*Author contributions.* IO has collected and prepared the CCI SIT RRDP presented in this paper, including pre-processing, estimation of uncertainties and flags. The CCI SIT RRDP is based on previous versions prepared by HSK within the initial phases of the CCI SI project. The initial versions included only sea ice freeboards and snow depth, with no uncertainties or flags provided until 2016,

https://ftp.spacecenter.dk/pub/SICCI/. IO further collocated the reference data with the satellite CDRs. IO, HSK, HS, RMFH wrote the initial manuscript, produced the figures, and specified the extended flagging procedure currently implemented. HSK, ER, SH, RMFH, and SK contributed by identifying relevant reference measurements and defining the temporal and spatial resolution together with the collocation procedures and initial uncertainty flagging procedures. They also contributed through discussions. HSK, ER, SK contributed to the development of the first phases of the CCI SIT RRDP, including validation. SH, SP, ER and HS contributed to satellite-derived CCI SIT CDRs from CryoSat-2 and Envisat. MB and SF contributed with ERS-1/2 data from the FDR4ALT project. DD contributed with NPI mooring data. All authors contributed to the revision of the manuscript, which was led by IO and HSK, together with RMFH.

*Competing interests.* The authors declare that they have no conflict of interest.

*Acknowledgements.* This publication was funded by the ESA's Climate Change Initiative (CCI) for sea ice (grant no. 4000126449/19/I-NB). The main contribution to this work was conducted while I. B. L. Olsen was affiliated with DTU Space. The project and its results are primarily associated with this institution. I. B. L. Olsen is now affiliated with DMI, which contributed to the revision process of the manuscript. We would like to thank DMI for their support during this phase.

We would also like to express our sincere gratitude to everyone involved in the collection, preparation, maintenance, and publication of the input data used in this study. These include, but are not limited to, the Beaufort Gyre Exploration Program based at the Woods Hole Oceanographic Institution (<https://www2.whoi.edu/site/beaufortgyre/>) in collaboration with researchers from Fisheries and Oceans Canada at the Institute of Ocean Sciences, the Norwegian Polar Institute, the North Pole Environmental Observatory and the Polar Science Center, the Russian-German BMBF-funded TRANSDRIFT project, the Alfred Wegener Institute, the Norwegian Meteorological Institute, the Cold Regions Research and Engineering Laboratory, the SCAR Antarctic Sea Ice Processes and Climate (ASPeCt) program ([aspect.antarctica.gov.au](http://aspect.antarctica.gov.au)), the U.S. Navy and Royal Submarines, and the Submarine Arctic Science Program, [The Nansen Legacy Arctic research project and the Multidisciplinary drifting Observatory for the Study of Arctic Climate \(MOSAic\) expedition](#). We acknowledge that it would not have been possible to create the Climate Change Initiative Sea Ice Thickness Round Robin Data Package without the up-to-date and publicly available reference data from the above sources.

We [acknowledge the use of AI-based language tools \(co-pilot and chatgpt\) to assist in checking the manuscript for consistency and clarity. These tools were used to support language refinement without altering the scientific content.](#)

We further acknowledge the important contributions of the CCI Sea Ice scientific leader, Thomas Lavergne, and project coordinator, Mari Anne Killie, both from the Norwegian Meteorological Institute (METNO). Their exceptional leadership, management, and insightful discussions have been pivotal to the success of this study.

[Finally, we would like to express our sincere appreciation to the reviewers for their thoughtful and constructive evaluations. Their insightful comments and suggestions have been invaluable in improving the clarity and overall quality of the manuscript.](#)

## 1185 References

- ERS missions: 20 years of observing Earth, ESA Special Publications (SP-1326), [https://esamultimedia.esa.int/multimedia/publications/SP-1326/SP-1326\\_ERS\\_web.pdf](https://esamultimedia.esa.int/multimedia/publications/SP-1326/SP-1326_ERS_web.pdf), 2013.
- Alexandrov, V., Sandven, S., Wahlin, J., and Johannessen, O. M.: The relation between sea ice thickness and freeboard in the Arctic, *The Cryosphere*, 4, 373–380, <https://doi.org/10.5194/tc-4-373-2010>, 2010.
- 1190 Andersen, O. B., Rose, S. K., Abulaitjiang, A., Zhang, S., and Fleury, S.: The DTU21 global mean sea surface and first evaluation, *Earth System Science Data*, 15, 4065–4075, <https://doi.org/10.5194/essd-15-4065-2023>, 2023.
- Arndt, S., Maaß, N., Rossmann, L., and Nicolaus, M.: From snow accumulation to snow depth distributions by quantifying meteoric ice fractions in the Weddell Sea, *The Cryosphere*, 18, 2001–2015, <https://doi.org/10.5194/tc-18-2001-2024>, 2024.
- ASSIST: Ice Watch ASSIST Data Network, accessed [23-07-2023], <https://icewatch.met.no/>, 2006.
- 1195 Beaven, S. G., LOCKHART, G. L., GOGINENI, S. P., HOSSETNMOSTAFA, A. R., JEZEK, K., GOW, A. J., PEROVICH, D. K., FUNG, A. K., and TJUATJA, S.: Laboratory measurements of radar backscatter from bare and snow-covered saline ice sheets, *International Journal of Remote Sensing*, 16, 851–876, <https://doi.org/10.1080/01431169508954448>, 1995.
- Behrendt, A., Dierking, W., Fahrbach, E., and Witte, H.: Sea ice draft in the Weddell Sea, measured by upward looking sonars, *Earth System Science Data*, 5, 209–226, <https://doi.org/10.5194/ESSD-5-209-2013>, 2013a.
- 1200 Behrendt, A., Dierking, W., Fahrbach, E., and Witte, H.: Sea ice draft measured by upward looking sonar at mooring site AWI227-4. PANGAEA, <https://doi.org/10.1594/PANGAEA.785805>, 2013b.
- Bell, S.: Measurement Good Practice Guide, A Beginner’s Guide to Uncertainty of Measurement, *Esscolab*, 11, [Online; accessed 2023-07-28], 1999.
- Belter, H. J., Janout, M. A., Krumpfen, T., Ross, E., Hölemann, J. A., Timokhov, L., Novikhin, A., Kassens, H., Wyatt, G., Rousseau, S., and Sadowy, D.: Daily mean sea ice draft from moored Upward-Looking Sonars in the Laptev Sea between 2013 and 2015, <https://doi.org/10.1594/PANGAEA.899275>, 2019.
- 1205 Belter, H. J., Janout, M. A., Hölemann, J. A., and Krumpfen, T.: Daily mean sea ice draft from moored upward-looking Acoustic Doppler Current Profilers (ADCPs) in the Laptev Sea from 2003 to 2016, <https://doi.org/10.1594/PANGAEA.912927>, 2020.
- Belter, H. J., Krumpfen, T., Hendricks, S., Hoelemann, J., Janout, M. A., Ricker, R., and Haas, C.: Satellite-based sea ice thickness changes in the Laptev Sea from 2002 to 2017: Comparison to mooring observations, *Cryosphere*, 14, 2189–2203, <https://doi.org/10.5194/TC-14-2189-2020>, 2020.
- 1210 Belter, H. J., Krumpfen, T., Janout, M. A., Ross, E., and Haas, C.: An Adaptive Approach to Derive Sea Ice Draft from Upward-Looking Acoustic Doppler Current Profilers (ADCPs), Validated by Upward-Looking Sonar (ULS) Data, *Remote Sensing*, 13, <https://doi.org/10.3390/rs13214335>, 2021.
- 1215 BGEP: The data were collected and made available by the Beaufort Gyre Exploration Program based at the Woods Hole Oceanographic Institution in collaboration with researchers from Fisheries and Oceans Canada at the Institute of Ocean Sciences., <https://www2.whoi.edu/site/beaufortgyre/data/mooring-data/>, [Online; accessed 2021-07-12], 2003.
- Bocquet, M., Fleury, S., Piras, F., Rinne, E., Sallila, H., Garnier, F., and Rémy, F.: Arctic sea ice radar freeboard retrieval from the European Remote-Sensing Satellite (ERS-2) using altimetry: toward sea ice thickness observation from 1995 to 2021, *The Cryosphere*, 17, 3013–3039, <https://doi.org/10.5194/tc-17-3013-2023>, 2023.
- 1220

- Bocquet, M., Fleury, S., Rémy, F., and Piras, F.: Arctic and Antarctic Sea Ice Thickness and Volume Changes From Observations Between 1994 and 2023, *Journal of Geophysical Research: Oceans*, 129, e2023JC020848, <https://doi.org/https://doi.org/10.1029/2023JC020848>, e2023JC020848 2023JC020848, 2024.
- 1225 Bocquet, M. Fleury, S.: Arctic and Antarctic sea ice thickness climate data record (ERS-1, ERS-2, Envisat, CryoSat-2), [https://doi.org/https://doi.org/10.6096/ctoh\\_sit\\_2023\\_01](https://doi.org/https://doi.org/10.6096/ctoh_sit_2023_01), 2023.
- Boggs, P. T. and Rogers, J. E.: Orthogonal Distance Regression,” in “Statistical analysis of measurement error models and applications: proceedings of the AMS-IMS-SIAM joint summer research conference held June 10-16, 1989, *Contemporary Mathematics*, 112, 186, 1990.
- Brodzik, M., Billingsley, B., Haran, T., Raup, B., and Savoie, M.: EASE-Grid 2.0: Incremental but Significant Improvements for Earth-Gridded Data Sets, *International Journal of Geo-Information*, 1, 32–45, <https://doi.org/10.3390/ijgi1010032>, 2012.
- 1230 Buynitskiy, V. K.: Structure, principal properties and strength of Antarctic sea ice, *Sov. Antarct. Exped. Inf. Bull.*, 65, 504–510, 1967.
- Carret, A., Fleury, S., Di Bella, A., Landy, J., Lawrence, I., Kurtz, N., Laforge, A., Bouffard, J., and Parrinello, T.: A multi-frequency altimetry snow depth product over Arctic sea ice, *Scientific Data*, 12, <https://doi.org/10.1038/s41597-024-04343-4>, 2025.
- Cavalieri, D. J., Markus, T., and Comiso, J. C.: AMSR-E/Aqua Daily L3 12.5 km Brightness Temperature, Sea Ice Concentration, Snow Depth Polar Grids, Version 3, [https://doi.org/10.5067/AMSR-E/AE\\_SI12.003](https://doi.org/10.5067/AMSR-E/AE_SI12.003), 2014.
- 1235 Cheng, Y., Cheng, B., Zheng, F., Vihma, T., Kontu, A., Yang, Q., and Liao, Z.: Air/snow, snow/ice and ice/water interfaces detection from high-resolution vertical temperature profiles measured by ice mass-balance buoys on an Arctic lake, *Annals of Glaciology*, 61, 309–319, <https://doi.org/10.1017/aog.2020.51>, 2020.
- Comiso, J., Cavalieri, D., and Markus, T.: Sea ice concentration, ice temperature, and snow depth using AMSR-E data, *IEEE Transactions on Geoscience and Remote Sensing*, 41, 243–252, <https://doi.org/10.1109/TGRS.2002.808317>, 2003.
- 1240 Cristea, A., Gerland, S., and Bratrein, M.: Results of regional scale sea ice and snow thickness surveys during Nansen Legacy/Synoptic Arctic Survey Joint Cruise 2 (JC2-2) in August – September 2021 using helicopter-borne electromagnetic induction sounding instrument (EM-bird), <https://doi.org/10.21334/NPOLAR.2023.C1CFD5DD>, 2023.
- Da Silva, E., Woolliams, E. R., Picot, N., Poisson, J.-C., Skourup, H., Moholdt, G., Fleury, S., Behnia, S., Favier, V., Arnaud, L., Aublanc, J., Fouqueau, V., Taburet, N., Renou, J., Yesou, H., Tarpanelli, A., Camici, S., Fredensborg Hansen, R. M., Nielsen, K., Vivier, F., Boy, F., Fjørtoft, R., Cancet, M., Ferrari, R., Picard, G., Tourian, M. J., Sneeuw, N., Munesa, E., Calzas, M., Paris, A., Le Meur, E., Rabatel, A., Valladeau, G., Bonnefond, P., Labroue, S., Andersen, O., El Hajj, M., Catapano, F., and Féménias, P.: Towards Operational Fiducial Reference Measurement (FRM) Data for the Calibration and Validation of the Sentinel-3 Surface Topography Mission over Inland Waters, Sea Ice, and Land Ice, *Remote Sensing*, 15, <https://doi.org/10.3390/rs15194826>, 2023.
- 1245 Divine, D., Bratrein, M., Jacobsen, J. A., and Gerland, S.: Results of regional scale sea ice and snow thickness surveys during Nansen Legacy Q1 research cruise in March 2021 using helicopter-borne electromagnetic induction sounding instrument (EM-bird)., <https://doi.org/10.21334/NPOLAR.2023.1A9CC2DF>, 2023.
- 1250 Divine, D. Bratrein, M. . J. J. . G. S.: Results of regional scale sea ice and snow thickness surveys during Nansen Legacy Q1 research cruise in March 2021 using helicopter-borne electromagnetic induction sounding instrument (EM-bird) [Data set], <https://doi.org/https://doi.org/10.21334/npolar.2023.1a9cc2df>, 2023a.
- 1255 Divine, D. Bratrein, M. . J. J. . G. S.: Results of regional scale sea ice and snow thickness surveys during Nansen Legacy/Synoptic Arctic Survey Joint Cruise 2 (JC2-2) in August – September 2021 using helicopter-borne electromagnetic induction sounding instrument (EM-bird) [Data set], <https://doi.org/https://doi.org/10.21334/npolar.2023.c1cfd5dd>, 2023b.

- Dubock, P. A., Spoto, F., Simpson, J., Spencer, D., Schutte, E., and Sontag, H.: The Envisat satellite and its integration, *ESA Bulletin*, 106, 1260 26–45, 2001.
- European Space Agency: CryoSat-2 Product Handbook Baseline E 1.0 - Draft B, [https://earth.esa.int/eogateway/documents/20142/0/CryoSat-Product-Handbook-Baseline-E-draft.pdf/fc311af8-b926-cf59-5e3a-6b81942e262f\\_c2-LI-ACS-ESL-5319](https://earth.esa.int/eogateway/documents/20142/0/CryoSat-Product-Handbook-Baseline-E-draft.pdf/fc311af8-b926-cf59-5e3a-6b81942e262f_c2-LI-ACS-ESL-5319), 2019.
- Fons, S., Kurtz, N., and Bagnardi, M.: A decade-plus of Antarctic sea ice thickness and volume estimates from CryoSat-2 using a physical model and waveform fitting, *The Cryosphere*, 17, 2487–2508, <https://doi.org/10.5194/tc-17-2487-2023>, 2023.
- 1265 Fredensborg Hansen, R. M.: cryo2iceant22-airborne-cryo2ice-weddell-sea-ice, <https://doi.org/10.5281/zenodo.13749342>, 2024.
- Fredensborg Hansen, R. M., Skourup, H., Rinne, E., Høyland, K. V., Landy, J. C., Merkouriadi, I., and Forsberg, R.: Arctic Freeboard and Snow Depth From Near-Coincident CryoSat-2 and ICESat-2 (CRYO2ICE) Observations: A First Examination of Winter Sea Ice During 2020–2022, *Earth and Space Science*, 11, e2023EA003313, <https://doi.org/https://doi.org/10.1029/2023EA003313>, e2023EA003313 2023EA003313, 2024a.
- 1270 Fredensborg Hansen, R. M., Skourup, H., Rinne, E., Jutila, A., Lawrence, I. R., Shepherd, A., Høyland, K. V., Li, J., Rodriguez-Morales, F., Simonsen, S. B., Wilkinson, J., Veyssiere, G., Yi, D., Forsberg, R., and Casal, T. G. D.: Exploring microwave penetration into snow on Antarctic summer sea ice along CryoSat-2 and ICESat-2 (CRYO2ICE) orbit from multi-frequency air- and spaceborne altimetry, *EGUsphere*, 2024, 1–53, <https://doi.org/10.5194/egusphere-2024-2854>, 2024b.
- Garnier, F., Fleury, S., Garric, G., Bouffard, J., Tsamados, M., Laforge, A., Bocquet, M., Fredensborg Hansen, R. M., and Remy, F.: Advances in altimetric snow depth estimates using bi-frequency SARAL and CryoSat-2 Ka–Ku measurements, *The Cryosphere*, 15, 5483–5512, <https://doi.org/10.5194/tc-15-5483-2021>, 2021.
- 1275 Giles, K., Laxon, S., Wingham, D., Wallis, D., Krabill, W., Leuschen, C., McAdoo, D., Manizade, S., and Raney, R.: Combined airborne laser and radar altimeter measurements over the Fram Strait in May 2002, *Remote Sensing of Environment*, 111, 182–194, <https://doi.org/10.1016/j.rse.2007.02.037>, *remote Sensing of the Cryosphere Special Issue*, 2007.
- 1280 Giles, K. A. and Hvidegaard, S. M.: Comparison of space borne radar altimetry and airborne laser altimetry over sea ice in the Fram Strait, *International Journal of Remote Sensing*, 27, 3105–3113, <https://doi.org/10.1080/01431160600563273>, 2006.
- Gregory, W., Lawrence, I. R., and Tsamados, M.: A Bayesian approach towards daily pan-Arctic sea ice freeboard estimates from combined CryoSat-2 and Sentinel-3 satellite observations, *The Cryosphere*, 15, 2857–2871, <https://doi.org/10.5194/tc-15-2857-2021>, 2021.
- Grosfeld, K., Treffeisen, R., Asseng, J., Bartsch, A., Bräuer, B., Fritzsche, B., Gerdes, R., Hendricks, S., Hiller, W., Heygster, G., 1285 Krumpfen, T., Lemke, P., Melsheimer, C., Nicolaus, M., Ricker, R., and Weigelt, M.: Online sea-ice knowledge and data platform <<https://data.meereisportal.de/relaunch/airborne?lang=de>>, <https://doi.org/10.2312/polfor.2016.011>, 2016.
- Guerreiro, K., Fleury, S., Zakharova, E., Rémy, F., and Kouraev, A.: Potential for estimation of snow depth on Arctic sea ice from CryoSat-2 and SARAL/AltiKa missions, *Remote Sensing of Environment*, 186, 339–349, <https://doi.org/https://doi.org/10.1016/j.rse.2016.07.013>, 2016.
- 1290 Guerreiro, K., Fleury, S., Zakharova, E., Kouraev, A., Rémy, F., and Maisongrande, P.: Comparison of CryoSat-2 and ENVISAT radar freeboard over Arctic sea ice: Toward an improved Envisat freeboard retrieval, *Cryosphere*, 11, 2059–2073, <https://doi.org/10.5194/TC-11-2059-2017>, 2017.
- Haas, C.: Sea Ice, third edition, Chapter 2: sea ice thickness distribution, Wiley Blackwell, <https://doi.org/10.1002/9781118778371>, 2016.
- Haas, C., Göbell, S., Hendricks, S., Martin, T., Pfaffhuber, A., and Saldern, C.: Airborne electromagnetic measurements of sea ice thickness: 1295 methods and applications, European Commission, 2007.

- Haas, C., Lobach, J., Hendricks, S., Rabenstein, L., and Pfaffling, A.: Helicopter-borne measurements of sea ice thickness, using a small and lightweight, digital EM system, *Journal of Applied Geophysics*, 67, 234–241, <https://doi.org/https://doi.org/10.1016/j.jappgeo.2008.05.005>, *airborne Geophysics*, 2009.
- 1300 Haas, C., Beckers, J., King, J., Silis, A., Stroeve, J., Wilkinson, J., Notenboom, B., Schweiger, A., and Hendricks, S.: Ice and Snow Thickness Variability and Change in the High Arctic Ocean Observed by In Situ Measurements, *Geophysical Research Letters*, 44, 10,462–10,469, <https://doi.org/10.1002/2017GL075434>, 2017.
- Hansen, E., Gerland, S., Granskog, M. A., Pavlova, O., Renner, A. H., Haapala, J., Løyning, T. B., and Tschudi, M.: Thinning of Arctic sea ice observed in Fram Strait: 1990–2011, *Journal of Geophysical Research: Oceans*, 118, 5202–5221, <https://doi.org/10.1002/jgrc.20393>, 2013.
- 1305 Hendricks, S. Paul, S. . R. E.: ESA Sea Ice Climate Change Initiative (Sea\_Ice\_cci): Northern hemisphere sea ice thickness from CryoSat-2 on the satellite swath (L2P), v3.0., <https://catalogue.ceda.ac.uk/uuid/c6504378f78c4ecd9f839b0434023eff>, 2024a.
- Hendricks, S. Paul, S. . R. E.: ESA Sea Ice Climate Change Initiative (Sea\_Ice\_cci): Northern hemisphere sea ice thickness from Envisat on the satellite swath (L2P), v3.0., <https://catalogue.ceda.ac.uk/uuid/92eb2ba942074bec804af6a8b5436bee>, 2024b.
- Hendricks, S. Paul, S. . R. E.: ESA Sea Ice Climate Change Initiative (Sea\_Ice\_cci): Southern hemisphere sea ice thickness from CryoSat-2 on the satellite swath (L2P), v3.0, <https://catalogue.ceda.ac.uk/uuid/861ad3c7f3a34ebd8be6f618a92bd8e3>, 2024c.
- 1310 Hendricks, S. Paul, S. . R. E.: ESA Sea Ice Climate Change Initiative (Sea\_Ice\_cci): Southern hemisphere sea ice thickness from Envisat on the satellite swath (L2P), v3.0., <https://catalogue.ceda.ac.uk/uuid/af96a1ec493f49caa39dc912d15f2b17>, 2024d.
- Hutchings, J., Delamere, J., and Heil, P.: The Ice Watch Manual - [https://icewatch.met.no/Ice\\_Watch\\_Manual\\_v4.1.pdf](https://icewatch.met.no/Ice_Watch_Manual_v4.1.pdf), <https://icewatch.met.no/>, <https://icewatch.met.no.>, 2018.
- 1315 Jutila, A., King, J., Ricker, R., Hendricks, S., Helm, V., Binder, T., and Herber, A.: Airborne snow depth on sea ice during the PAMARCMIP2017 campaign in the Arctic Ocean, Version 1, <https://doi.org/10.1594/PANGAEA.932668>, 2021.
- Jutila, A., Hendricks, S., Ricker, R., von Albedyll, L., Krumpfen, T., and Haas, C.: Retrieval and parameterisation of sea-ice bulk density from airborne multi-sensor measurements, *The Cryosphere*, 16, 259–275, <https://doi.org/10.5194/TC-16-259-2022>, 2022a.
- Jutila, A., King, J., Paden, J., Ricker, R., Hendricks, S., Polashenski, C., Helm, V., Binder, T., and Haas, C.: High-Resolution Snow Depth on Arctic Sea Ice From Low-Altitude Airborne Microwave Radar Data, *IEEE Transactions on Geoscience and Remote Sensing*, 60, 1–16, <https://doi.org/10.1109/TGRS.2021.3063756>, 2022b.
- 1320 Jutila, A., Hendricks, S., Ricker, R., von Albedyll, L., and Haas, C.: Airborne sea ice parameters during the PAMARCMIP2017 campaign in the Arctic Ocean, Version 2, <https://doi.org/10.1594/PANGAEA.966009>, 2024a.
- Jutila, A., Hendricks, S., Ricker, R., von Albedyll, L., and Haas, C.: Airborne sea ice parameters during the IceBird Winter 2019 campaign in the Arctic Ocean, Version 2, <https://doi.org/10.1594/PANGAEA.966057>, 2024b.
- 1325 Kacimi, S. and Kwok, R.: The Antarctic sea ice cover from ICESat-2 and CryoSat-2: freeboard, snow depth, and ice thickness, *The Cryosphere*, 14, 4453–4474, <https://doi.org/10.5194/tc-14-4453-2020>, 2020.
- Kacimi, S. and Kwok, R.: Arctic Snow Depth, Ice Thickness, and Volume From ICESat-2 and CryoSat-2: 2018–2021, *Geophysical Research Letters*, 49, e2021GL097448, <https://doi.org/10.1029/2021GL097448>, e2021GL097448 2021GL097448, 2022.
- 1330 Kern, M., Cullen, R., Berruti, B., Bouffard, J., Casal, T., Drinkwater, M. R., Gabriele, A., Lecuyot, A., Ludwig, M., Midthassel, R., Navas Traver, I., Parrinello, T., Ressler, G., Andersson, E., Martin-Puig, C., Andersen, O., Bartsch, A., Farrell, S., Fleury, S., Gascoin, S., Guillot, A., Humbert, A., Rinne, E., Shepherd, A., van den Broeke, M. R., and Yackel, J.: The Copernicus Polar Ice and Snow Topography Altimeter (CRISTAL) high-priority candidate mission, *The Cryosphere*, 14, 2235–2251, <https://doi.org/10.5194/tc-14-2235-2020>, 2020.

- Kern, S.: ESA-CCI\_Phase2\_Standardized\_Manual\_Visual\_Ship-Based\_SeaIceObservations\_v02, <https://doi.org/10.26050/WDCC/ESACCIPSMVBSIS>  
1335 2020.
- Kern, S., Khvorostovsky, K., Skourup, H., Rinne, E., Parsakhoo, Z. S., Djepa, V., Wadhams, P., and Sandven, S.: The impact of snow depth, snow density and ice density on sea ice thickness retrieval from satellite radar altimetry: results from the ESA-CCI Sea Ice ECV Project Round Robin Exercise, *The Cryosphere*, 9, 37–52, <https://doi.org/10.5194/tc-9-37-2015>, 2015.
- Kern, S., Ozsoy-Çiçek, B., and Worby, A. P.: Antarctic Sea-Ice Thickness Retrieval from ICESat: Inter-Comparison of Different Approaches,  
1340 *Remote Sensing*, 8, 538, <https://doi.org/10.3390/rs8070538>, 2016.
- King, J., Howell, S., Derksen, C., Rutter, N., Toose, P., Beckers, J. F., Haas, C., Kurtz, N., and Richter-Menge, J.: Evaluation of Operation IceBridge quick-look snow depth estimates on sea ice, *Geophysical Research Letters*, 42, 9302–9310, <https://doi.org/https://doi.org/10.1002/2015GL066389>, 2015.
- King, J., Skourup, H., Hvidegaard, S. M., Rösel, A., Gerland, S., Spreen, G., Polashenski, C., Helm, V., and Liston, G. E.:  
1345 Comparison of Freeboard Retrieval and Ice Thickness Calculation From ALS, ASIRAS, and CryoSat-2 in the Norwegian Arctic to Field Measurements Made During the N-ICE2015 Expedition, *Journal of Geophysical Research: Oceans*, 123, 1123–1141, <https://doi.org/https://doi.org/10.1002/2017JC013233>, 2018.
- Krishfield, R. and Proshutinsky, A.: BGOS ULS Data Processing Procedure, [https://www2.whoi.edu/site/beaufortgyre/wp-content/uploads/sites/108/2020/04/BGOS\\_ULS\\_Data\\_Processing\\_Procedure\\_85684.pdf](https://www2.whoi.edu/site/beaufortgyre/wp-content/uploads/sites/108/2020/04/BGOS_ULS_Data_Processing_Procedure_85684.pdf), 2006.
- 1350 Kurtz, N., Studinger, M., Harbeck, J., Onana, V., and Yi., and D.: IceBridge L4 Sea Ice Freeboard, Snow Depth, and Thickness, Version 1, <https://doi.org/10.5067/G519SHCKWQV6>, [Online; accessed 2023-07-12], 2015.
- Kurtz, N., Studinger, M., Harbeck, J., Onana, V., and Yi, D.: IceBridge Sea Ice Freeboard, Snow Depth, and Thickness Quick Look, Version 1, <https://doi.org/10.5067/GRIXZ91DE0L9>, 2016.
- Kurtz, N. T. and Farrell, S. L.: Large-scale surveys of snow depth on Arctic sea ice from Operation IceBridge, *Geophysical Research Letters*,  
1355 38, <https://doi.org/https://doi.org/10.1029/2011GL049216>, 2011.
- Kurtz, N. T., Farrell, S. L., Studinger, M., Galin, N., Harbeck, J. P., Lindsay, R., Onana, V. D., Panzer, B., and Sonntag, J. G.: Sea ice thickness, freeboard, and snow depth products from Operation IceBridge airborne data, *The Cryosphere*, 7, 1035–1056, <https://doi.org/10.5194/tc-7-1035-2013>, 2013.
- Kurtz, N. T., Galin, N., and Studinger, M.: An improved CryoSat-2 sea ice freeboard retrieval algorithm through the use of waveform fitting,  
1360 *The Cryosphere*, 8, 1217–1237, <https://doi.org/10.5194/tc-8-1217-2014>, 2014.
- Kwok, R. and Kacimi, S.: Three years of sea ice freeboard, snow depth, and ice thickness of the Weddell Sea from Operation IceBridge and CryoSat-2, *The Cryosphere*, 12, 2789–2801, <https://doi.org/10.5194/tc-12-2789-2018>, 2018.
- Kwok, R. and Markus, T.: Potential basin-scale estimates of Arctic snow depth with sea ice freeboards from CryoSat-2 and ICESat-2: An exploratory analysis, *Advances in Space Research*, 62, 1243–1250, <https://doi.org/https://doi.org/10.1016/j.asr.2017.09.007>, the CryoSat  
1365 Satellite Altimetry Mission: Eight Years of Scientific Exploitation, 2018.
- Kwok, R., Kurtz, N. T., Brucker, L., Ivanoff, A., Newman, T., Farrell, S. L., King, J., Howell, S., Webster, M. A., Paden, J., Leuschen, C., MacGregor, J. A., Richter-Menge, J., Harbeck, J., and Tschudi, M.: Intercomparison of snow depth retrievals over Arctic sea ice from radar data acquired by Operation IceBridges, *The Cryosphere*, 11, 2571–2593, <https://doi.org/10.5194/tc-11-2571-2017>, 2017.
- Kwok, R., Kacimi, S., Webster, M., Kurtz, N., and Petty, A.: Arctic Snow Depth and Sea Ice Thickness From ICESat-2 and CryoSat-2 Free-  
1370 boards: A First Examination, *Journal of Geophysical Research: Oceans*, 125, e2019JC016008, <https://doi.org/10.1029/2019JC016008>, 2020.

- Landy, J. C., Petty, A. A., Tsamados, M., and J. C. Stroeve, J. C.: Sea ice roughness overlooked as a key source of uncertainty in CryoSat-2 ice freeboard retrievals., *Journal of Geophysical Research: Oceans*, 125, <https://doi.org/10.1029/2019JC015820>, 2020.
- 1375 Landy, J. C., Dawson, G. J., Tsamados, M., Bushuk, M., Stroeve, J. C., Howell, S. E. L., Krumpen, T., Babb, D. G., Komarov, A. S., Heorton, H. D. B. S., Belter, H. J., and Aksenov, Y.: A year-round satellite sea-ice thickness record from CryoSat-2, *Nature*, 609, 517–522, <https://doi.org/10.1038/s41586-022-05058-5>, 2022.
- Lawrence, I. R., Tsamados, M. C., Stroeve, J. C., Armitage, T. W. K., and Ridout, A. L.: Estimating snow depth over Arctic sea ice from calibrated dual-frequency radar freeboards, *The Cryosphere*, 12, 3551–3564, <https://doi.org/10.5194/tc-12-3551-2018>, 2018.
- 1380 Lawrence, I. R., Ridout, A. L., Shepherd, A., and Tilling, R.: A Simulation of Snow on Antarctic Sea Ice Based on Satellite Data and Climate Reanalyses, *Journal of Geophysical Research: Oceans*, 129, e2022JC019002, <https://doi.org/10.1029/2022JC019002>, e2022JC019002 2022JC019002, 2024.
- Laxon, S., Peacock, N., and Smith, D.: High interannual variability of sea ice thickness in the Arctic region, *Nature*, pp. 947–950, <https://doi.org/10.1038/nature020505>, 2003.
- 1385 Laxon, S. W., Giles, K. A., Ridout, A. L., Wingham, D. J., Willatt, R., Cullen, R., Kwok, R., Schweiger, A., Zhang, J., Haas, C., Hendricks, S., Krishfield, R., Kurtz, N., Farrell, S., and Davidson, M.: CryoSat-2 estimates of Arctic sea ice thickness and volume, *Geophysical Research Letters*, 40, 732–737, <https://doi.org/10.1002/grl.50193>, 2013.
- Lee, J.-E., Lee, G. W., Earle, M., and Nitu, R.: Uncertainty Analysis for Evaluating the Accuracy of Snow Depth Measurements, *Hydrology and Earth System Sciences Discussions*, 12, 4157–4190, <https://doi.org/10.5194/hessd-12-4157-2015>, 2015.
- 1390 Lei, R., Cheng, B., Hoppmann, M., and Zuo, G.: Snow depth and sea ice thickness derived from the measurements of SIMBA buoys deployed in the Arctic Ocean during the Legs 1a, 1, and 3 of the MOSAiC campaign in 2019-2020, <https://doi.org/10.1594/PANGAEA.938244>, 2021.
- MacGregor, J. A., Boisvert, L. N., Medley, B., Petty, A. A., Harbeck, J. P., Bell, R. E., Blair, J. B., Blanchard-Wrigglesworth, E., Buckley, E. M., Christoffersen, M. S., Cochran, J. R., Csathó, B. M., De Marco, E. L., Dominguez, R. T., Fahnestock, M. A., Farrell, S. L., Gogineni, S. P., Greenbaum, J. S., Hansen, C. M., Hofton, M. A., Holt, J. W., Jezek, K. C., Koenig, L. S., Kurtz, N. T., Kwok, R., Larsen, 1395 C. F., Leuschen, C. J., Locke, C. D., Manizade, S. S., Martin, S., Neumann, T. A., Nowicki, S. M., Paden, J. D., Richter-Menge, J. A., Rignot, E. J., Rodríguez-Morales, F., Siegfried, M. R., Smith, B. E., Sonntag, J. G., Studinger, M., Tinto, K. J., Truffer, M., Wagner, T. P., Woods, J. E., Young, D. A., and Yungel, J. K.: The Scientific Legacy of NASA's Operation IceBridge, *Reviews of Geophysics*, 59, e2020RG000712, <https://doi.org/10.1029/2020RG000712>, 2021.
- 1400 Mahoney, A. R., Eicken, H., Fukamachi, Y., Ohshima, K. I., Simizu, D., Kambhamettu, C., Rohith, M. V., Hendricks, S., and Jones, J.: Taking a look at both sides of the ice: Comparison of ice thickness and drift speed as observed from moored, airborne and shore-based instruments near Barrow, Alaska, *Annals of Glaciology*, 56, 363–372, <https://doi.org/10.3189/2015AoG69A565>, 2015.
- Maksym, T., Stammerjohn, S. E., Ackley, S., and Massom, R.: Antarctic Sea Ice: A Polar Opposite?, *Oceanography*, 25, 140–151, <http://www.jstor.org/stable/24861407>, [Online; accessed 2023-07-31], 2012.
- 1405 Mallett, R. D. C., Lawrence, I. R., Stroeve, J. C., Landy, J. C., and Tsamados, M.: Brief communication: Conventional assumptions involving the speed of radar waves in snow introduce systematic underestimates to sea ice thickness and seasonal growth rate estimates, *The Cryosphere*, 14, 251–260, <https://doi.org/10.5194/tc-14-251-2020>, 2020.
- Markus, T. and Cavalieri, D. J.: Snow Depth Distribution Over Sea Ice in the Southern Ocean from Satellite Passive Microwave Data, pp. 19–39, *American Geophysical Union (AGU)*, <https://doi.org/10.1029/AR074p0019>, 1998.

- Markus, T., Massom, R., Worby, A., Lytle, V., Kurtz, N., and Maksym, T.: Freeboard, snow depth and sea-ice roughness in East Antarctica from in situ and multiple satellite data, *Annals of Glaciology*, 52, 242–248, <https://doi.org/10.3189/172756411795931570>, 2011.
- 1410 Melling, H., Johnston, P., and Riedel, D. A.: Measurements of the Underside Topography of Sea Ice by Moored Subsea Sonar, *Journal of Atmospheric and Oceanic Technology*, 12, 589–602, <https://api.semanticscholar.org/CorpusID:140548130>, 1995.
- Morison, J. H., Aagaard, Dr, K., Moritz, R., McPhee, M., Heiberg, A., Steele, M., and Andersen, R.: North Pole Environmental Observatory (NPEO) Oceanographic Mooring Data., <https://doi.org/10.5065/D6P84921>, [Online; accessed 2023-07-12], 2016.
- 1415 Nandan, V., Geldsetzer, T., Yackel, J., Mahmud, M., Scharien, R., Howell, S., King, J., Ricker, R., and Else, B.: Effect of Snow Salinity on CryoSat-2 Arctic First-Year Sea Ice Freeboard Measurements, *Geophysical Research Letters*, 44, 10,419–10,426, <https://doi.org/10.1002/2017GL074506>, 2017.
- Nicolaus, M. and Katlein, C.: Observations of the Snow Depth on Arctic Sea Ice, *Journal of Geophysical Research: Oceans*, 122, 7167–7183, <https://doi.org/10.1002/2017JC012838>, 2017.
- 1420 Nicolaus, M., Hoppmann, M., Arndt, S., Hendricks, S., Katlein, C., König-Langlo, G., Nicolaus, A., Rossmann, L., Schiller, M., Schwegmann, S., Langevin, D., and Bartsch, A.: Snow height and air temperature on sea ice from Snow Buoy measurements, <https://doi.org/10.1594/PANGAEA.875638>, 2017.
- Nicolaus, M., Hoppmann, M., Arndt, S., Hendricks, S., Katlein, C., Nicolaus, A., Rossmann, L., Schiller, M., and Schwegmann, S.: Snow Depth and Air Temperature Seasonality on Sea Ice Derived From Snow Buoy Measurements, *Frontiers in Marine Science*, 8, 377, <https://doi.org/10.3389/FMARS.2021.655446/BIBTEX>, 2021.
- 1425 NSIDC: Submarine Upward Looking Sonar Ice Draft Profile Data and Statistics, Version 1, <https://doi.org/10.7265/N54Q7RWK>, 1998.
- NSIDC: Submarine Upward Looking Sonar Ice Draft Profile Data and Statistics, Version 1 USER GUIDE, [https://nsidc.org/sites/default/files/g01360-v001-userguide\\_1\\_0.pdf](https://nsidc.org/sites/default/files/g01360-v001-userguide_1_0.pdf), 1998, 2006.
- Olsen, I. L. and Skourup, H.: Sea ice thickness reference measurements (ESA CCI SIT RRDP), Dataset, <https://doi.org/10.11583/DTU.24787341>, 2024a.
- 1430 Olsen, I. L. and Skourup, H.: Source code for the creation of the ESA CCI SIT RRDP, <https://github.com/Idalundtorp/ESACCI->, 2024b.
- Ozsoy-Cicek, B., Kern, S., Ackley, S. F., Xie, H., and Tekeli, A. E.: Intercomparisons of Antarctic sea ice types from visual ship, RADARSAT-1 SAR, Envisat ASAR, QuikSCAT, and AMSR-E satellite observations in the Bellingshausen Sea, *Deep Sea Research Part II: Topical Studies in Oceanography*, 58, 1092–1111, <https://doi.org/https://doi.org/10.1016/j.dsr2.2010.10.031>, antarctic Sea Ice Research during the International Polar Year 2007-2009, 2011.
- 1435 Paul, S., Hendricks, S., Ricker, R., Kern, S., and Rinne, E.: Empirical parametrization of Envisat freeboard retrieval of Arctic and Antarctic sea ice based on CryoSat-2: progress in the ESA Climate Change Initiative, *The Cryosphere*, 12, 2437–2460, <https://doi.org/10.5194/tc-12-2437-2018>, 2018.
- Paul, S., Sallila, H., Hendricks, S., and Rinne, E.: ESA CCI+ Climate Change Initiative Phase 1, D2.1 Sea Ice Thickness Algorithm Theoretical Basis Document (ATBD), v.3.1, <https://climate.esa.int/en/projects/sea-ice/Sea-Ice-Key-Documents/>, 2021.
- 1440 Paul, S., Hendricks, S., Skourup, H., Sallila, H., Rinne, E., and Lavergne, T.: The ESA CCI Sea-Ice Thickness CDR: Current State and Evolutions, in: *ESA Living Planet Symposium 2022*, Bonn, 2022.
- Perovich, D., Richter-Menge, J., and Polashenski, C.: Observing and understanding climate change: Monitoring the mass balance, motion, and thickness of Arctic sea ice, <http://imb-crrel-dartmouth.org>, 2022.

- 1445 Petty, A. A., Keeney, N., Cabaj, A., Kushner, P., and Bagnardi, M.: Winter Arctic sea ice thickness from ICESat-2: upgrades to freeboard and snow loading estimates and an assessment of the first three winters of data collection, *The Cryosphere*, 17, 127–156, <https://doi.org/10.5194/tc-17-127-2023>, 2023.
- Polashenski, C., Perovich, D., Richter-Menge, J., and Elder, B.: Seasonal ice mass-balance buoys: adapting tools to the changing Arctic, *Annals of Glaciology*, 52, 18–26, <https://doi.org/10.3189/172756411795931516>, 2011.
- 1450 Quartly, G. D., Rinne, E., Passaro, M., Andersen, O. B., Dinardo, S., Fleury, S., Guillot, A., Hendricks, S., Kurekin, A. A., Müller, F. L., Ricker, R., Skourup, H., and Tsamados, M.: Retrieving Sea Level and Freeboard in the Arctic: A Review of Current Radar Altimetry Methodologies and Future Perspectives, *Remote Sensing*, 11, <https://doi.org/10.3390/rs11070881>, 2019.
- Richter-Menge, J., Gascard, J.-C., and Andersen, S.: State of the Arctic Sea Ice Cover, *EOS Transactions American Geophysical Union*, 87, 253–260, <https://doi.org/10.1029/2006EO250002>, 2006a.
- 1455 Richter-Menge, J. A., Perovich, D. K., Elder, B. C., Claffey, K., Rigor, I., and Ortmeier, M.: Ice mass-balance buoys: a tool for measuring and attributing changes in the thickness of the Arctic sea-ice cover, *Annals of Glaciology*, 44, 205–210, <https://doi.org/10.3189/172756406781811727>, 2006b.
- Ricker, R., Hendricks, S., Helm, V., Skourup, H., and Davidson, M.: Sensitivity of CryoSat-2 Arctic sea-ice freeboard and thickness on radar-waveform interpretation, *The Cryosphere*, 8, 1607–1622, <https://doi.org/10.5194/tc-8-1607-2014>, 2014.
- 1460 Roca, M., Laxon, S., and Zelli, C.: The EnviSat RA-2 Instrument Design and Tracking Performance, *IEEE Transactions on Geoscience and Remote Sensing*, 47, 3489–3506, <https://doi.org/10.1109/TGRS.2009.2020793>, 2009.
- Rothrock, D. A. and Wensnahan, M.: The Accuracy of Sea Ice Drafts Measured from U.S. Navy Submarines, *Journal of Atmospheric and Oceanic Technology*, 24, 1936–1949, <https://doi.org/10.1175/JTECH2097.1>, 2007.
- Sallila, H., Farrell, S. L., McCurry, J., and Rinne, E.: Assessment of contemporary satellite sea ice thickness products for Arctic sea ice, *The Cryosphere*, 13, 1187–1213, <https://doi.org/10.5194/tc-13-1187-2019>, 2019.
- 1465 Schwegmann, S., Rinne, E., Ricker, R., Hendricks, S., and Helm, V.: About the consistency between Envisat and CryoSat-2 radar freeboard retrieval over Antarctic sea ice, *The Cryosphere*, 10, 1415–1425, <https://doi.org/10.5194/tc-10-1415-2016>, 2016.
- SCICEX: Science Ice Exercise Data Collection. Boulder, Colorado USA: National Snow and Ice Data Center, <https://doi.org/10.7265/N5930R3Z>, 2009, 2014.
- 1470 Shalina, E. V. and Sandven, S.: Snow depth on Arctic sea ice from historical in situ data, *The Cryosphere*, 12, 1867–1886, <https://doi.org/10.5194/tc-12-1867-2018>, 2018.
- Shen, X., Ke, C.-Q., and Li, H.: Snow depth product over Antarctic sea ice from 2002 to 2020 using multisource passive microwave radiometers, *Earth System Science Data*, 14, 619–636, <https://doi.org/10.5194/essd-14-619-2022>, 2022.
- Stroeve, J., Liston, G. E., Buzzard, S., Zhou, L., Mallett, R., Barrett, A., Tschudi, M., Tsamados, M., Itkin, P., and Stewart, J. S.: A Lagrangian Snow Evolution System for Sea Ice Applications (SnowModel-LG): Part II—Analyses, *Journal of Geophysical Research: Oceans*, 125, e2019JC015900, <https://doi.org/10.1029/2019JC015900>, 2020a.
- 1475 Stroeve, J., Nandan, V., Willatt, R., Tonboe, R., Hendricks, S., Ricker, R., Mead, J., Mallett, R., Huntemann, M., Itkin, P., Schneebeli, M., Krampe, D., Spreen, G., Wilkinson, J., Matero, I., Hoppmann, M., and Tsamados, M.: Surface-based Ku- and Ka-band polarimetric radar for sea ice studies, *The Cryosphere*, 14, 4405–4426, <https://doi.org/10.5194/tc-14-4405-2020>, 2020b.
- 1480 Sumata, H.: Monthly sea ice thickness distribution in Fram Strait [Data set], <https://doi.org/https://doi.org/10.21334/npolar.2022.b94cb848>, 2022.

- Sumata, H., Divine, D., and de Steur, L.: Monthly mean sea ice draft from the Fram Strait Arctic Outflow Observatory since 1990., <https://doi.org/10.21334/npolar.2021.5b717274>, 2021.
- 1485 Taylor, J. R.: *An Introduction to Error Analysis - the study of uncertainties in physical measurements*, University Science Books, California, United States of America, 2nd. ed., 1939.
- Tilling, R. L., Ridout, A., and Shepherd, A.: Estimating Arctic sea ice thickness and volume using CryoSat-2 radar altimeter data, *Advances in Space Research*, 62, 1203–1225, <https://doi.org/10.1016/j.asr.2017.10.051>, the CryoSat Satellite Altimetry Mission: Eight Years of Scientific Exploitation, 2018.
- 1490 Tucker, W. B., Perovich, D. K., Gow, A. J., Weeks, W. F., and Drinkwater, M. R.: Physical properties of sea ice relevant to remote sensing, in: *Microwave Remote Sensing of Sea Ice*, edited by Frank D. Carsey, <https://doi.org/10.1029/GM068p0009>, 1992.
- Ulaby, F., Moore, R. K., and Fung, A. K.: *Microwave remote sensing: From theory to applications (vol. 3)*, Artech House, Norwood, MA., 1986.
- U.S.Fleet: *Polar Icebreakers in a Changing World*, chapter 7 icebreaking environments and challenges to U.S. Fleet, <https://doi.org/10.17226/11753>, [Online; accessed 2023-07-29], 2007.
- 1495 von Abedyll, L., Kubiczek, J. M., von Bock und Polach, F., and Haas, C.: Sea ice thickness, ice loads, and navigability during the North Pole cruise CC110823 of Le Commandant Charcot in August 2023, Cruise report, Alfred Wegener Institute, Helmholtz Centre for Polar and Marine Research, Bremerhaven, Germany, 2024.
- von Albedyll, L., Haas, C., and Grodofzig, R.: EM-Bird ice thickness measurements in the Transpolar Drift during MOSAiC 2019/2020, part 1, <https://doi.org/10.1594/PANGAEA.934578>, 2021.
- 1500 Wadhams, P., Tucker III, W. B., Krabill, W. B., Swift, R. N., Comiso, J. C., and Davis, N. R.: Relationship between sea ice freeboard and draft in the Arctic Basin, and implications for ice thickness monitoring, *Journal of Geophysical Research: Oceans*, 97, 20 325–20 334, <https://doi.org/https://doi.org/10.1029/92JC02014>, 1992.
- Wang, X., Zhou, H., and Ji, M.: Spatial-temporal variations of one-year ice in Antarctic different regions, 1988–2020, *Ecological Indicators*, 154, 110 889, <https://doi.org/https://doi.org/10.1016/j.ecolind.2023.110889>, 2023.
- 1505 Warren, S. G., Rigor, I. G., Untersteiner, N., Radionov, V. F., Bryazgin, N. N., Aleksandrov, Y. I., and Colony, R.: Snow Depth on Arctic Sea Ice, *Journal of Climate*, 12, 1814 – 1829, [https://doi.org/10.1175/1520-0442\(1999\)012<1814:SDOASI>2.0.CO;2](https://doi.org/10.1175/1520-0442(1999)012<1814:SDOASI>2.0.CO;2), 1999.
- Willatt, R., Laxon, S., Giles, K., Cullen, R., Haas, C., and Helm, V.: Ku-band radar penetration into snow cover on Arctic sea ice using airborne data, *Annals of Glaciology*, 52, 197–205, <https://doi.org/10.3189/172756411795931589>, 2011.
- 1510 Willatt, R. C., Giles, K. A., Laxon, S. W., Stone-Drake, L., and Worby, A. P.: Field Investigations of Ku-Band Radar Penetration Into Snow Cover on Antarctic Sea Ice, *IEEE Transactions on Geoscience and Remote Sensing*, 48, 365–372, <https://doi.org/10.1109/TGRS.2009.2028237>, 2010.
- Wingham, D., Francis, C., Baker, S., Bouzinac, C., Brockley, D., Cullen, R., de Chateau-Thierry, P., Laxon, S., Mallow, U., Mavrocordatos, C., Phalippou, L., Ratier, G., Rey, L., Rostan, F., Viau, P., and Wallis, D.: CryoSat: A mission to determine the fluctuations in Earth's land and marine ice fields, *Advances in Space Research*, 37, 841–871, <https://doi.org/https://doi.org/10.1016/j.asr.2005.07.027>, natural Hazards and Oceanographic Processes from Satellite Data, 2006.
- 1515 Worby, A., Allison, I., and Dirita, V.: ANTARCTIC CRC COOPERATIVE RESEARCH CENTRE FOR THE ANTARCTIC AND SOUTHERN OCEAN ENVIRONMENT; A Technique for Making Ship-Based Observations of Antarctic Sea Ice Thickness and Characteristics PART I, Observational Technique and Results PART II User Operating Manual, <http://www.antarc.utas.edu.au/aspect.>, 1999.

- 1520 Worby, A. P., Geiger, C. A., Paget, M. J., Van Woert, M. L., Ackley, S. F., and Deliberty, T. L.: Thickness Distribution of Antarctic Sea Ice, *Journal of Geophysical Research*, 113, 5–92, <https://doi.org/10.1029/2007JC004254>, 2008a.
- Worby, A. P., Geiger, C. A., Paget, M. J., Woert, M. L. V., Ackley, S. F., and DeLiberty, T. L.: ASPeCt data — antarctic sea ice processes climate (ASPeCt), <https://aspect.antarctica.gov.au/data.html>, [Online; accessed 2023-07-12], 2008b.
- 1525 Zeliang Liao, Bin Cheng, J. Z. T. V. K. J. Q. Y. Y. Y. L. Z. Z. L. Y. Q. and Cheng, X.: Snow depth and ice thickness derived from SIMBA ice mass balance buoy data using an automated algorithm, *International Journal of Digital Earth*, 12, 962–979, <https://doi.org/10.1080/17538947.2018.1545877>, 2019.
- Zhou, L., Stroeve, J., Xu, S., Petty, A., Tilling, R., Winstrup, M., Rostosky, P., Lawrence, I. R., Liston, G. E., Ridout, A., Tsamados, M., and Nandan, V.: Inter-comparison of snow depth over Arctic sea ice from reanalysis reconstructions and satellite retrieval, *The Cryosphere*, 15, 345–367, <https://doi.org/10.5194/tc-15-345-2021>, 2021.
- 1530 Zygmuntowska, M., Rampal, P., Ivanova, N., and Smedsrud, L. H.: Uncertainties in Arctic sea ice thickness and volume: new estimates and implications for trends, *The Cryosphere*, 8, 705–720, <https://doi.org/10.5194/tc-8-705-2014>, 2014.
- Øyvind, F. and Sundfjord, A.: Sea ice draft and sea ice and upper ocean velocity from mooring observations in the northwestern Barents Sea from 2018 onward, <https://doi.org/10.21334/NPOLAR.2024.C19E8A7D>, 2025.

## Appendix A: Acronym table

**Table A1.** Acronym table - for Acronyms given to campaigns included in the CCI SIT RRDP, see Table 1.

<b>Abbreviation</b>	<b>Definition</b>
<u><a href="#">AEM</a></u>	<u><a href="#">Airborne Electromagnetic (measurements)</a></u>
ATM	Airborne Topographic Mapper
CCI	Climate Change Initiative
CDR	Climate Data Record
CRISTAL	Polar Ice and Snow Topography Altimeter
CryoVEx	CryoSat Validation Experiment
EASE2	Equal-Area Scalable Earth grid, version 2
ECV	Essential Climate Variable
EM	Electromagnetic
Envisat	Environmental Satellite
ERS-1/2	European Remote Sensing Satellites 1 and 2
ESA	European Space Agency
FDR4ALT	Fundamental Data Records for Altimetry
FRB	Freeboard
FRM	Fiducial Reference Measurements
GNSS	Global Navigation Satellite System
<u><a href="#">HEM</a></u>	<u><a href="#">Helicopter Borne Electromagnetic (measurements)</a></u>
ICESat	Ice, Cloud and land Elevation Satellite
LiDAR	Light Detection and Ranging
NASA	National Aeronautics and Space Administration
NH	Northern Hemisphere
NSIDC	National Snow and Ice Data Center
RA	Radar Altimeter
RRDP	Round Robin Data Package
SAR	Synthetic Aperture Radar
SH	Southern Hemisphere
SD	Snow Depth
SID	Sea Ice Draft
SIRAL	SAR interferometric radar altimeter
SIT	Sea Ice Thickness
ULS	Upward Looking Sonar
WGS	World Geodetic System

## Appendix B: Statistics of comparison between satellite and reference data

1535 The following tables show statistics linked to the comparison of CCI SIT RRDP to Envisat CDR and CryoSat-2 CDR. The comparison includes the standard deviation (std) and average of reference and satellite data, respectively. The Root Mean Square Error (RMSE), Pearson correlation coefficient (R) ( only shown in plots 6–9) and Coefficient of determination ( $R^2$ ) for both the best fit and for the ( $y = x$ ) fit, as would be the ideal case.

Due to the nature of  $R^2$  being a calculation between a true value and a fit this calculation is highly sensitive to which variable  
1540 is being examined. In the case below the ( $R^2$ ) value is calculated between the satellite CDRs and the predictions.

**Table B1.** Statistics of results CryoSat-2, LS= Least Squares, ODR= Orthogonal Distance Regression

Campaign	variable	Avg. (obs)	Avg. (CS-2)	std. (obs)	std. (CS-2)	bias (obs-sat)	$R^2$ ODR	RMSE ODR	$R^2$ LS	RMSE LS	$R^2(y=x)$	RMSE(y=x)	points	ODR fit
		[m]	[m]	[m]	[m]	[m]		[m]		[m]		[m]		
BGEP	SID	0.94	1.16	0.43	0.44	-0.22	0.47	0.32	0.48	0.32	0.15	0.41	193	y=0.75 x + 0.46
Nansen_legacy	SID	0.65	0.74	0.34	0.32	-0.10	0.04	0.32	0.12	0.30	-0.45	0.39	19	y=0.60 x + 0.37
NPLFS	SID	1.59	1.54	0.42	0.88	0.05	-8679.13	82.27	0.02	0.87	-0.36	1.03	154	y=194.45 x + -307.50
SCICEX	SID	2.49	1.97	0.57	0.39	0.52	0.36	0.32	0.37	0.31	-2.10	0.69	97	y=0.51 x + 0.67
TRANSDRIFT	SID	1.08	0.83	0.50	0.23	0.25	0.33	0.19	0.34	0.18	-3.49	0.48	67	y=0.31 x + 0.50
AEM: (AWI + MOSAIC)	SIT	2.46	2.55	1.07	1.23	-0.08	0.25	1.07	0.34	1.00	0.26	1.06	627	y= 1.01 x + 0.09
ASSIST	SIT	0.50	1.01	0.45	0.73	-0.51	0.09	0.75	0.10	0.69	-0.48	0.89	560	y=0.33 x + 0.56
IMB-CRREL	SIT	1.71	1.49	0.78	0.67	0.22	0.02	0.73	0.02	0.66	-1.11	0.97	1238	y=0.16 x + 0.92
MOSAIC: SIMBA	SIT	1.45	1.61	0.46	0.59	-0.15	0.42	0.50	0.44	0.44	0.36	0.47	729	y=0.67 x + 0.41
OIB	SIT	2.46	2.43	1.05	0.94	0.03	0.21	0.84	0.35	0.76	0.07	0.91	6465	y= 0.86 x + 0.32
AEM-AWI	SD	0.14	0.24	0.10	0.08	-0.11	-1.06	0.14	0.29	0.07	-1.77	0.14	155	y= 1.44 x + 0.12
SB-AWI	SD	0.30	0.25	0.21	0.08	0.05	0.02	0.08	0.05	0.08	-5.96	0.21	1302	y=0.16 x + 0.19
ASSIST	SD	0.10	0.13	0.11	0.08	-0.03	-2.35	0.19	0.32	0.07	-0.39	0.10	388	y= 1.69 x + 0.07
IMB-CRREL	SD	0.26	0.23	0.23	0.08	0.03	-0.01	0.08	0.00	0.08	-8.71	0.24	1626	y=0.04 x + 0.20
MOSAIC: SIMBA	SD	0.19	0.29	0.07	0.07	-0.09	-8.97	0.23	0.05	0.07	-2.13	0.13	729	y= 3.33 x + -0.33
OIB	SD	0.23	0.30	0.11	0.08	-0.08	-1.78	0.16	0.31	0.07	-1.29	0.12	7498	y= 1.48 x + 0.06
OIB	FRB	0.19	0.24	0.12	0.13	-0.05	0.14	0.12	0.21	0.11	-0.21	0.14	6501	y=0.74 x + 0.07
ASPeCi	SIT	0.62	1.34	0.44	0.56	-0.71	0.00	0.56	0.00	0.56	-2.20	1.00	488	y=0.05 x + 1.30
ASPeCi	SD	0.20	0.19	0.19	0.07	0.01	-2.57	0.14	0.08	0.07	-5.48	0.18	491	y=0.73 x + 0.09
SB-AWI:SH	SD	0.66	0.25	0.38	0.08	0.41	-0.07	0.10	0.05	0.08	-48.10	0.57	979	y= -0.12 x + 0.28

**Table B2.** Statistics of results Envisat, LS= Least Squares, ODR= Orthogonal Distance Regression

Campaign	variable	Avg. (obs) [m]	Avg. (ENV) [m]	std. (obs) [m]	std. (ENV) [m]	bias (obs-sat) [m]	$R^2$ ODR	RMSE ODR [m]	$R^2$ LS	RMSE LS [m]	$R^2(y=x)$	RMSE( $y=x$ )	points	ODR fit
BGEP	SID	1.12	1.09	0.49	0.40	0.03	0.57	0.26	0.57	0.26	0.33	0.32	183	$y=0.66x+0.36$
	SID	2.16	1.53	0.65	0.66	0.64	-0.59	0.83	0.06	0.64	-1.45	1.03	140	$y=1.05x-0.75$
	SCICEX	1.27	1.14	0.86	0.38	0.12	0.52	0.26	0.53	0.26	-1.97	0.65	100	$y=0.36x+0.69$
	TRANSDRIFT	1.43	0.85	0.70	0.31	0.58	0.50	0.22	0.53	0.22	-5.10	0.78	55	$y=0.40x+0.30$
AEM-AWI	SIT	1.69	1.39	1.03	0.76	0.29	0.13	0.72	0.20	0.67	-0.78	1.01	473	$y=0.53x+0.37$
	SIT	0.48	0.61	0.58	0.15	-0.13	0.06	0.15	0.06	0.15	-13.30	0.58	39	$y=0.06x+0.58$
	IMB-CRREL	1.89	1.27	0.91	0.71	0.63	0.02	0.75	0.02	0.71	-2.00	1.24	497	$y=0.17x+0.69$
	OIB	2.29	1.88	0.93	0.76	0.41	-0.17	0.83	0.10	0.73	-1.00	1.08	733	$y=0.69x+0.34$
ASSIST	SD	0.05	0.12	0.02	0.04	-0.08	-1.05	0.07	0.31	0.04	-2.58	0.08	39	$y=4.04x-0.04$
	SD	0.21	0.18	0.15	0.08	0.03	0.01	0.08	0.02	0.08	-3.43	0.16	768	$y=0.11x+0.14$
	SD	0.17	0.25	0.10	0.09	-0.08	-0.98	0.13	0.33	0.07	-0.84	0.12	1155	$y=1.52x+0.04$
	FRB	0.03	0.15	0.01	0.05	-0.12	-4830.56	3.83	0.00	0.05	-5.49	0.13	39	$y=376.03x-11.33$
AEM-AWI-FRB	FRB	0.19	0.17	0.14	0.11	0.02	-0.04	0.11	0.03	0.10	-1.34	0.16	748	$y=0.32x+0.10$
	SID	0.83	1.30	0.65	0.90	-0.47	-0.23	0.99	0.02	0.89	-0.61	1.14	243	$y=0.86x+0.58$
	SIT	0.72	1.34	0.51	0.69	-0.62	0.01	0.69	0.01	0.69	-1.16	1.02	734	$y=0.20x+1.18$
	FRB	0.21	0.19	0.18	0.09	0.02	-0.37	0.10	0.19	0.08	-2.61	0.16	739	$y=0.56x+0.08$
OIB-SH	FRB	0.45	0.39	0.24	0.17	0.06	0.21	0.16	0.24	0.15	-0.68	0.23	363	$y=0.49x+0.14$